MODELING AND CONTROL OF AUTONOMOUS UNDERWATER VEHICLE MANIPULATOR SYSTEMS

A THESIS SUBMITTED TO
THE GRADUATE SCHOOL OF NATURAL AND APPLIED SCIENCES
OF
MIDDLE EAST TECHNICAL UNIVERSITY

BY

OZAN KORKMAZ

IN PARTIAL FULFILLMENT OF THE REQUIREMENTS
FOR
THE DEGREE OF DOCTOR OF PHILOSOPHY
IN
MECHANICAL ENGINEERING

SEPTEMBER 2012

Approval of the thesis:

MODELING AND CONTROL OF AUTONOMOUS UNDERWATER VEHICLE MANIPULATOR SYSTEMS

submitted by **OZAN KORKMAZ** in partial fulfillment of the requirements for the degree of **Doctor of Philosophy in Mechanical Engineering Department, Middle East Technical University** by,

Prof. Dr. Canan ÖZGEN _____
Dean, Graduate School of **Natural and Applied Sciences**

Prof. Dr. Süha ORAL _____
Head of Department, **Mechanical Engineering**

Prof. Dr. S. Kemal İDER
Supervisor, **Mechanical Engineering Dept., METU** _____

Prof. Dr. M. Kemal ÖZGÖREN
Co-Supervisor, **Mechanical Engineering Dept., METU** _____

Examining Committee Members:

Prof. Dr. Reşit SOYLU _____
Mechanical Engineering Dept., METU

Prof. Dr. S. Kemal İDER _____
Mechanical Engineering Dept., METU

Prof. Dr. M. Kemal LEBLEBİCİOĞLU _____
Electrical and Electronics Engineering Dept., METU

Asst. Prof. Dr. Yiğit YAZICIOĞLU _____
Mechanical Engineering Dept., METU

Assoc. Prof. Dr. Metin U. SALAMCI _____
Mechanical Engineering Dept., Gazi University

Date: 14.09.2012

I hereby declare that all information in this document has been obtained and presented in accordance with academic rules and ethical conduct. I also declare that, as required by these rules and conduct, I have fully cited and referenced all material and results that are not original to this work.

Name, Last name : Ozan KORKMAZ

Signature :

ABSTRACT

MODELING AND CONTROL OF AUTONOMOUS UNDERWATER VEHICLE MANIPULATOR SYSTEMS

KORKMAZ, Ozan
Ph.D., Department of Mechanical Engineering
Supervisor: Prof. Dr. S. Kemal İDER
Co-Supervisor: Prof. Dr. M. Kemal ÖZGÖREN

September 2012, 154 pages

In this thesis, dynamic modeling and nonlinear control of autonomous underwater vehicle manipulator systems are presented. Mainly, two types of systems consisting of a 6-DOF AUV equipped with a 6-DOF manipulator subsystem (UVMS) and with an 8-DOF redundant manipulator subsystem (UVRMS) are modeled considering hydrostatic forces and hydrodynamic effects such as added mass, lift, drag and side forces. The shadowing effects of the bodies on each other are introduced when computing the hydrodynamic forces. The system equations of motion are derived recursively using Newton–Euler formulation. The inverse dynamics control algorithms are formulated and trajectory tracking control of the systems is achieved by assigning separate tasks for the end effector of the manipulator and for the underwater vehicle. The proposed inverse dynamics controller utilizes the full nonlinear model of the system and consists of a linearizing control law that uses the feedback of positions and velocities of the joints and the underwater vehicle in order to cancel off the nonlinearities of the system. The PD control is applied after this

complicated feedback linearization process yielding second order error dynamics. The thruster dynamics is also incorporated into the control system design. The stability analysis is performed in the presence of parametric uncertainty and disturbing ocean current. The effectiveness of the control methods are demonstrated by simulations for typical underwater missions.

Keywords: underwater vehicle manipulator system, modeling, inverse dynamics control, feedback linearization.

ÖZ

OTONOM SUALTI ARACI MANİPÜLATÖR SİSTEMLERİNİN MODELLENMESİ VE KONTROLÜ

KORKMAZ, Ozan
Doktora , Makina Mühendisliği Bölümü
Tez Yöneticisi: Prof. Dr. S. Kemal İDER
Ortak Tez Yöneticisi: Prof. Dr. M. Kemal ÖZGÖREN

Eylül 2012, 154 sayfa

Bu tezde, otonom sualtı aracı manipülatör sistemlerinin dinamik modellenmesi ve doğrusal olmayan kontrolü ele alınmıştır. Temel olarak, 6 serbestlik dereceli otonom sualtı aracı ile birlikte 6 serbestlik dereceli manipülatör alt sistemi (UVMS) ve 8 serbestlik dereceli manipülatör alt sisteminden (UVRMS) oluşan iki ayrı sistem, hidrostatik kuvvetler ve eklenmiş kütle, dinamik kaldırma, sürüklenme ve yanal kuvvetler gibi hidrodinamik etkiler dikkate alınarak modellenmiştir. Hidrodinamik kuvvetler hesaplanırken gövdelerin birbiri üzerindeki gölgeleme etkileri tanıtılmıştır. Newton–Euler formülasyonu kullanılarak sistem hareket denklemleri türetilmiştir. Ters dinamik kontrol algoritmaları formüle edilmiş ve sistemlerin yörünge takip kontrolü manipülatörün uç işlemcisi ve sualtı aracına ayrı görevler tanımlayarak sağlanmıştır. Önerilen ters dinamik kontrolcü, sistemlerin doğrusal olmayan modelinden yararlanmaktadır ve sistemlerdeki doğrusalsızlığı yok etmek için sualtı aracı ile eklemlerin pozisyon ve hız geribildirimlerini kullanan doğrusallaştırıcı kontrol yasasından oluşmaktadır. PD kontrolü ikinci derece hata dinamiğini sağlayacak şekilde, bu karmaşık geribildirime dayanan doğrusallaştırma süreci

sonrasında uygulanmıştır. Kontrol sistemi tasarımına itki dinamiği de dahil edilmiştir. Parametrik belirsizliğin ve bozucu okyanus akıntısının varlığında kararlılık analizi yapılmıştır. Kontrol yöntemlerinin etkinliği tipik sualtı görevleri için benzetimlerle gösterilmiştir.

Anahtar kelimeler: sualtı aracı manipülatör sistemi, modelleme, ters dinamik kontrol, geribildirimle doğrusallaştırma.

To My Family

ACKNOWLEDGMENTS

I would like to express my deepest gratitude to my supervisors Prof. Dr. S. Kemal İDER and Prof. Dr. M. Kemal ÖZGÖREN for their guidance, advice, criticism, encouragements and understanding throughout the thesis.

I would also like to express my thanks to my Thesis Monitoring Committee members, Prof. Dr. M. Kemal LEBLEBİCİOĞLU and Assoc. Prof. Dr. Yiğit YAZICIOĞLU for their constructive comments and guidance throughout my study.

The support of TÜBİTAK SAGE is also acknowledged.

My greatest thanks go to my family for their trust, patience, understanding and continuous support.

TABLE OF CONTENTS

ABSTRACT iv
ÖZ vi
ACKNOWLEDGMENTS ix
TABLE OF CONTENTS x
LIST OF TABLES xiii
LIST OF FIGURES xiv
LIST OF SYMBOLS xvii
CHAPTERS
1. INTRODUCTION 1
1.1 Overview 1
1.2 Literature Survey 6
1.2.1 Literature Survey on Modeling and Control of UUVs 6
1.2.2 Literature Survey on Modeling and Control of UVMSs 8
1.3 Motivation and Contribution 10
1.4 Outline 12
2. UVMS KINEMATICS 14
2.1 Underwater Vehicle Kinematics 14
2.1.1 Coordinate Transformations 18
2.1.1.1 Velocity Level Transformation 18
2.1.1.2 Acceleration Level Transformation 21
2.2 Manipulator Kinematics with Moving Base 24
2.2.1 Sign Convention 24
2.2.2 Link Orientation Expressions 25
2.2.3 Angular Velocity Expressions 25
2.2.4 Angular Acceleration Expressions 26
2.2.5 Link Origin and Mass Center Location Expressions 27

2.2.6 Velocity Expressions 27
2.2.7 Acceleration Expressions 28
2.3 UVMS Kinematics Having Regular Manipulator 29
2.4 UVMS Kinematics Having Redundant Manipulator 34
3. UVMS DYNAMICS 40
3.1 Underwater Vehicle Dynamics 40
3.1.1 Newton-Euler Equations for the AUV 40
3.2 Manipulator Dynamics 43
3.2.1 Newton-Euler Equations for Regular Manipulator Subsystem 44
3.2.2 Newton-Euler Equations for Redundant Manipulator Subsystem 47
3.3 Hydrostatic Forces and Moments 49
3.4 Hydrodynamic Effects 52
3.4.1 Added Mass/Inertia Forces and Moments 52
3.4.2 Damping Forces and Moments 55
3.4.2.1 Damping Forces 55
3.4.2.1.1 Drag Forces 56
3.4.2.1.2 Lift Forces 58
3.4.2.1.3 Side Forces 60
3.4.2.2 Damping Moments 64
3.4.3 The Shadowing Effect 65
3.4.4 The Effect of Ocean Currents 67
3.5 Thruster Dynamics 68
3.6 Underwater Vehicle Regular Manipulator System Dynamics 72
3.6.1 The Elimination of the Generalized Constraint Forces 73
3.7 Underwater Vehicle Redundant Manipulator System Dynamics 76
4. TRAJECTORY PLANNING AND CONTROLLER DESIGN 79
4.1 Task Equations 79
4.1.1 Position Level Equations 79
4.1.2 Velocity Level Equations 82
4.1.3 Acceleration Level Equations 85
4.2 Inverse Dynamics Controller Design for Fully Actuated UVMS 89

4.3 Inverse Dynamics Controller Design for Underactuated UVMS 92
4.4 Inverse Dynamics Controller Design for Underactuated UVRMS 94
4.5 Thruster Controller Design 96
4.6 Trajectory Planning 98
5. CONTROL SIMULATIONS 101
5.1 Simulink Model 101
5.2 Simulation Results 104
5.2.1 Fully Actuated UVMS Results 106
5.2.2 Underactuated UVMS Results 119
5.2.3 Underactuated UVRMS Results 126
6. DISCUSSIONS AND CONCLUSIONS 136
REFERENCES 140
APPENDICES 147
A. SYSTEM JACOBIAN MATRICES 147
B. HYDRODYNAMIC DATA 151
VITA 153

LIST OF TABLES

TABLES

Table 2.1 Vehicle Motions 14

Table 2.2 UVMS DH Parameters 30

Table 2.3 UVRMS DH Parameters 35

Table 3.1 UVMS Unknowns 73

Table 3.2 UVRMS Unknowns 78

Table 5.1 Test Scenarios and Missions 105

Table 5.2 Parametric Uncertainty Combinations 106

Table 5.3 UVMS Mass and Geometry Properties 107

Table 5.4 Thruster Parameters 110

Table 5.5 UVRMS Mass and Geometry Properties 126

Table 5.6 Geological Sampling Mission Results 135

LIST OF FIGURES

FIGURES

Figure 1.1 Efforts on Raising the Wreckage of the Aircraft 3

Figure 1.2 Titanic 2010 Expedition 4

Figure 1.3 Water Sampling AUV and NASA's Satellite View 5

Figure 1.4 AUV ISiMI 6

Figure 1.5 AUV SAUVIM 7

Figure 2.1 Vehicle Reference Frames 15

Figure 2.2 DH Sign Convention 24

Figure 2.3 Underwater Vehicle Manipulator System 29

Figure 2.4 Underwater Vehicle Redundant Manipulator System 34

Figure 3.1 Hydrostatic Forces 50

Figure 3.2 Damping Forces & Current Frame 55

Figure 3.3 Apparent Mass Factor 59

Figure 3.4 The Side Force Coefficient Variations 61

Figure 3.5 Shadowing Effects 66

Figure 3.6 Thruster Model 69

Figure 3.7 Thrusters' Configuration 70

Figure 4.1 End-effector Orientation 80

Figure 4.2 Singular Configurations 98

Figure 5.1 UVMS Simulink Model 103
Figure 5.2 UVMS Initial Configuration 108
Figure 5.3 UVMS Closed Loop Responses (C1) 112
Figure 5.4 UVMS Position Errors (C1) 113
Figure 5.5 UVMS Control Forces and Torques (C1) 114
Figure 5.6 UVMS Joint Displacements (C1) 114
Figure 5.7 UVMS Control Forces and Torques (C2) 115
Figure 5.8 UVMS Propeller Speed Responses (C2) 115
Figure 5.9 UVMS Closed Loop Responses (C2) 116
Figure 5.10 UVMS Position Errors (C2) 117
Figure 5.11 UVMS Thruster Motor Control Torques (C2) 118
Figure 5.12 Effect of Damping Ratio on Responses 119
Figure 5.13 u-UVMS Closed Loop Responses (C1) 121
Figure 5.14 u-UVMS Position Errors (C1) 122
Figure 5.15 u-UVMS Closed Loop Responses (C2) 123
Figure 5.16 u-UVMS Position Errors (C2) 124
Figure 5.17 u-UVMS Control Forces and Torques (C2) 125
Figure 5.18 u-UVMS Propeller Speed Responses (C2) 125
Figure 5.19 u-UVMS Thruster Motor Control Torques (C2) 125
Figure 5.20 u-UVRMS Initial Configuration 127
Figure 5.21 u-UVRMS Closed Loop Responses (C1) 129
Figure 5.22 u-UVRMS Position Errors (C1) 130
Figure 5.23 u-UVRMS Closed Loop Responses (C2) 131
Figure 5.24 u-UVRMS Position Errors (C2) 132

Figure 5.25 u-UVRMS Control Forces and Torques (C2) 133
Figure 5.26 u-UVRMS Propeller Speed Responses (C2) 133
Figure 5.27 u-UVRMS Thruster Motor Control Torques (C2) 133

LIST OF SYMBOLS

Basic Latin Letters

a_i : Effective Length of the i^{th} Body

$\overline{a}_{O_i/O_j}^{(k)}$: Acceleration Vector of Point-O_i with respect to Point-O_j as Expressed in k^{th} Reference Frame

$\hat{C}^{(i,j)}$: Transformation Matrix from j^{th} Reference Frame to i^{th} Reference Frame

C_{D_i} : Drag Coefficient of the i^{th} Body

C_{L_i} : Lift Coefficient of the i^{th} Body

C_{S_i} : Side Coefficient of the i^{th} Body

d_i : Diameter of the i^{th} Body

g : Gravitational Acceleration

$\hat{E}_m$: Rotation Matrix of the End-Effector of the Manipulator

$\hat{E}_v$: Rotation Matrix of the AUV

$\overline{e}_p$: Position Error Vector

$\overline{f}_{ij}^{(k)}$: Vector of Forces Applied by Body i on Body j as Expressed in k^{th} Reference Frame

$\hat{J}_m$: Manipulator Jacobian Matrix

$\hat{J}_{O_i}$: Inertia Matrix of Point-O_i

$\hat{J}_v$: AUV Jacobian Matrix

$\hat{K}_p$: Position Feedback Gain Matrix

$\hat{K}_v$: Velocity Feedback Gain Matrix

l_i : Length of the i^{th} Body

m_i : Mass of the i^{th} Body

$\bar{m}_{ij}^{(k)}$: Vector of Moments Applied by Body i on Body j as Expressed in k^{th} Reference Frame

O_i : Origin of the i^{th} Reference Frame

p : Roll Velocity Component of AUV

$\bar{p}_{O_i/O_j}^{(k)}$: Position Vector of Point-O_i with respect to Point-O_j as Expressed in k^{th} Reference Frame

p_{th_i} : Pitch of the Propeller of the i^{th} thruster

q : Pitch Velocity Component of AUV

q_{∞_i} : Dynamic Pressure of the i^{th} Body

r : Yaw Velocity Component of AUV

r_i : Radius of the i^{th} Body

S_i : Frontal Area of the i^{th} Body

s_i : Offset of the i^{th} Body

T : The Period of the Motion

t : Time

u : Surge Velocity Component of AUV

$\bar{u}$: Commanded Input Vector

$\bar{u}_i$: i^{th} Unit Vector

v : Sway Velocity Component of AUV

$\bar{v}_{O_i/O_j}^{(k)}$: Velocity Vector of Point-O_i with respect to Point-O_j as Expressed in k^{th} Reference Frame

w : Heave Velocity Component of AUV

Greek Letters

α_i : Twist Angle of the i^{th} Body

α_t : Angle of Attack

$\bar{\alpha}_{i/j}^{(k)}$: Angular Acceleration Vector of Body-*i* with respect to Body-*j* as Expressed in k^{th} Reference Frame

β_t : Angle of Side Slip of the i^{th} Body

Δx : The Amount Change in x Component

δ : Deflection

ϕ_i : i^{th} Euler Angle of AUV

$\bar{\eta}$: AUV Body-Fixed Velocity Vector

$\hat{\mu}$: Thruster Configuration Matrix

θ_i : Rotation Angle of the i^{th} Body

ρ : Density, Specific Weight

ς : Damping Ratio

τ_k : Motor Torque of the Propeller of the i^{th} Thruster

υ_i : Volume Swept by the i^{th} Body

Ω_i : Angular Velocity of the Propeller of the i^{th} Thruster

ω_i : i^{th} Controller Bandwidth

$\bar{\omega}_{i/j}^{(k)}$: Angular Velocity Vector of Body-*i* with respect to Body-*j* as Expressed in k^{th} Reference Frame

$\bar{\xi}$: Generalized Coordinates Vector of the System in Earth-Fixed Reference Frame

ψ_i : i^{th} Euler Angle of Manipulator

$\bar{\zeta}$: Generalized Coordinates Vector of AUV in Earth-Fixed Reference Frame

$\bar{\zeta}_{ee}$: Generalized Coordinates Vector of End-effector of Manipulator in Earth- Fixed Reference Frame

Overhead Symbols

.	: First Time Derivative
..	: Second Time Derivative
$\rightarrow$	: Vector
–	: Column Vector
^	: Matrix
~	: Skew-Symmetric Matrix

Abbreviations

AUV	: Autonomous Underwater Vehicle
DC	: Direct Current
DH	: Denavit-Hartenberg
DOF	: Degree of Freedom
ISE	: Integral of Square of Error
ITAE	: Integral of Time Multiplied by the Absolute Value of Error
NASA	: National Aeronautics and Space Administration
PD	: Proportional plus Derivative
RF	: Reference Frame
ROV	: Remotely Operated Vehicle
US	: United States
UUV	: Unmanned Underwater Vehicle
UVMS	: Underwater Vehicle Manipulator System
UVRMS	: Underwater Vehicle Redundant Manipulator System

CHAPTER I

INTRODUCTION

1.1 Overview

Underwater Vehicle Manipulator Systems (UVMSs) are great point of concern for years and research studies especially focusing on modeling and control of these unmanned systems date back to 1980s beginning with *Unmanned Underwater Vehicles* (UUVs). UUVs can be classified into two groups; namely *Remotely Operated Vehicles (ROVs*) and *Autonomous Underwater Vehicle (AUVs).*

The term ROV denotes an underwater vehicle physically linked, via the tether, to an operator that can be on a submarine or on a surface ship [1]. The tether is used to establish communication between the ROV and the ship and also in charge of transmitting power to the vehicle.

Extensive uses of ROVs are currently limited due mainly to high operational costs and safety requirements. Besides that trained and skilled operators are necessary to execute the task precisely and they are often required to be close to the system [1,2]. In the past several decades, the AUVs have evolved as a consequence of various research efforts arising from the demand in autonomy of the vehicle and minimized the need for the presence of human operators.

An AUV is defined as an untethered underwater vehicle that is driven through the water by a propulsion system, controlled autonomously by an onboard computer. The main advantages of the AUVs compared to the ROVs are their decreased sizes and

increased maneuvering capabilities. Autonomy greatly reduces operational costs since there is no human operator involved.

In order to handle high precision underwater manipulations on the other hand, AUVs are equipped with *teleoperators* which are controlled by a human operator in a surface vessel. Even in such a case, new problems arise due to the time delays introduced by the vessel-manipulator communication system [1,2].

To overcome all the limitations stated above, the recent research efforts are aimed at developing systems consisting of AUVs together with one or more autonomous robotic manipulators in order to perform more challenging and high precision tasks in contact with the hazardous environment of the sea water, which are called as fully autonomous UVMSs.

UVMSs have a lot of applications today in different areas such as science, environment and military. In science and environment for example, these systems are used to map the sea floor leading to oceanographic investigations, to take samples to analyze the geological characteristics, to monitor the sea water for both biodiversity research and pollution measurements and to repair and maintain the underwater structures like pipelines or oil rigs.

In military, UVMSs have significant role in underwater reconnaissance and surveillance, maritime safety and security and especially sea mine detection and disposal.

In order to stress the importance of these above-mentioned unmanned underwater systems, a few striking real-life events and engineering problems which happened only 2-3 years ago can be considered.

Air France Plane Crash: Air France Flight 447 was a scheduled commercial flight from Rio de Janeiro, Brazil to Paris, France. On 1 June 2009, the Airbus A330-200 airliner serving the flight crashed into the Atlantic Ocean, killing all 216 passengers

and 12 crew [3]. Earlier 2011, two types of ROVs (see Figure 1.1) dove to 4.000 m depths in the Atlantic Ocean to locate, map, and raise the wreckage. Researchers from Woods Hole Oceanographic Institute used their Remus 6000 machines, torpedo-like tubes fitted with cameras, side scan sonar, sensors and a fiber-optic tether, working in a grid pattern, to locate the wreckage in a 3.900 miles squared area. Then, working from an ocean-going cable-laying ship, operators with Phoenix International, Largo, Md., used their Remora 6000 to work the bottom, recover the flight's black boxes and later, rig large pieces of the wreckage to allow recovery by ship's cranes [4].

Figure 1.1 Efforts on Raising the Wreckage of the Aircraft [4]

Titanic Ship Wreck: The 100 year-old Titanic ship wreck was mapped in a 2010 expedition led by National Geographic, Woods Hole Oceanographic Institution, and the Waitt Institute of Discovery. The three dimensional map of a roughly 15 miles squared area was pieced together by engineers and scientists using ROVs and AUVs working at 12.600 ft depths and fitted with side scan sonar systems and cameras. To map the site, researchers used the Remus vehicles in tandem using low-resolution sonar equipment. That was followed by high-resolution sonar used in mapping a smaller area that contains the wreck. After that, researchers used a ROV fitted with

high-definition cameras to photograph the field highlighted by the AUVs as seen in Figure 1.2. For the first time, viewers are able look at the wreck site as if the ocean were removed [5].

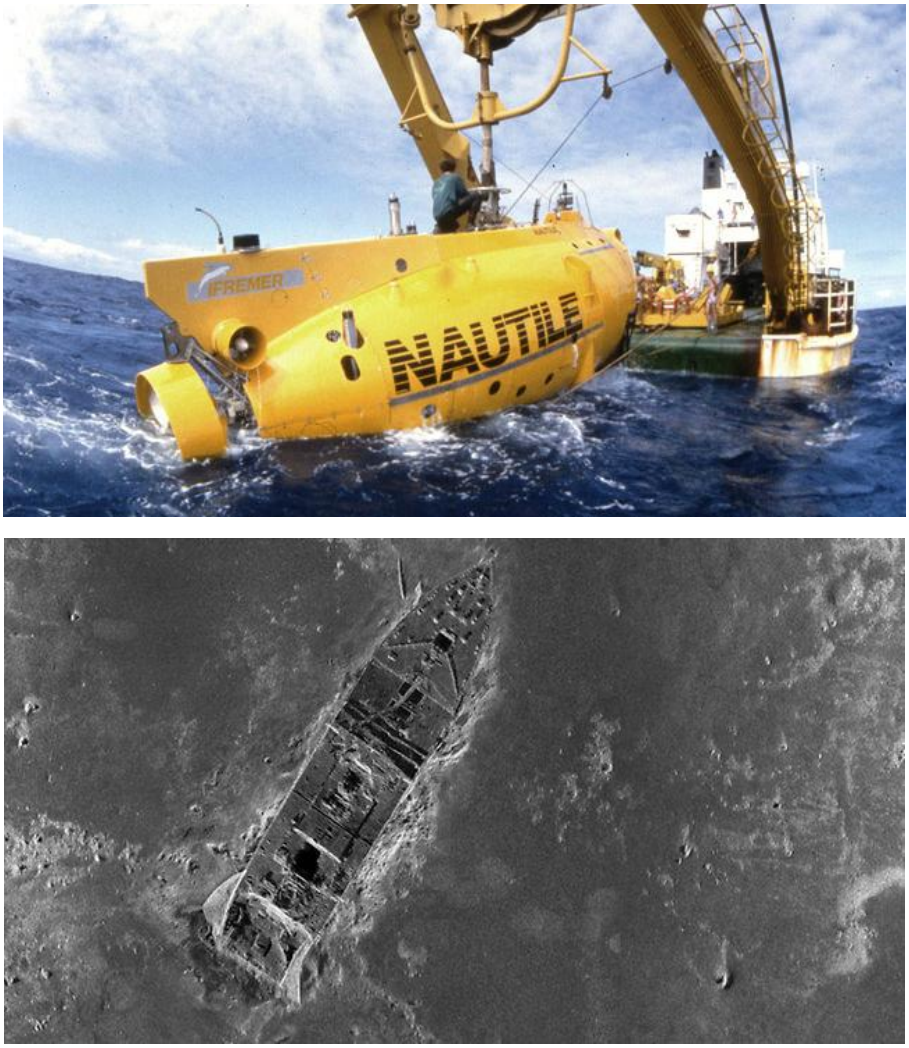

Figure 1.2 Titanic 2010 Expedition [6,7]

Oil Spill in the Gulf of Mexico: This catastrophic event happened a few miles away from the U.S. and lasted at least three months starting from 20 April 2010. It is considered to be one of the largest accidental marine oil spill in the history of the petroleum industry. The spill stemmed from a sea-floor oil gusher that resulted from the explosion of Deepwater Horizon, the mobile offshore drilling unit. On 15 July

2010, the gushing wellhead was capped, after it had released about millions of barrels of crude oil causing extensive damage to marine and wildlife habitats [8].

Monterey Bay Aquarium Research Institute's AUV as seen in Figure 1.3 participated in a cruise to investigate subsurface oil during May 27th to June 4th, 2010. It was in charge of mapping, sampling, and analyzing the subsurface hydrocarbon plumes to determine their distributions and how they interact with the oceanic environment. The AUV used its sensors to measure temperature, salinity, pressure, density, dissolved oxygen concentration etc. in a volume of oceanic water ranging from 900 to 1200 meters deep [9].

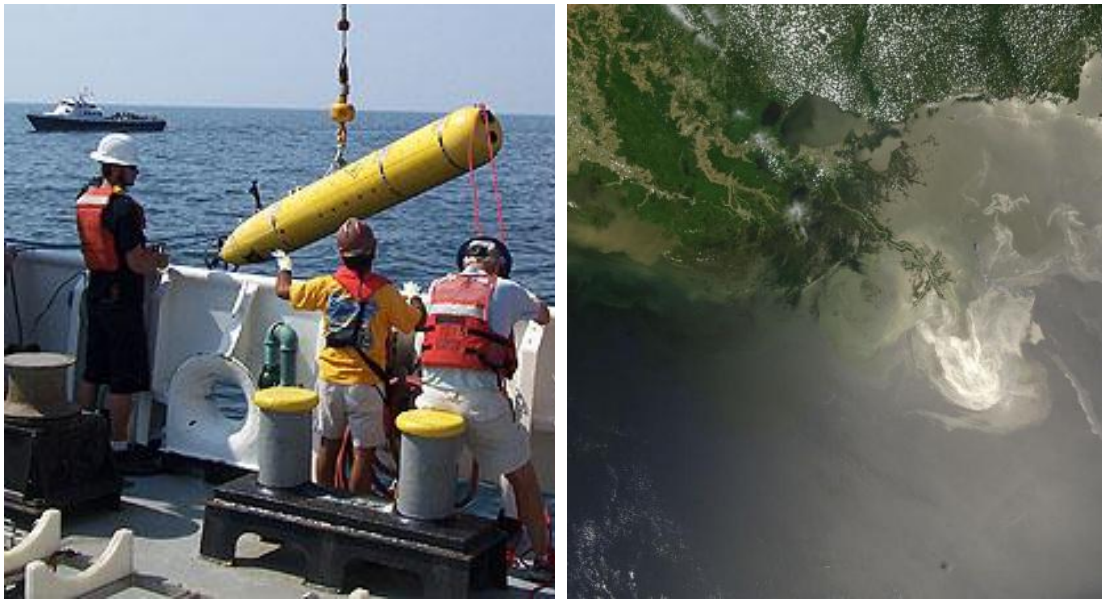

Figure 1.3 Water Sampling AUV and NASA's Satellite View [9,10]

These worldwide events showed clearly that these systems can play vital roles in different kinds of missions individually or collectively and have strategic importance both in civil applications and in the military operations. Therefore, it can be stated that the force for developing and improving UVMSs is driven not only to meet the needs of Turkey which is surrounded by waters on three sides but also help solving global problems.

1.2 Literature Survey

Underwater task execution is as expected more difficult relatively due to the surrounding media. This media involves the disturbing effects of underwater currents and may change rapidly. This necessitates the inclusion of all significant effects that oceanic environment creates into the system modeling and controller design. The working environment created by these effects on the other hand attract the researchers developing more realistic system models and create a desire for continuous improvement on the control methods for all kinds of unmanned underwater systems.

1.2.1 Literature Survey on Modeling and Control of UUVs

There are several researchers who dealt with deriving dynamic models for ROVs and AUVs in the literature. A detailed description and dynamic analysis of ROVs can be found in [11-16].

Goheen and Jefferys [11] developed ROV models using data gathered during simple free-running trials, processed by system identification and parameter estimation algorithms. Fossen *et al.* [12] presented nonlinear modeling of marine vehicles in 6-DOF by deriving equations of motion in vectorial form using both Newton-Euler and Lagrange equations.

Yuh and Choi [13] designed an omni-directional ROV with four vertical thrusters. Jun et al. [14] designed a small AUV called ISiMI and performed some maneuvering tests to compare the results by experiments.

Figure 1.4 AUV ISiMI [14]

Marani *et al.* [15] designed a semi autonomous underwater vehicle called SAUVIM for underwater intervention missions. A more detailed survey on AUV's designed worldwide especially during the 90's can be obtained in [16].

Figure 1.5 AUV SAUVIM [15]

Several control methods have been proposed by various authors [17-27]; namely adaptive control, sliding mode control, learning control based on neural networks and fuzzy control.

Yoerger and Slotine [17] proposed sliding mode controller for robust trajectory control of an AUV and showed by simulation the performance degradation depending on the model uncertainty. Healey and Lienard [18] used sliding mode approach to robustly control the underwater vehicles.

Goheen and Jefferys [19] investigated multi input-multi output self-tuning controller as an autopilot with two different schemes. Nakamura and Savant [20] developed a nonlinear tracking control algorithm considering only kinematic motion of an AUV.

Yuh *et al.* [21, 22] presented adaptive control methods using a non-regressor based algorithm. Hybrid adaptive controller of an AUV was developed by Tabaii *et al.* [23]. Hoang and Kreuzer [24] proposed adaptive PD-controller for an ROV and demonstrated effectiveness by means of numerical simulations and experiments.

Wang *et al*. [25] proposed an online self organizing neuro-fuzzy controller for AUVs. Craven *et al*. [26] proposed a fuzzy controller to produce autopilots for simultaneous control of multiple degrees of freedom for an AUV. Ishii *et al.* [27] studied a neural network based controller and tested experimentally against disturbances.

1.2.2 Literature Survey on Modeling and Control of UVMSs

The dynamic modeling and control of UVMSs are much more complicated than those of UUVs because of the coupled motion of the AUV and the manipulator. The interaction of these subsystems with the fluid environment complicates the problem further. The studies on the UVMSs in the literature are given in [28-47].

Tarn et al. [28] developed a dynamic model for an underwater vehicle with an n-axis robot arm based on Kane's method and incorporated major external environmental forces into the model; namely added mass, drag, fluid acceleration, and buoyancy.

McMillan *et al.* [29] developed a dynamic simulation algorithm based on the articulated body dynamics for a UVMS using Newton-Euler formulation including the added mass, drag and fluid acceleration effects.

Mahesh *et al.* [30] derived the equations of motion for UVMS using NBOD2 method and proposed an adaptive control strategy for the coordinated control of an underwater vehicle having planar motion and its 3-DOF robotic manipulator in the presence of parameter uncertainties and the water current while ignoring the effects of thruster dynamics.

Diaz et al. [31] and De Wit *et al.* [32] proposed a nonlinear robust control method for a 3-DOF vehicle with a 3-DOF manipulator system in planar motion taking into account the thruster dynamics to control the position and attitude of the vehicle expressed in the inertial frame and the joint positions of the manipulator.

Ishitsuka *et al*. [33] proposed resolved acceleration control of an UVMS consisting of a previously designed AUV called Twin Burger and a 2-link planar manipulator by taking into account external wave disturbance.

McLain *et al*. [34] showed by experiments that the dynamic interaction between the robot arm and the vehicle can be significant.

Antonelli *et al*. [35] designed an adaptive controller based on a sliding mode and a virtual decomposition approaches for UVMSs using a reduced system regressor in the control law by taking into account thruster effects and ocean currents.

Chung *et al.* [36] proposed a disturbance observer based independent joint controller for a four-link model of a planar underactuated UVMS which is robust to model uncertainty and external disturbances.

Sarkar and Podder [37,38] proposed motion coordination algorithm for a UVMS consisting of an AUV and a 3-DOF planar manipulator working in the vertical plane that generates the desired trajectories for both of the vehicle and the manipulator in such a way that the total hydrodynamic drag on the system is minimized. The dynamic model was derived using Lagrange approach including thruster effects.

Several researchers [39-43] dealt with developing control methods using fuzzy techniques for redundancy resolution of UVMSs.

Antonelli and Chiaverini [39,40] proposed fuzzy controllers for 9-DOF and 12-DOF UVMSs using a task priority inverse kinematics approach for redundancy resolution to manage the vehicle/arm coordination. Dos Santos *et al.* [41] proposed a fuzzy controller for 6-DOF UVMS considering singularity avoidance.

Soylu *et al.* [42] proposed a fault-tolerant fuzzy-based redundancy resolution method to distribute the human pilot end-effector command over the ROV and the manipulator while satisfying a hierarchy of secondary objectives.

Suboh *et al.* [43] investigated the performance of the fuzzy model reference adaptive control applied on 2-DOF underwater planar manipulator while ignoring the coupled effects between manipulator and vehicle.

Han *et al.* [44] recently proposed a robust optimal control algorithm with a disturbance observer that minimizes the restoring moments during manipulation of the 11-DOF UVMS. The values for the hydrodynamic coefficients are approximated and thruster effects and random external disturbances together with the ocean currents are also studied.

Cui and Yuh [45] developed a unified force controller which combines adaptive impedance control with hybrid position and force control by means of fuzzy switching for a UVMS consisting of an AUV and a 3-DOF manipulator

Lapierre *et al.* [46] reported a control method applied to a spherical underwater vehicle equipped with a two-link robot manipulator which is based on force control to stabilize the platform when the manipulator works in free or constrained space.

Antonelli *et al.* [47] developed force control method for 9-DOF UVMS by taking into account possible occurrence of loss of contact due to vehicle movement during the task.

Yatoh and Sagara [48] proposed continuous and discrete time resolved acceleration control methods for a UVMS having a 2 link manipulator and showed the effectiveness by experiments.

1.3 Motivation and Contribution

The research presented in this thesis focuses on the modeling and control of fully autonomous underwater vehicle manipulator systems. In the modeling stage, it is intended to derive a dynamic model which is as realistic as possible. To this end, the hydrodynamic forces of the manipulator links which have significant fineness ratio

are also considered in addition to those of the vehicle. Besides, the shadowing effects are included in the computation of these forces.

On the other hand, although there are quite number of studies related to controlling UVMSs, most are related with systems having planar manipulators. To the best of our knowledge, no research has been reported in the literature yet, addressing the modeling and control of UVMSs having a *spatial* and/or *redundant* manipulator using inverse dynamics control approach.

In the view of the examples and studies given in the previous sections, main goals of this research are listed as follows:

1. Deriving a more realistic dynamic model for rigid multibody systems working in underwater environment
    a. Deriving equations of motion of a manipulator with a moving base.
    b. Modeling rigid multibody systems subjected to both hydrostatic and hydrodynamic effects *in three dimensions* considering
        i. lift, drag and side forces/moments as well as added mass force and added inertia moments,
        ii. the shadowing effects of the bodies acting on each other during manipulation,
        iii. the effects due to the external disturbances such as ocean currents,
        iv. the effects due to thrusters.

2. Developing inverse dynamics control algorithms for 12-DOF UVMSs including thrusters consisting of
    a. fully actuated AUV and fully actuated, 6-DOF spatial manipulator (UVMS)
    b. underactuated AUV and fully actuated, 6-DOF spatial manipulator (u-UVMS)

3. Developing an inverse dynamics control algorithm for 14-DOF system including thrusters consisting of underactuated AUV and fully actuated, 8-DOF spatial redundant manipulator (u-UVRMS).

4. Testing developed controllers against external disturbance and parametric uncertainty in hydrodynamic coefficients of both subsystems and thruster constants by computer simulations.

5. Comparing the results of these three systems (i.e. UVMS, u-UVMS and u-UVRMS) in terms of tracking errors and discussing the main advantages and disadvantages in between.

1.4 Outline

The remaining part of the thesis is comprised of the following chapters:

Chapter II presents the basic kinematic equations of UVMSs. First, kinematic relations of AUV subsystem are derived in body-fixed frame. Then, coordinate transformations are introduced to state these equations expressed in inertial frame at velocity and acceleration levels. Next, recursive kinematic relations of multibody systems with a moving base are derived. Finally, the kinematic equations for both regular and redundant manipulators with a moving base are given.

Chapter III covers the derivation of the dynamic models of the UVMSs. First, the dynamic equations of motion of the AUV and the manipulator subsystems are derived one by one to obtain the final form of the equations of the whole system. Basic hydrodynamic forces and the effect of the ocean currents on the systems are explained. The thruster model is introduced and its incorporation to the dynamic equations is clarified.

Chapter IV presents the inverse dynamics control methods developed for tracking the desired trajectories of the UVMSs as well as the thrusters. The task equations are formulated and the expressions relating the task variables to the joint variables are explained. Trajectories for both of the AUV and the end-effector of the manipulator subsystem are defined for typical underwater missions like mine detection and geological sampling. The position error dynamics of the systems under consideration are formulated.

In Chapter V, the effectiveness of the control methods explained in Chapter IV is tested in MATLAB/Simulink environment and the results are presented for all three types of systems. Simulink models are developed in order to generate the system equations of motion by producing relevant matrices and vectors and to apply the control algorithm at each sampling time. Finally, the simulation results of the systems are compared with each other in terms of the closed loop responses and the errors. The main advantages and disadvantages are discussed in detail.

Chapter VI reviews and concludes the comparisons of the simulations and presents recommendations for future work.

CHAPTER II

UVMS KINEMATICS

In this chapter, the basic kinematic equations of UVMSs are presented. First, kinematic relations of AUV subsystem are derived in body-fixed frame. Then, coordinate transformations are introduced to state these equations expressed in inertial frame at velocity and acceleration levels. Next, recursive kinematic relations of multibody systems with a moving base are derived. Finally, the kinematic equations for both regular and redundant manipulators with a moving base are given.

2.1 Underwater Vehicle Kinematics

The motion of underwater vehicles in 6-DOF consists of 6 independent coordinates necessary to determine the position of the body with its commonly accepted notation defined in [49] as seen in Table 2.1.

Table 2.1 Vehicle Motions

DOF	Description	Generalized Forces	Velocity (Body-Fixed RF)	Position (Inertial RF)
1	translational motion along the x-axis (surge)	X	u	x_v
2	translational motion along the y-axis (sway)	Y	v	y_v
3	translational motion along the z-axis (heave)	Z	w	z_v
4	angular motion about the x-axis (roll)	K	p	ϕ_1
5	angular motion about the y-axis (pitch)	M	q	ϕ_2
6	angular motion about the z-axis (yaw)	N	r	ϕ_3

The first three coordinates correspond to the translational motion along the x, y and z axes while the remaining three coordinates are used to describe rotational motion about these axes. These motions are illustrated in Figure 2.1.

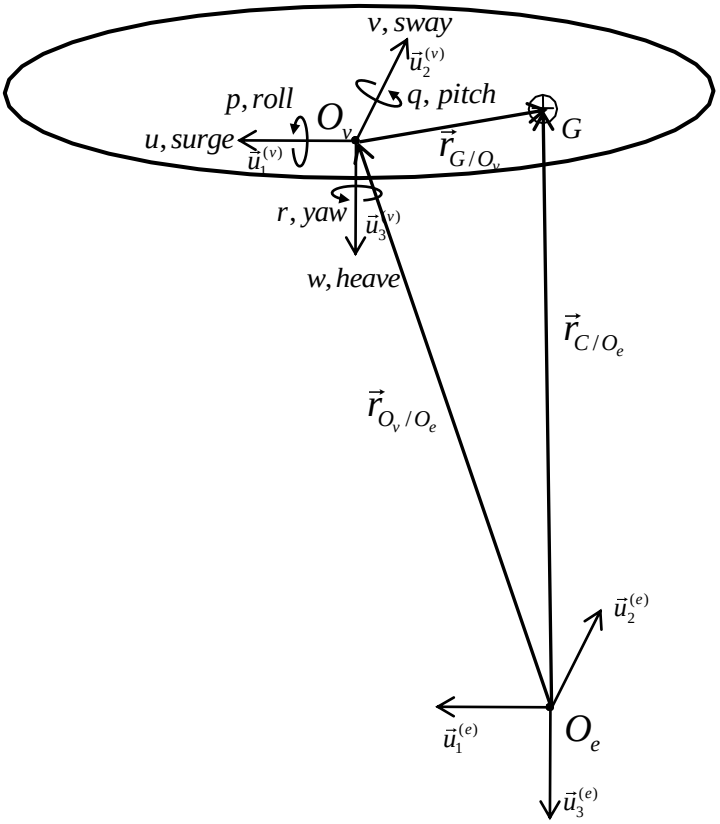

Figure 2.1 Vehicle Reference Frames

In Figure 2.1, the superscript "*e*" is used to denote vectors defined or expressed in inertial reference frame with origin O_e. Earth is taken to be the inertial reference frame assuming that its motion does not affect the motion of the system. Similarly, the superscript "*v*" is used to denote vectors defined or expressed in vehicle's body fixed reference frame with origin O_v.

The motions of AUV can be described by the following vectors,

$$\bar{\zeta} = \left[\bar{\zeta}_L^T \quad \vdots \quad \bar{\zeta}_A^T \right]^T = \left[x_v \quad y_v \quad z_v \quad \vdots \quad \phi_1 \quad \phi_2 \quad \phi_3 \right]^T \tag{2.1}$$

$$\bar{\eta} = \left[\bar{\eta}_L^T \quad \vdots \quad \bar{\eta}_A^T \right]^T = \left[u \quad v \quad w \quad \vdots \quad p \quad q \quad r \right]^T \tag{2.2}$$

where $\bar{\zeta}$ is the generalized coordinates vector consisting of the linear displacements and angular displacements (i.e. Euler angles) of the vehicle as expressed in inertial reference frame, $\bar{\eta}$ shows linear and angular velocity components of the vehicle with respect to Earth-fixed reference frame as expressed in its own frame. That is,

$$\bar{\eta} = \begin{bmatrix} \bar{v}_{O_v/O_e}^{(v)} \\ \bar{\omega}_{v/e}^{(v)} \end{bmatrix} \tag{2.3}$$

The angular acceleration of the AUV can be obtained by differentiating $\bar{\omega}_{v/e}^{(v)}$ with respect to $\Im_e$ as

$$\bar{\alpha}_{v/e}^{(v)} = D_e \bar{\omega}_{v/e}^{(v)} = D_v \bar{\omega}_{v/e}^{(v)} + \tilde{\omega}_{v/e}^{(v)} \bar{\omega}_{v/e}^{(v)} = D_v \bar{\omega}_{v/e}^{(v)} = \dot{\bar{\omega}}_{v/e}^{(v)} \tag{2.4}$$

Hence,

$$\bar{\alpha}_{v/e}^{(v)} = \begin{bmatrix} \dot{p} \\ \dot{q} \\ \dot{r} \end{bmatrix} = \dot{\bar{\eta}}_A \tag{2.5}$$

The position of the mass center of the vehicle with respect to the origin of $\Im_e$ can be written in vectorial form as

$$\vec{r}_{C/O_e} = \vec{r}_{G/O_v} + \vec{r}_{O_v/O_e} \tag{2.6}$$

Differentiating Equation (2.6) with respect to $\Im_e$ gives the velocity relation as

$$D_e \vec{r}_C = D_e \vec{r}_G + D_e \vec{r}_{O_v/O_e} \tag{2.7}$$

$$D_e\vec{r}_C = D_v\vec{r}_G + \vec{\omega}_{v/e}\times\vec{r}_G + D_e\vec{r}_{O_v/O_e} \tag{2.8}$$

which can be expressed in $\Im_v$ as

$$\left\{D_e\vec{r}_C\right\}^v = \left\{D_v\vec{r}_G\right\}^v + \left\{\vec{\omega}_{v/e}\times\vec{r}_G\right\}^v + \left\{D_e\vec{r}_{O_v/O_e}\right\}^v \tag{2.9}$$

Noting that components x_G, y_G, z_G of the position vector of the mass center of the AUV are constant in $\Im_v$, therefore

$$\left\{D_v\vec{r}_G\right\}^v = 0 \tag{2.10}$$

Equation (2.9) can be written in matrix form as

$$\bar{v}_C^{(v)} = \tilde{\omega}_{v/e}^{(v)}\bar{r}_G^{(v)} + \bar{\eta}_L = \begin{bmatrix} 0 & -r & q \\ r & 0 & -p \\ -q & p & 0 \end{bmatrix}\begin{bmatrix} x_G \\ y_G \\ z_G \end{bmatrix} + \begin{bmatrix} u \\ v \\ w \end{bmatrix} = \begin{bmatrix} u - ry_G + qz_G \\ v + rx_G - pz_G \\ w - qx_G + py_G \end{bmatrix} \tag{2.11}$$

reminding that

$$\left\{D_e\vec{r}_{O_v/O_e}\right\}^v = \bar{\eta}_L . \tag{2.12}$$

Remark:

The skew-symmetric matrix operator (~) converts a vector $\bar{x}=\begin{bmatrix} a & b & c \end{bmatrix}^T$ *to a matrix as* $\tilde{x} = \begin{bmatrix} 0 & -c & b \\ c & 0 & -a \\ -b & a & 0 \end{bmatrix}$.

The acceleration vector of the origin of $\Im_v$ can be obtained by taking derivative of the velocity vector $\bar{v}_{O_v/O_e}^{(v)}$ with respect to $\Im_e$ as

$$\bar{a}_{O_v/O_e}^{(v)} = D_e\bar{v}_{O_v/O_e}^{(v)} \tag{2.13}$$

Proceeding further gives

$$D_e\bar{v}_{O_v/O_e}^{(v)} = D_v\bar{v}_{O_v/O_e}^{(v)} + \bar{\omega}_{v/e}\times\bar{v}_{O_v/O_e}^{(v)} \tag{2.14}$$

$$\bar{a}_{O_v/O_e}^{(v)} = \dot{\bar{\eta}}_L + \tilde{\omega}_{v/e}^{(v)}\bar{\eta}_L = \begin{bmatrix} \dot{u} - rv + qw \\ \dot{v} + ru - pw \\ \dot{w} - qu + pv \end{bmatrix} \tag{2.15}$$

In order to find the acceleration of the mass center, Equation (2.11) is further differentiated as below

$$D_e\vec{v}_C = D_v\vec{v}_C + \vec{\omega}_{v/e}\times\vec{v}_C \tag{2.16}$$

which can also be expressed in $\Im_v$ as

$$\{D_e\vec{v}_C\}^{(v)} = \{D_v\vec{v}_C\}^{(v)} + \{\vec{\omega}_{v/e}\times\vec{v}_C\}^{(v)} \tag{2.17}$$

This relation can also be written in matrix form as in the following

$$\bar{a}_C^{(v)} = \dot{\bar{v}}_C^{(v)} + \tilde{\omega}_{v/e}^{(v)}\bar{v}_C^{(v)} = \begin{bmatrix} \dot{u} - rv + qw - x_G(r^2+q^2) + y_G(pq-\dot{r}) + z_G(pr+\dot{q}) \\ \dot{v} + ur - pw + x_G(pq+\dot{r}) - y_G(p^2+r^2) + z_G(qr-\dot{p}) \\ \dot{w} - qu + pv + x_G(pr-\dot{q}) + y_G(qr+\dot{p}) - z_G(p^2+q^2) \end{bmatrix} \tag{2.18}$$

2.1.1 Coordinate Transformations

In order to express position, velocity and acceleration relations of the AUV in terms of Earth fixed coordinates, one needs to transform the kinematic equations from $\Im_v$ to $\Im_e$.

2.1.1.1 Velocity Level Transformation

The vehicle's path relative to the inertial reference frame can be described using Rotated Frame Based 321 (yaw, pitch, roll) Euler angle sequence.

This sequence is more commonly used in vehicle dynamics as shown below.

$$\Im_e \xrightarrow[\vec{u}_3^{(e)}=\vec{u}_3^{(m)}]{\phi_3} \Im_m \xrightarrow[\vec{u}_2^{(m)}=\vec{u}_2^{(n)}]{\phi_2} \Im_n \xrightarrow[\vec{u}_1^{(n)}=\vec{u}_1^{(v)}]{\phi_1} \Im_v$$

where $\Im_e$, $\Im_v$ stand for the Earth-fixed frame & AUV body-fixed frame respectively and $\Im_m$ & $\Im_n$ are the intermediate frames.

In order to find coordinate transformation matrix of the vehicle, elementary rotation matrices are used to transform the coordinates expressed in $\Im_v$ to those expressed in $\Im_e$ as in the following equation.

$$\hat{C}^{(e,v)} = \hat{C}^{(e,m)}\hat{C}^{(m,n)}\hat{C}^{(n,v)} \tag{2.19}$$

where

$$\hat{C}^{(e,m)} = e^{\tilde{u}_3\phi_3} = \begin{bmatrix} c\phi_3 & -s\phi_3 & 0 \\ s\phi_3 & c\phi_3 & 0 \\ 0 & 0 & 1 \end{bmatrix} \tag{2.20}$$

$$\hat{C}^{(m,n)} = e^{\tilde{u}_2\phi_2} = \begin{bmatrix} c\phi_2 & 0 & s\phi_2 \\ 0 & 1 & 0 \\ -s\phi_2 & 0 & c\phi_2 \end{bmatrix} \tag{2.21}$$

$$\hat{C}^{(n,v)} = e^{\tilde{u}_1\phi_1} = \begin{bmatrix} 1 & 0 & 0 \\ 0 & c\phi_1 & -s\phi_1 \\ 0 & s\phi_1 & c\phi_1 \end{bmatrix} \tag{2.22}$$

In expanded form,

$$\hat{C}^{(e,v)} = \begin{bmatrix} c\phi_3 c\phi_2 & c\phi_3 s\phi_2 s\phi_1 - s\phi_3 c\phi_1 & c\phi_3 s\phi_2 c\phi_1 + s\phi_3 s\phi_1 \\ s\phi_3 c\phi_2 & s\phi_3 s\phi_2 s\phi_1 + c\phi_3 c\phi_1 & s\phi_3 s\phi_2 c\phi_1 - c\phi_3 s\phi_1 \\ -s\phi_2 & c\phi_2 s\phi_1 & c\phi_2 c\phi_1 \end{bmatrix} \tag{2.23}$$

where $s\phi_i = \sin\phi_i$ & $c\phi_i = \cos\phi_i$ $i=1,2,3.$ and ϕ_i $i=1,2,3.$ are the Euler angles of the yaw, pitch, roll sequence of the AUV.

Linear velocities expressed in $\Im_v$ are transformed to those expressed in $\Im_e$ using the following relationship.

$$\begin{bmatrix} \dot{x}_v \\ \dot{y}_v \\ \dot{z}_v \end{bmatrix} = \hat{C}^{(e,v)} \begin{bmatrix} u \\ v \\ w \end{bmatrix} \tag{2.24}$$

Equation (2.24) can be written in compact form as

$$\dot{\bar{\zeta}}_L = \hat{C}^{(e,v)} \bar{\eta}_L \tag{2.25}$$

Remark:
The transformation matrix $\hat{C}$ is orthonormal which satisfies

$$\hat{C}^{(a,b)} = \left[\hat{C}^{(b,a)}\right]^{-1} = \left[\hat{C}^{(b,a)}\right]^{T} \tag{2.26}$$

The angular velocity of the AUV can also be expressed in terms of the Euler angles as

$$\bar{\omega}_{v/e} = \dot{\phi}_3 \bar{u}_3^{(e)} + \dot{\phi}_2 \bar{u}_2^{(m)} + \dot{\phi}_1 \bar{u}_1^{(n)} \tag{2.27}$$

Combining Equation (2.27) with the definition $\bar{\eta}_A$ leads to

$$\begin{bmatrix} p \\ q \\ r \end{bmatrix} = \hat{C}^{(v,e)} \dot{\phi}_3 \bar{u}_3 + \hat{C}^{(v,n)} \hat{C}^{(n,m)} \dot{\phi}_2 \bar{u}_2 + \hat{C}^{(v,n)} \dot{\phi}_1 \bar{u}_1 \tag{2.28}$$

and to the following compact form

$$\dot{\bar{\zeta}}_A = \hat{E}_v^{-1} \bar{\eta}_A \tag{2.29}$$

where $\hat{E}_v(\phi) \in \Re^{3x3}$ is obtained as

$$\hat{E}_v = \begin{bmatrix} 1 & 0 & -s\phi_2 \\ 0 & c\phi_1 & s\phi_1 c\phi_2 \\ 0 & -s\phi_1 & c\phi_1 c\phi_2 \end{bmatrix} \tag{2.30}$$

and $\dot{\bar{\zeta}}_A(\dot{\phi}) \in \Re^{3x1}$ consists of the Euler rates as below

$$\dot{\bar{\zeta}}_A = \begin{bmatrix} \dot{\phi}_1 \\ \dot{\phi}_2 \\ \dot{\phi}_3 \end{bmatrix} \tag{2.31}$$

In Equation (2.29), $\hat{E}_v$ is called the rotation matrix of AUV. It should be noted that $\det(\hat{E}_v) = 0$ when $c\phi_2 = 0$. That means singularity takes place when the intermediate angle $\phi_2 = \pm\pi/2$. Such a singularity will not matter since vehicle does not experience any kind of motion directing its nose up or down.

Finally, taking both of the linear and angular coordinate transformations into account and combining Equation (2.25) and Equation (2.29) in augmented form yields

$$\dot{\bar{\zeta}} = \hat{J}_v \bar{\eta} \tag{2.32}$$

where $\dot{\bar{\zeta}} \in \Re^{6x1}$

$$\dot{\bar{\zeta}} = \begin{bmatrix} \dot{\bar{\zeta}}_L \\ \dot{\bar{\zeta}}_A \end{bmatrix} \tag{2.33}$$

and $\hat{J}_v \in \Re^{6x6}$ is the Jacobian matrix of the AUV can be written as

$$\hat{J}_v = \begin{bmatrix} \hat{C}^{(e,v)} & 0_{3x3} \\ 0_{3x3} & \hat{E}_v^{-1} \end{bmatrix} \tag{2.34}$$

2.1.1.2 Acceleration Level Transformation

Let the acceleration expression given in Equation (2.15) be factored as

$$\bar{a}_{O_v/O_e}^{(v)} = \dot{\bar{\eta}}_L + \bar{J}_{L_{b,v}} \tag{2.35}$$

where $\bar{J}_{L_{b,v}} \in \Re^{3x1}$ is a function of $\bar{\eta}$ and is obtained as

$$\bar{J}_{L_{b,v}} = \begin{bmatrix} -rv + qw \\ ru - pw \\ -qu + pv \end{bmatrix} \tag{2.36}$$

Combining the Equation (2.5) and the Equation (2.35) yields

$$\begin{bmatrix} \bar{a}_{O_v/O_e}^{(v)} \\ \bar{\alpha}_{v/e}^{(v)} \end{bmatrix} = \dot{\bar{\eta}} + \bar{J}_{b,v} \tag{2.37}$$

where $\bar{J}_{b,v}(\bar{\eta}) \in \Re^{6x1}$

$$\bar{J}_{b,v} = \begin{bmatrix} \bar{J}_{L_{b,v}} \\ \bar{0} \end{bmatrix} \tag{2.38}$$

The acceleration expressions expressed in $\Im_v$ is transformed to the one expressed in $\Im_e$ using the following relationships

$$\ddot{\bar{\zeta}}_L = \hat{C}^{(e,v)} \bar{a}_{O_v/O_e}^{(v)} \tag{2.39}$$

where

$$\ddot{\bar{\zeta}}_L = \begin{bmatrix} \ddot{x}_v \\ \ddot{y}_v \\ \ddot{z}_v \end{bmatrix} \tag{2.40}$$

On the other hand, the angular acceleration expressions can be obtained by differentiating Equation (2.28) and written in expanded form as

$$\dot{p} = \ddot{\phi}_1 - \ddot{\phi}_3 s\phi_2 - \dot{\phi}_3 \dot{\phi}_2 c\phi_2 \tag{2.41}$$

$$\dot{q} = \ddot{\phi}_2 c\phi_1 + \left[\ddot{\phi}_3 s\phi_1 + \dot{\phi}_3\dot{\phi}_1 c\phi_1\right] c\phi_2 - \dot{\phi}_2\left[\dot{\phi}_1 + \dot{\phi}_3 s\phi_2\right] s\phi_1 \tag{2.42}$$

$$\dot{r} = -\ddot{\phi}_2 s\phi_1 + \left[\ddot{\phi}_3 c\phi_1 - \dot{\phi}_3\dot{\phi}_1 s\phi_1\right] c\phi_2 - \dot{\phi}_2\left[\dot{\phi}_1 + \dot{\phi}_3 s\phi_2\right] c\phi_1 \tag{2.43}$$

Equations (2.41) – (2.43) can be written in compact form as

$$\bar{\alpha}_{v/e}^{(v)} = \hat{E}_v \ddot{\bar{\zeta}}_A + \hat{E}_1 \tag{2.44}$$

where $\hat{E}_1\left(\phi, \dot{\phi}\right) \in \Re^{3x1}$ is obtained as

$$\hat{E}_1 = \begin{bmatrix} -\dot{\phi}_3\dot{\phi}_2 c\phi_2 \\ \dot{\phi}_3\dot{\phi}_1 c\phi_1 c\phi_2 - \dot{\phi}_2\left(\dot{\phi}_1 + \dot{\phi}_3 s\phi_2\right) s\phi_1 \\ -\dot{\phi}_3\dot{\phi}_1 s\phi_1 c\phi_2 - \dot{\phi}_2\left(\dot{\phi}_1 + \dot{\phi}_3 s\phi_2\right) c\phi_1 \end{bmatrix} \tag{2.45}$$

and

$$\ddot{\bar{\zeta}}_A = \begin{bmatrix} \ddot{\phi}_1 \\ \ddot{\phi}_2 \\ \ddot{\phi}_3 \end{bmatrix} \tag{2.46}$$

As the next step, combining Equations (2.39) and (2.44) gives

$$\ddot{\bar{\zeta}} = \hat{J}_v \begin{bmatrix} \bar{a}_{O_v/O_e}^{(v)} \\ \bar{\alpha}_{v/e}^{(v)} \end{bmatrix} + \bar{T}_{b,v} \tag{2.47}$$

where $\ddot{\bar{\zeta}} \in \Re^{6x1}$

$$\ddot{\bar{\zeta}} = \begin{bmatrix} \ddot{\bar{\zeta}}_L \\ \ddot{\bar{\zeta}}_A \end{bmatrix} \tag{2.48}$$

and $\bar{T}_{b,v}\left(\phi, \dot{\phi}\right) \in \Re^{6x1}$

$$\bar{T}_{b,v} = \begin{bmatrix} \bar{0} \\ -\hat{E}_v^{-1}\hat{E}_1 \end{bmatrix} \tag{2.49}$$

Consequently, the following acceleration relationship is obtained utilizing Equation (2.37) and Equation (2.47) as

$$\ddot{\bar{\zeta}} = \hat{J}_v \dot{\bar{\eta}} + \bar{a}_{b_v} \tag{2.50}$$

where $\bar{a}_{bv}$ is a bias vector which is a function of $\bar{\eta}$, $\bar{\phi}$ and $\dot{\bar{\phi}}$.

$$\bar{a}_{b_v} = \hat{J}_v \bar{J}_{b,v} + \bar{T}_{b,v} \tag{2.51}$$

2.2 Manipulator Kinematics with Moving Base

2.2.1 Sign Convention

Denavit-Hartenberg (DH) sign convention is commonly used in robotic applications especially for manipulators having single axis joints (i.e. revolute, prismatic etc.) due to its advantage in kinematic and dynamic analysis [50]. In this study, DH convention is used for the same reasoning and can be illustrated in Figure 2.2 for the sake of completeness.

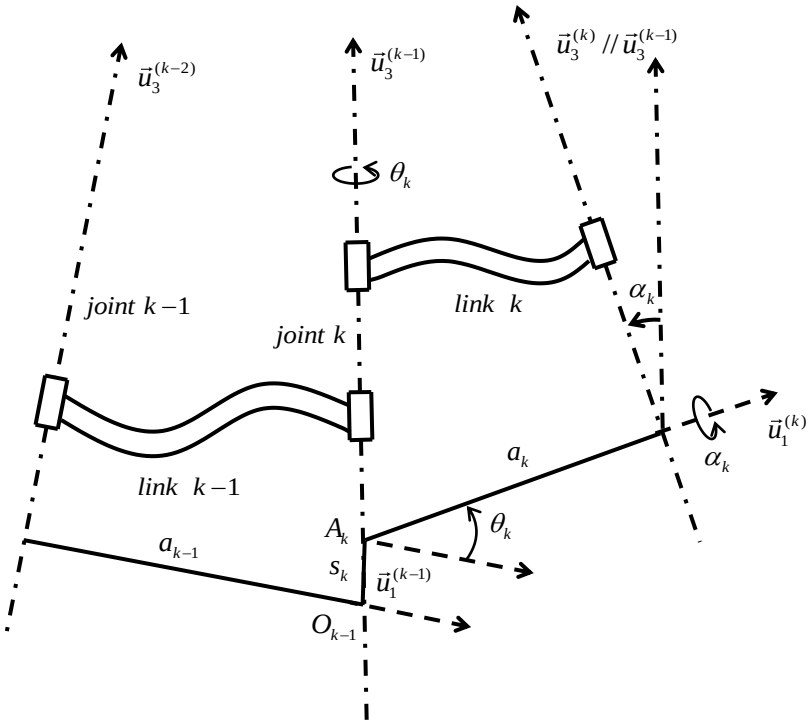

Figure 2.2 DH Sign Convention [50]

DH sign convention has two kinds of parameters namely: *link parameters* and *joint parameters* defined as follows.

Effective length of link-k

$a_k = A_k O_k$ along $\vec{u}_1^{(k)}$

Offset of link-k with respect to link k-1 along the joint axis

$s_k = O_{k-1} A_k$ along $\vec{u}_3^{(k-1)}$

Twist angle of link-k

$\alpha_k = angle\left\{\vec{u}_3^{(k-1)} \longrightarrow \vec{u}_3^{(k)} \text{ about } \vec{u}_1^{(k)}\right\}$

Rotation angle of link k with respect to link k-1 about joint axis

$\theta_k = angle\left\{\vec{u}_1^{(k-1)} \longrightarrow \vec{u}_1^{(k)} \text{ about } \vec{u}_3^{(k-1)}\right\}$

2.2.2 Link Orientation Expressions

Orientation matrix that transforms the coordinates of k^{th} reference frame $\Im_k$ to the frame of interest $\Im_0$ is defined as

$$\hat{C}^{(0,k)} = \hat{C}^{(0,1)}\hat{C}^{(0,2)}...\hat{C}^{(k-2,k-1)}\hat{C}^{(k-1,k)} \tag{2.52}$$

where

$$\boxed{\hat{C}^{(k-1,k)} = e^{\tilde{u}_3\theta_k} e^{\tilde{u}_1\alpha_k}} \tag{2.53}$$

2.2.3 Angular Velocity Expressions

Let the angular velocity of the k^{th} link with respect to $\Im_e$ as expressed in the frame of interest $\Im_0$ be denoted as $\bar{\omega}_k = \bar{\omega}_{k/e}^{(0)}$.

The angular velocity expression takes the matrix form as

$$\boxed{\bar{\omega}_k = \bar{\omega}_{k-1} + \dot{\theta}_k \hat{C}^{(0,k-1)} \bar{u}_3} \quad \boxed{k = 1, 2, ..., n.} \tag{2.54}$$

where

$$\bar{\omega}_{k-1} = \bar{\omega}_{k-1/e}^{(0)} \tag{2.55}$$

$$\bar{\omega}_0 = \bar{\omega}_{0/e}^{(0)} = \hat{T}^{(0,e)} \bar{\omega}_{0/e}^{(e)} \tag{2.56}$$

noting that n denotes the number of links of the manipulator and $\hat{T}^{(0,e)}$ is rotation matrix which can be a function of the Euler angles.

2.2.4 Angular Acceleration Expressions

Let the angular acceleration of the k^{th} link with respect to $\Im_e$ as expressed in the frame of interest $\Im_0$ be denoted as $\bar{\alpha}_k = \bar{\alpha}_{k/e}^{(0)}$. It can be derived by differentiating Equation (2.54) with respect to $\Im_e$ as

$$\bar{\alpha}_k = D_e \left[\bar{\omega}_{k-1} + \dot{\theta}_k \hat{C}^{(0,k-1)} \bar{u}_3 \right] \tag{2.57}$$

$$\bar{\alpha}_k = D_0 \left[\bar{\omega}_{k-1} + \dot{\theta}_k \hat{C}^{(0,k-1)} \bar{u}_3 \right] + \tilde{\omega}_{0/e} \left[\bar{\omega}_{k-1} + \dot{\theta}_k \hat{C}^{(0,k-1)} \bar{u}_3 \right] \tag{2.58}$$

$$\bar{\alpha}_k = \bar{\alpha}_{k-1} + \ddot{\theta}_k \hat{C}^{(0,k-1)} \bar{u}_3 + \dot{\theta}_k \tilde{\omega}_{k-1/0} \hat{C}^{(0,k-1)} \bar{u}_3 + \tilde{\omega}_{0/e} \bar{\omega}_{k-1} + \tilde{\omega}_{0/e} \dot{\theta}_k \hat{C}^{(0,k-1)} \bar{u}_3 \tag{2.59}$$

$$\bar{\alpha}_k = \bar{\alpha}_{k-1} + \ddot{\theta}_k \hat{C}^{(0,k-1)} \bar{u}_3 + \dot{\theta}_k \left[\tilde{\omega}_{k-1/0} + \tilde{\omega}_{0/e} \right] \hat{C}^{(0,k-1)} \bar{u}_3 + \tilde{\omega}_{0/e} \bar{\omega}_{k-1/e} \tag{2.60}$$

$$\boxed{\bar{\alpha}_k = \bar{\alpha}_{k-1} + \ddot{\theta}_k \hat{C}^{(0,k-1)} \bar{u}_3 + \dot{\theta}_k \tilde{\omega}_{k-1} \hat{C}^{(0,k-1)} \bar{u}_3 + \tilde{\omega}_0 \bar{\omega}_{k-1}} \quad \boxed{k = 1, 2, ..., n.} \tag{2.61}$$

where

$$\bar{\alpha}_0 = \bar{\alpha}_{0/e}^{(0)} \neq 0 \tag{2.62}$$

2.2.5 Link Origin and Mass Center Location Expressions

The distance $\bar{p}_{O_k} = \overrightarrow{O_k O_e}$ between the origin of body-fixed frame $\Im_k$ of the k^{th} link with respect to the origin of $\Im_e$ can be written in the frame of interest $\Im_0$ as

$$\boxed{\bar{p}_{O_k} = \bar{p}_{O_{k-1}} + \hat{C}^{(0,k)}\bar{r}_{O_k}} \quad \boxed{k = 1, 2, ..., n.} \tag{2.63}$$

where $\bar{r}_{O_k} = \bar{r}^{(k)}_{O_k/O_{k-1}}$ is the position vector of the origin of $\Im_k$ of the k^{th} link with respect to that of the *k-1*th link expressed in $\Im_k$.

The distance $\bar{p}_{G_k} = \overrightarrow{O_{G_k} O_e}$ between the mass center of the k^{th} link and the origin of the $\Im_e$ can be written in the frame of interest $\Im_0$ as

$$\boxed{\bar{p}_{G_k} = \bar{p}_{O_{k-1}} + \hat{C}^{(0,k)}\bar{r}_{G_k}} \quad \boxed{k = 1, 2, ..., n.} \tag{2.64}$$

where $\bar{r}_{G_k} = \bar{r}^{(k)}_{G_k/O_{k-1}}$ is the position vector of the mass center of the k^{th} link with respect to the origin of body fixed frame of the *k-1*th link expressed in $\Im_k$.

2.2.6 Velocity Expressions

Let the velocity of the origin of the body fixed frame of k^{th} link with respect to $\Im_e$ as expressed in the frame of interest $\Im_0$ be denoted as $\bar{v}_{O_k} = \bar{v}^{(0)}_{O_k/O_e}$. It can be derived by differentiating Equation (2.64) with respect to $\Im_e$ as

$$\bar{v}_{O_k} = D_e\left[\bar{p}_{O_{k-1}} + \hat{C}^{(0,k)}\bar{r}_{O_k}\right] \tag{2.65}$$

$$\bar{v}_{O_k} = D_0\left[\bar{p}_{O_{k-1}} + \hat{C}^{(0,k)}\bar{r}_{O_k}\right] + \tilde{\omega}_{0/e}\left[\bar{p}_{O_{k-1}} + \hat{C}^{(0,k)}\bar{r}_{O_k}\right] \tag{2.66}$$

$$\bar{v}_{O_k} = \bar{v}_{O_{k-1}} + \left[\tilde{\omega}_{k/0} + \tilde{\omega}_{0/e}\right]\hat{C}^{(0,k)}\bar{r}_{O_k} + \tilde{\omega}_{0/e}\bar{p}_{O_{k-1}} \tag{2.67}$$

$$\boxed{\bar{v}_{O_k} = \bar{v}_{O_{k-1}} + \tilde{\omega}_k \hat{C}^{(0,k)} \bar{r}_{O_k} + \tilde{\omega}_0 \bar{p}_{O_{k-1}}} \quad \boxed{k = 1, 2, ..., n.} \tag{2.68}$$

where

$$\bar{v}_{O_0} = \bar{v}^{(0)}_{O_0/O_e} \neq 0. \tag{2.69}$$

Similarly, the velocity of the mass center of k^{th} link with respect to $\Im_e$ as expressed in the frame of interest $\Im_0$ can be denoted as $\bar{v}_{G_k} = \bar{v}^{(0)}_{G_k/O_e}$ and derived as

$$\boxed{\bar{v}_{G_k} = \bar{v}_{O_{k-1}} + \tilde{\omega}_k \hat{C}^{(0,k)} \bar{r}_{G_k} + \tilde{\omega}_0 \bar{p}_{O_{k-1}}} \quad \boxed{k = 1, 2, ..., n.} \tag{2.70}$$

2.2.7 Acceleration Expressions

Let the acceleration of the origin of the body fixed frame of k^{th} link with respect to $\Im_e$ as expressed in the frame of interest $\Im_0$ be denoted as $\bar{a}_{O_k} = \bar{a}^{(0)}_{O_k/O_e}$. It can be derived by differentiating Equation (2.68) with respect to $\Im_e$ as

$$\bar{a}_{O_k} = D_e \left[\bar{v}_{O_{k-1}} + \tilde{\omega}_k \hat{C}^{(0,k)} \bar{r}_{O_k} + \tilde{\omega}_{0/e} \bar{p}_{O_{k-1}} \right] \tag{2.71}$$

$$\bar{a}_{O_k} = D_0 \left[\bar{v}_{O_{k-1}} + \tilde{\omega}_k \hat{C}^{(0,k)} \bar{r}_{O_k} + \tilde{\omega}_{0/e} \bar{p}_{O_{k-1}} \right] + \tilde{\omega}_{0/e} \left[\bar{v}_{O_{k-1}} + \tilde{\omega}_k \hat{C}^{(0,k)} \bar{r}_{O_k} + \tilde{\omega}_{0/e} \bar{p}_{O_{k-1}} \right] \tag{2.72}$$

$$\bar{a}_{O_k} = \bar{a}_{O_{k-1}} + \left[\tilde{\omega}_k \tilde{\omega}_{k/0} + \tilde{\omega}_{0/e} \tilde{\omega}_k + \tilde{\alpha}_k \right] \hat{C}^{(0,k)} \bar{r}_{O_k} + \left[\tilde{\alpha}_{0/e} + \tilde{\omega}^2_{0/e} \right] \bar{p}_{O_{k-1}} + 2\tilde{\omega}_{0/e} \bar{v}_{O_{k-1}} \tag{2.73}$$

$$\boxed{\bar{a}_{O_k} = \bar{a}_{O_{k-1}} + \left[\tilde{\alpha}_k + \tilde{\omega}^2_k \right] \hat{C}^{(0,k)} \bar{r}_{O_k} + \left[\tilde{\alpha}_0 + \tilde{\omega}^2_0 \right] \bar{p}_{O_{k-1}} + 2\tilde{\omega}_0 \bar{v}_{O_{k-1}}} \quad \boxed{k = 1, 2, ..., n.} \tag{2.74}$$

where

$$\bar{a}_{O_0} = \bar{a}^{(0)}_{O_0/O_e} \neq 0. \tag{2.75}$$

Similarly, the acceleration of the mass center of k^{th} link with respect to $\Im_e$ as expressed in the frame of interest $\Im_0$ can be denoted as $\bar{a}_{G_k} = \bar{a}^{(0)}_{G_k/O_e}$ and derived as

$$\boxed{\bar{a}_{G_k} = \bar{a}_{O_{k-1}} + \left[\tilde{\alpha}_k + \tilde{\omega}_k^2\right]\hat{C}^{(0,k)}\bar{r}_{G_k} + \left[\tilde{\alpha}_0 + \tilde{\omega}_0^2\right]\bar{p}_{O_{k-1}} + 2\tilde{\omega}_0\bar{v}_{O_{k-1}}} \quad \boxed{k = 1, 2, ..., n.} \tag{2.76}$$

2.3 UVMS Kinematics Having Regular Manipulator

The UVMS under consideration is a 12-DOF system consisting of an AUV in 6-DOF equipped with a 6-DOF manipulator as seen in Figure 2.3. It is a kinematically redundant system. In other words, it has more degrees of freedom than required to locate an object in task space using its end-effector. Though, any DOF that is added to 6-DOF vehicle increase the redundancy of the system at that extent.

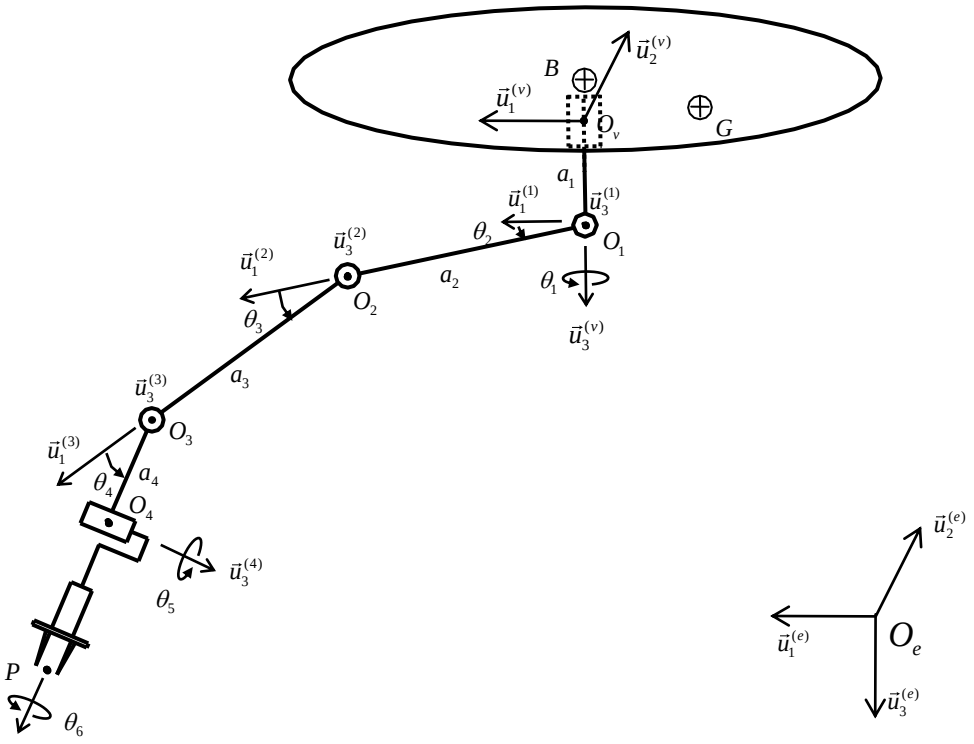

Figure 2.3 Underwater Vehicle Manipulator System

The spatial manipulator has a 6R serial configuration. The AUV has three planes of symmetry with a prolate spheroidal shape while the manipulator links are assumed to be cylindrical aluminum bars.

The base frame of the manipulator is selected to be coincident with the AUV's body fixed frame with origin O_v. The inertial reference frame is selected conventionally as a NED (north-east-down) earth-fixed frame attached to a convenient location in the vicinity of the UVMS. Point-G and Point-B are respectively the centers of gravity and buoyancy. The origin of the body-fixed frame the k^{th} link is shown by O_k. The tip point of the end-effector is taken as Point-P. Since the system links do not have any offsets, all s_k's are taken to be equal to zero.

The DH parameters of the system are given in Table 2.2.

Table 2.2 UVMS DH Parameters

DOF	**1**	**2**	**3**	**4**	**5**	**6**
α_k	$\frac{\pi}{2}$	0	0	$-\frac{\pi}{2}$	$\frac{\pi}{2}$	0
a_k	a_1	a_2	a_3	a_4	a_5	a_6
θ_k *or* δ_k	θ_1	θ_2	θ_3	θ_4	θ_5	θ_6
s_k *or* d_k	0	0	0	0	0	0

In following, the expressions of the position, velocity and acceleration of the body frame origins and the mass centers are derived *recursively* as well as angular velocities and angular accelerations. All of the matrix representations of these relations are expressed with respect to $\Im_e$ but $\Im_v$ is used for the frame of interest.

Before deriving the position equations, link to link rotation matrices are written as

$$
\begin{aligned}
\hat{C}^{(0,1)} &= e^{\tilde{u}_3\theta_1} e^{\tilde{u}_1\pi/2} \\
\hat{C}^{(0,2)} &= e^{\tilde{u}_3\theta_1} e^{-\tilde{u}_2\theta_2} e^{\tilde{u}_1\pi/2} \\
\hat{C}^{(0,3)} &= e^{\tilde{u}_3\theta_1} e^{-\tilde{u}_2\theta_{23}} e^{\tilde{u}_1\pi/2} \\
\hat{C}^{(0,4)} &= e^{\tilde{u}_3\theta_1} e^{-\tilde{u}_2\theta_{234}} \\
\hat{C}^{(0,5)} &= e^{\tilde{u}_3\theta_1} e^{-\tilde{u}_2\theta_{234}} e^{\tilde{u}_3\theta_5} e^{\tilde{u}_1\pi/2} \\
\hat{C}^{(0,6)} &= e^{\tilde{u}_3\theta_1} e^{-\tilde{u}_2\theta_{234}} e^{\tilde{u}_3\theta_5} e^{-\tilde{u}_2\theta_6} e^{\tilde{u}_1\pi/2}
\end{aligned}
\tag{2.77}
$$

The position vectors of the link origins of the manipulator are given below

$$
\begin{aligned}
\overline{p}_{O_v} &= \overline{\zeta}_L \\
\overline{p}_{O_1} &= \overline{p}_{O_v} + a_1\overline{u}_3 \\
\overline{p}_{O_2} &= \overline{p}_{O_1} + a_2\hat{C}^{(0,2)}\overline{u}_1 \\
\overline{p}_{O_3} &= \overline{p}_{O_2} + a_3\hat{C}^{(0,3)}\overline{u}_1 \\
\overline{p}_{O_4} &= \overline{p}_{O_3} + a_4\hat{C}^{(0,4)}\overline{u}_1 \\
\overline{p}_{O_5} &= \overline{p}_{O_4} + a_5\hat{C}^{(0,5)}\overline{u}_3 \\
\overline{p}_P &= \overline{p}_{O_5} + a_6\hat{C}^{(0,6)}\overline{u}_3
\end{aligned}
\tag{2.78}
$$

The positions of the mass centers of the links are obtained by means of the previously derived position equations of the link origins.

$$
\begin{aligned}
\overline{p}_{G_1} &= \overline{p}_{O_v} + \frac{a_1}{2}\overline{u}_3 \\
\overline{p}_{G_2} &= \overline{p}_{O_1} + \frac{a_2}{2}\hat{C}^{(0,2)}\overline{u}_1 \\
\overline{p}_{G_3} &= \overline{p}_{O_2} + \frac{a_3}{2}\hat{C}^{(0,3)}\overline{u}_1 \\
\overline{p}_{G_4} &= \overline{p}_{O_3} + \frac{a_4}{2}\hat{C}^{(0,4)}\overline{u}_1 \\
\overline{p}_{G_5} &= \overline{p}_{O_4} + \frac{a_5}{2}\hat{C}^{(0,5)}\overline{u}_3 \\
\overline{p}_P &= \overline{p}_{O_5} + \frac{a_6}{2}\hat{C}^{(0,6)}\overline{u}_3
\end{aligned}
\tag{2.79}
$$

The angular velocities of the links are calculated recursively as

$$
\begin{aligned}
\bar{\omega}_v &= p\bar{u}_1 + q\bar{u}_2 + r\bar{u}_3 \\
\bar{\omega}_1 &= \bar{\omega}_v + \dot{\theta}_1\bar{u}_3 \\
\bar{\omega}_2 &= \bar{\omega}_1 + \dot{\theta}_2\hat{C}^{(0,1)}\bar{u}_3 \\
\bar{\omega}_3 &= \bar{\omega}_2 + \dot{\theta}_3\hat{C}^{(0,2)}\bar{u}_3 \\
\bar{\omega}_4 &= \bar{\omega}_3 + \dot{\theta}_4\hat{C}^{(0,3)}\bar{u}_3 \\
\bar{\omega}_5 &= \bar{\omega}_4 + \dot{\theta}_5\hat{C}^{(0,4)}\bar{u}_3 \\
\bar{\omega}_6 &= \bar{\omega}_5 + \dot{\theta}_6\hat{C}^{(0,5)}\bar{u}_3
\end{aligned}
\tag{2.80}
$$

The velocities of the link origins are obtained by using the angular velocities

$$
\begin{aligned}
\bar{v}_{O_v} &= \bar{\eta}_L = u\bar{u}_1 + v\bar{u}_2 + w\bar{u}_3 \\
\bar{v}_{O_1} &= \bar{v}_{O_v} + a_1\tilde{\omega}_1\bar{u}_3 + \tilde{\omega}_v\bar{p}_{O_v} \\
\bar{v}_{O_2} &= \bar{v}_{O_1} + a_2\tilde{\omega}_2\hat{C}^{(0,2)}\bar{u}_1 + \tilde{\omega}_v\bar{p}_{O_1} \\
\bar{v}_{O_3} &= \bar{v}_{O_2} + a_3\tilde{\omega}_3\hat{C}^{(0,3)}\bar{u}_1 + \tilde{\omega}_v\bar{p}_{O_2} \\
\bar{v}_{O_4} &= \bar{v}_{O_3} + a_4\tilde{\omega}_4\hat{C}^{(0,4)}\bar{u}_1 + \tilde{\omega}_v\bar{p}_{O_3} \\
\bar{v}_{O_5} &= \bar{v}_{O_4} + a_5\tilde{\omega}_5\hat{C}^{(0,5)}\bar{u}_3 + \tilde{\omega}_v\bar{p}_{O_4} \\
\bar{v}_P &= \bar{v}_{O_5} + a_6\tilde{\omega}_6\hat{C}^{(0,6)}\bar{u}_3 + \tilde{\omega}_v\bar{p}_{O_5}
\end{aligned}
\tag{2.81}
$$

The velocities of the mass centers of the links are

$$
\begin{aligned}
\bar{v}_{G_1} &= \bar{v}_{O_v} + \frac{a_1}{2}\tilde{\omega}_1\bar{u}_3 + \tilde{\omega}_v\bar{p}_{O_v} \\
\bar{v}_{G_2} &= \bar{v}_{O_1} + \frac{a_2}{2}\tilde{\omega}_2\hat{C}^{(0,2)}\bar{u}_1 + \tilde{\omega}_v\bar{p}_{O_1} \\
\bar{v}_{G_3} &= \bar{v}_{O_2} + \frac{a_3}{2}\tilde{\omega}_3\hat{C}^{(0,3)}\bar{u}_1 + \tilde{\omega}_v\bar{p}_{O_2} \\
\bar{v}_{G_4} &= \bar{v}_{O_3} + \frac{a_4}{2}\tilde{\omega}_4\hat{C}^{(0,4)}\bar{u}_1 + \tilde{\omega}_v\bar{p}_{O_3} \\
\bar{v}_{G_5} &= \bar{v}_{O_4} + \frac{a_5}{2}\tilde{\omega}_5\hat{C}^{(0,5)}\bar{u}_3 + \tilde{\omega}_v\bar{p}_{O_4} \\
\bar{v}_P &= \bar{v}_{O_5} + \frac{a_6}{2}\tilde{\omega}_6\hat{C}^{(0,6)}\bar{u}_3 + \tilde{\omega}_v\bar{p}_{O_5}
\end{aligned}
\tag{2.82}
$$

The angular accelerations of the links are obtained as

$$
\begin{aligned}
\bar{\alpha}_v &= \dot{p}\bar{u}_1 + \dot{q}\bar{u}_2 + \dot{r}\bar{u}_3 \\
\bar{\alpha}_1 &= \bar{\alpha}_v + \ddot{\theta}_1\bar{u}_3 + \dot{\theta}_1\tilde{\omega}_v\bar{u}_3 \\
\bar{\alpha}_2 &= \bar{\alpha}_1 + \ddot{\theta}_2\hat{C}^{(0,1)}\bar{u}_3 + \dot{\theta}_2\tilde{\omega}_1\hat{C}^{(0,1)}\bar{u}_3 + \tilde{\omega}_v\bar{\omega}_1 \\
\bar{\alpha}_3 &= \bar{\alpha}_2 + \ddot{\theta}_3\hat{C}^{(0,2)}\bar{u}_3 + \dot{\theta}_3\tilde{\omega}_2\hat{C}^{(0,2)}\bar{u}_3 + \tilde{\omega}_v\bar{\omega}_2 \\
\bar{\alpha}_4 &= \bar{\alpha}_3 + \ddot{\theta}_4\hat{C}^{(0,3)}\bar{u}_3 + \dot{\theta}_4\tilde{\omega}_3\hat{C}^{(0,3)}\bar{u}_3 + \tilde{\omega}_v\bar{\omega}_3 \\
\bar{\alpha}_5 &= \bar{\alpha}_4 + \ddot{\theta}_5\hat{C}^{(0,4)}\bar{u}_3 + \dot{\theta}_5\tilde{\omega}_4\hat{C}^{(0,4)}\bar{u}_3 + \tilde{\omega}_v\bar{\omega}_4 \\
\bar{\alpha}_6 &= \bar{\alpha}_5 + \ddot{\theta}_6\hat{C}^{(0,5)}\bar{u}_3 + \dot{\theta}_6\tilde{\omega}_5\hat{C}^{(0,5)}\bar{u}_3 + \tilde{\omega}_v\bar{\omega}_5
\end{aligned}
\tag{2.83}
$$

The accelerations of the link origins are as follows

$$
\begin{aligned}
\bar{a}_{O_v} &= \left(\dot{u} - rv + qw\right)\bar{u}_1 + \left(\dot{v} + ru - pw\right)\bar{u}_2 + \left(\dot{w} - qu + pv\right)\bar{u}_3 \\
\bar{a}_{O_1} &= \bar{a}_{O_v} + a_1\left[\tilde{\alpha}_1 + \tilde{\omega}_1^2\right]\bar{u}_3 + \left[\tilde{\alpha}_v + \tilde{\omega}_v^2\right]\bar{p}_{O_v} + 2\tilde{\omega}_v\bar{v}_{O_v} \\
\bar{a}_{O_2} &= \bar{a}_{O_1} + a_2\left[\tilde{\alpha}_2 + \tilde{\omega}_2^2\right]\hat{C}^{(0,2)}\bar{u}_1 + \left[\tilde{\alpha}_v + \tilde{\omega}_v^2\right]\bar{p}_{O_1} + 2\tilde{\omega}_v\bar{v}_{O_1} \\
\bar{a}_{O_3} &= \bar{a}_{O_2} + a_3\left[\tilde{\alpha}_3 + \tilde{\omega}_3^2\right]\hat{C}^{(0,3)}\bar{u}_1 + \left[\tilde{\alpha}_v + \tilde{\omega}_v^2\right]\bar{p}_{O_2} + 2\tilde{\omega}_v\bar{v}_{O_2} \\
\bar{a}_{O_4} &= \bar{a}_{O_3} + a_4\left[\tilde{\alpha}_4 + \tilde{\omega}_4^2\right]\hat{C}^{(0,4)}\bar{u}_1 + \left[\tilde{\alpha}_v + \tilde{\omega}_v^2\right]\bar{p}_{O_3} + 2\tilde{\omega}_v\bar{v}_{O_3} \\
\bar{a}_{O_5} &= \bar{a}_{O_4} + a_5\left[\tilde{\alpha}_5 + \tilde{\omega}_5^2\right]\hat{C}^{(0,5)}\bar{u}_3 + \left[\tilde{\alpha}_v + \tilde{\omega}_v^2\right]\bar{p}_{O_4} + 2\tilde{\omega}_v\bar{v}_{O_4} \\
\bar{a}_P &= \bar{a}_{O_5} + a_6\left[\tilde{\alpha}_6 + \tilde{\omega}_6^2\right]\hat{C}^{(0,6)}\bar{u}_3 + \left[\tilde{\alpha}_v + \tilde{\omega}_v^2\right]\bar{p}_{O_5} + 2\tilde{\omega}_v\bar{v}_{O_5}
\end{aligned}
\tag{2.84}
$$

In the equation group (2.85), the accelerations of the mass centers are given as

$$
\begin{aligned}
\bar{a}_{G_1} &= \bar{a}_{O_v} + \frac{a_1}{2}\left[\tilde{\alpha}_1 + \tilde{\omega}_1^2\right]\bar{u}_3 + \left[\tilde{\alpha}_v + \tilde{\omega}_v^2\right]\bar{p}_{O_v} + 2\tilde{\omega}_v\bar{v}_{O_v} \\
\bar{a}_{G_2} &= \bar{a}_{O_1} + \frac{a_2}{2}\left[\tilde{\alpha}_2 + \tilde{\omega}_2^2\right]\hat{C}^{(0,2)}\bar{u}_1 + \left[\tilde{\alpha}_v + \tilde{\omega}_v^2\right]\bar{p}_{O_1} + 2\tilde{\omega}_v\bar{v}_{O_1} \\
\bar{a}_{G_3} &= \bar{a}_{O_2} + \frac{a_3}{2}\left[\tilde{\alpha}_3 + \tilde{\omega}_3^2\right]\hat{C}^{(0,3)}\bar{u}_1 + \left[\tilde{\alpha}_v + \tilde{\omega}_v^2\right]\bar{p}_{O_2} + 2\tilde{\omega}_v\bar{v}_{O_2} \\
\bar{a}_{G_4} &= \bar{a}_{O_3} + \frac{a_4}{2}\left[\tilde{\alpha}_4 + \tilde{\omega}_4^2\right]\hat{C}^{(0,4)}\bar{u}_1 + \left[\tilde{\alpha}_v + \tilde{\omega}_v^2\right]\bar{p}_{O_3} + 2\tilde{\omega}_v\bar{v}_{O_3} \\
\bar{a}_{G_5} &= \bar{a}_{O_4} + \frac{a_5}{2}\left[\tilde{\alpha}_5 + \tilde{\omega}_5^2\right]\hat{C}^{(0,5)}\bar{u}_3 + \left[\tilde{\alpha}_v + \tilde{\omega}_v^2\right]\bar{p}_{O_4} + 2\tilde{\omega}_v\bar{v}_{O_4} \\
\bar{a}_{G_6} &= \bar{a}_{O_5} + \frac{a_6}{2}\left[\tilde{\alpha}_6 + \tilde{\omega}_6^2\right]\hat{C}^{(0,6)}\bar{u}_3 + \left[\tilde{\alpha}_v + \tilde{\omega}_v^2\right]\bar{p}_{O_5} + 2\tilde{\omega}_v\bar{v}_{O_5}
\end{aligned}
\tag{2.85}
$$

2.4 UVMS Kinematics Having Redundant Manipulator

The 14-DOF UVMS consists of an AUV which has 4 thrusters and 8-DOF manipulator (i.e. u-UVRMS) as seen in Figure 2.4. It is also a kinematically redundant system. This time, it has an underactuated AUV subsystem which has no thrusters in sway and yaw directions. The redundant manipulator of u-UVRMS is designed in such a way that it will compensate the motions of the AUV where there is no control. Though, it is aimed to minimize the disturbing effect of the manipulator on the AUV during manipulation of the end-effector. The reason why it is designed as a 8-DOF redundant manipulator is that system will be controlled by a total of 12 actuators in 12-DOF task space.

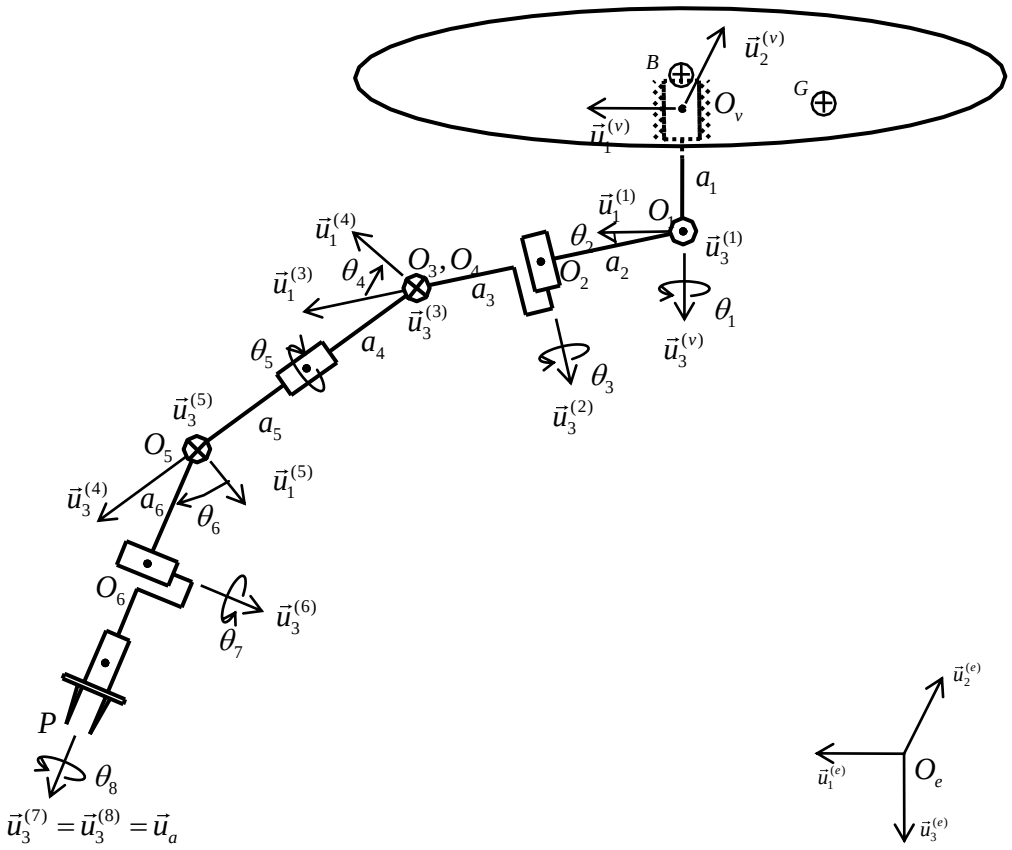

Figure 2.4 Underwater Vehicle Redundant Manipulator System

As seen from Figure 2.4, system has two more joints compared to fully actuated UVMS. The joint that connects second and third links is used to compensate to sway motion. Uncontrolled yaw motion is compensated by the first joint of the manipulator. The joint placed between the fourth and fifth links gives support to the AUV by decreasing rolling interaction between the subsystems. The DH parameters of the system are given in Table 2.3.

Table 2.3 UVRMS DH Parameters

DOF	**1**	**2**	**3**	**4**	**5**	**6**	**7**	**8**
α_k	$\frac{\pi}{2}$	$-\frac{\pi}{2}$	$-\frac{\pi}{2}$	$\frac{\pi}{2}$	$\frac{\pi}{2}$	$\frac{\pi}{2}$	$\frac{\pi}{2}$	0
a_k	a_1	a_2	a_3	a_4	a_5	a_6	a_7	a_8
θ_k *or* δ_k	θ_1	θ_2	θ_3	θ_4	θ_5	θ_6	θ_7	θ_8
s_k *or* d_k	0	0	0	0	0	0	0	0

In following, the expressions of the position, velocity and acceleration of the body frame origins and the mass centers are derived *recursively* as well as angular velocities and angular accelerations. All of the matrix representations of these relations are expressed with respect to $\Im_e$ but $\Im_v$ is used for the frame of interest.

Before deriving the position equations link to link rotation matrices are written as

$$
\begin{aligned}
\hat{C}^{(0,1)} &= e^{\tilde{u}_3\theta_1}e^{\tilde{u}_1\pi/2} \\
\hat{C}^{(0,2)} &= e^{\tilde{u}_3\theta_1}e^{-\tilde{u}_2\theta_2} \\
\hat{C}^{(0,3)} &= e^{\tilde{u}_3\theta_1}e^{-\tilde{u}_2\theta_2}e^{\tilde{u}_3\theta_3}e^{-\tilde{u}_1\pi/2} \\
\hat{C}^{(0,4)} &= e^{\tilde{u}_3\theta_1}e^{-\tilde{u}_2\theta_2}e^{\tilde{u}_3\theta_3}e^{\tilde{u}_2\theta_4}e^{-\tilde{u}_1\pi} \\
\hat{C}^{(0,5)} &= e^{\tilde{u}_3\theta_1}e^{-\tilde{u}_2\theta_2}e^{\tilde{u}_3\theta_3}e^{\tilde{u}_2\theta_4}e^{\tilde{u}_3\theta_5}e^{-\tilde{u}_1\pi/2} \\
\hat{C}^{(0,6)} &= e^{\tilde{u}_3\theta_1}e^{-\tilde{u}_2\theta_2}e^{\tilde{u}_3\theta_3}e^{\tilde{u}_2\theta_4}e^{\tilde{u}_3\theta_5}e^{\tilde{u}_2\theta_6} \\
\hat{C}^{(0,7)} &= e^{\tilde{u}_3\theta_1}e^{-\tilde{u}_2\theta_2}e^{\tilde{u}_3\theta_3}e^{\tilde{u}_2\theta_4}e^{\tilde{u}_3\theta_5}e^{\tilde{u}_2\theta_6}e^{\tilde{u}_3\theta_7}e^{\tilde{u}_1\pi/2} \\
\hat{C}^{(0,8)} &= e^{\tilde{u}_3\theta_1}e^{-\tilde{u}_2\theta_2}e^{\tilde{u}_3\theta_3}e^{\tilde{u}_2\theta_4}e^{\tilde{u}_3\theta_5}e^{\tilde{u}_2\theta_6}e^{\tilde{u}_3\theta_7}e^{-\tilde{u}_2\theta_8}e^{\tilde{u}_1\pi/2}
\end{aligned}
\tag{2.86}
$$

The position vectors of the link origins of the manipulator are given below

$$
\begin{aligned}
\overline{p}_{O_v} &= \overline{\zeta}_L \\
\overline{p}_{O_1} &= \overline{p}_{O_v} + a_1\overline{u}_3 \\
\overline{p}_{O_2} &= \overline{p}_{O_1} + a_2\hat{C}^{(0,2)}\overline{u}_1 \\
\overline{p}_{O_3} &= \overline{p}_{O_4} = \overline{p}_{O_2} + a_3\hat{C}^{(0,3)}\overline{u}_1 \\
\overline{p}_{O_5} &= \overline{p}_{O_4} + a_{45}\hat{C}^{(0,4)}\overline{u}_3 \\
\overline{p}_{O_6} &= \overline{p}_{O_5} + a_6\hat{C}^{(0,6)}\overline{u}_1 \\
\overline{p}_{O_7} &= \overline{p}_{O_6} + a_7\hat{C}^{(0,7)}\overline{u}_3 \\
\overline{p}_P &= \overline{p}_{O_7} + a_8\hat{C}^{(0,8)}\overline{u}_3
\end{aligned}
\tag{2.87}
$$

The positions of the mass centers of the links are obtained by means of the previously derived position equations of the link origins.

$$
\begin{aligned}
\overline{p}_{G_1} &= \overline{p}_{O_v} + \frac{a_1}{2}\overline{u}_3 \\
\overline{p}_{G_2} &= \overline{p}_{O_1} + \frac{a_2}{2}\hat{C}^{(0,2)}\overline{u}_1 \\
\overline{p}_{G_3} &= \overline{p}_{O_2} + \frac{a_3}{2}\hat{C}^{(0,3)}\overline{u}_1 \\
\overline{p}_{G_4} &= \overline{p}_{O_3} + \frac{a_4}{2}\hat{C}^{(0,4)}\overline{u}_3 \\
\overline{p}_{G_5} &= \overline{p}_{O_4} + \left(a_4 + \frac{a_5}{2}\right)\hat{C}^{(0,4)}\overline{u}_3 \\
\overline{p}_{G_6} &= \overline{p}_{O_5} + \frac{a_6}{2}\hat{C}^{(0,6)}\overline{u}_1 \\
\overline{p}_{G_7} &= \overline{p}_{O_6} + \frac{a_7}{2}\hat{C}^{(0,7)}\overline{u}_3 \\
\overline{p}_{G_8} &= \overline{p}_{O_7} + \frac{a_8}{2}\hat{C}^{(0,8)}\overline{u}_3
\end{aligned}
\tag{2.88}
$$

The angular velocities of the links are calculated recursively as

$$
\begin{aligned}
\bar{\omega}_v &= p\bar{u}_1 + q\bar{u}_2 + r\bar{u}_3 \\
\bar{\omega}_1 &= \bar{\omega}_v + \dot{\theta}_1\bar{u}_3 \\
\bar{\omega}_2 &= \bar{\omega}_1 + \dot{\theta}_2\hat{C}^{(0,1)}\bar{u}_3 \\
\bar{\omega}_3 &= \bar{\omega}_2 + \dot{\theta}_3\hat{C}^{(0,2)}\bar{u}_3 \\
\bar{\omega}_4 &= \bar{\omega}_3 + \dot{\theta}_4\hat{C}^{(0,3)}\bar{u}_3 \\
\bar{\omega}_5 &= \bar{\omega}_4 + \dot{\theta}_5\hat{C}^{(0,4)}\bar{u}_3 \\
\bar{\omega}_6 &= \bar{\omega}_5 + \dot{\theta}_6\hat{C}^{(0,5)}\bar{u}_3 \\
\bar{\omega}_7 &= \bar{\omega}_6 + \dot{\theta}_7\hat{C}^{(0,6)}\bar{u}_3 \\
\bar{\omega}_8 &= \bar{\omega}_7 + \dot{\theta}_8\hat{C}^{(0,7)}\bar{u}_3
\end{aligned}
\tag{2.89}
$$

The velocities of the link origins are obtained by using the angular velocities

$$
\begin{aligned}
\bar{v}_{O_v} &= \bar{\eta}_L = u\bar{u}_1 + v\bar{u}_2 + w\bar{u}_3 \\
\bar{v}_{O_1} &= \bar{v}_{O_v} + a_1\tilde{\omega}_1\bar{u}_3 + \tilde{\omega}_v\bar{p}_{O_v} \\
\bar{v}_{O_2} &= \bar{v}_{O_1} + a_2\tilde{\omega}_2\hat{C}^{(0,2)}\bar{u}_1 + \tilde{\omega}_v\bar{p}_{O_1} \\
\bar{v}_{O_3} &= \bar{v}_{O_4} = \bar{v}_{O_2} + a_3\tilde{\omega}_3\hat{C}^{(0,3)}\bar{u}_1 + \tilde{\omega}_v\bar{p}_{O_2} \\
\bar{v}_{O_5} &= \bar{v}_{O_4} + a_{45}\tilde{\omega}_5\hat{C}^{(0,4)}\bar{u}_3 + \tilde{\omega}_v\bar{p}_{O_4} \\
\bar{v}_{O_6} &= \bar{v}_{O_5} + a_6\tilde{\omega}_6\hat{C}^{(0,6)}\bar{u}_1 + \tilde{\omega}_v\bar{p}_{O_5} \\
\bar{v}_{O_7} &= \bar{v}_{O_6} + a_7\tilde{\omega}_7\hat{C}^{(0,7)}\bar{u}_3 + \tilde{\omega}_v\bar{p}_{O_6} \\
\bar{v}_P &= \bar{v}_{O_7} + a_8\tilde{\omega}_8\hat{C}^{(0,8)}\bar{u}_3 + \tilde{\omega}_v\bar{p}_{O_7}
\end{aligned}
\tag{2.90}
$$

The velocities of the mass centers of the links are

$$
\begin{aligned}
\bar{v}_{G_1} &= \bar{v}_{O_v} + \frac{a_1}{2}\tilde{\omega}_1\bar{u}_3 + \tilde{\omega}_v\bar{p}_{O_v} \\
\bar{v}_{G_2} &= \bar{v}_{O_1} + \frac{a_2}{2}\tilde{\omega}_2\hat{C}^{(0,2)}\bar{u}_1 + \tilde{\omega}_v\bar{p}_{O_1} \\
\bar{v}_{G_3} &= \bar{v}_{O_2} + \frac{a_3}{2}\tilde{\omega}_3\hat{C}^{(0,3)}\bar{u}_1 + \tilde{\omega}_v\bar{p}_{O_2} \\
\bar{v}_{G_4} &= \bar{v}_{O_3} + \frac{a_4}{2}\tilde{\omega}_4\hat{C}^{(0,4)}\bar{u}_3 + \tilde{\omega}_v\bar{p}_{O_3} \\
\bar{v}_{G_5} &= \bar{v}_{O_4} + \left(a_4 + \frac{a_5}{2}\right)\tilde{\omega}_5\hat{C}^{(0,4)}\bar{u}_3 + \tilde{\omega}_v\bar{p}_{O_4}
\end{aligned}
\tag{2.91}
$$

$$\bar{v}_{G_6} = \bar{v}_{O_5} + \frac{a_6}{2}\tilde{\omega}_6\hat{C}^{(0,6)}\bar{u}_1 + \tilde{\omega}_v\bar{p}_{O_5}$$
$$\bar{v}_{G_7} = \bar{v}_{O_6} + \frac{a_7}{2}\tilde{\omega}_7\hat{C}^{(0,7)}\bar{u}_3 + \tilde{\omega}_v\bar{p}_{O_6}$$
$$\bar{v}_{G_8} = \bar{v}_{O_7} + \frac{a_8}{2}\tilde{\omega}_8\hat{C}^{(0,8)}\bar{u}_3 + \tilde{\omega}_v\bar{p}_{O_7}$$

The angular accelerations of the links are obtained as

$$\begin{aligned}
\bar{\alpha}_v &= \dot{p}\bar{u}_1 + \dot{q}\bar{u}_2 + \dot{r}\bar{u}_3 \\
\bar{\alpha}_1 &= \bar{\alpha}_v + \ddot{\theta}_1\bar{u}_3 + \dot{\theta}_1\tilde{\omega}_v\bar{u}_3 \\
\bar{\alpha}_2 &= \bar{\alpha}_1 + \ddot{\theta}_2\hat{C}^{(0,1)}\bar{u}_3 + \dot{\theta}_2\tilde{\omega}_1\hat{C}^{(0,1)}\bar{u}_3 + \tilde{\omega}_v\bar{\omega}_1 \\
\bar{\alpha}_3 &= \bar{\alpha}_2 + \ddot{\theta}_3\hat{C}^{(0,2)}\bar{u}_3 + \dot{\theta}_3\tilde{\omega}_2\hat{C}^{(0,2)}\bar{u}_3 + \tilde{\omega}_v\bar{\omega}_2 \\
\bar{\alpha}_4 &= \bar{\alpha}_3 + \ddot{\theta}_4\hat{C}^{(0,3)}\bar{u}_3 + \dot{\theta}_4\tilde{\omega}_3\hat{C}^{(0,3)}\bar{u}_3 + \tilde{\omega}_v\bar{\omega}_3 \\
\bar{\alpha}_5 &= \bar{\alpha}_4 + \ddot{\theta}_5\hat{C}^{(0,4)}\bar{u}_3 + \dot{\theta}_5\tilde{\omega}_4\hat{C}^{(0,4)}\bar{u}_3 + \tilde{\omega}_v\bar{\omega}_4 \\
\bar{\alpha}_6 &= \bar{\alpha}_5 + \ddot{\theta}_6\hat{C}^{(0,5)}\bar{u}_3 + \dot{\theta}_6\tilde{\omega}_5\hat{C}^{(0,5)}\bar{u}_3 + \tilde{\omega}_v\bar{\omega}_5 \\
\bar{\alpha}_7 &= \bar{\alpha}_6 + \ddot{\theta}_7\hat{C}^{(0,6)}\bar{u}_3 + \dot{\theta}_7\tilde{\omega}_6\hat{C}^{(0,6)}\bar{u}_3 + \tilde{\omega}_v\bar{\omega}_6 \\
\bar{\alpha}_8 &= \bar{\alpha}_7 + \ddot{\theta}_8\hat{C}^{(0,7)}\bar{u}_3 + \dot{\theta}_8\tilde{\omega}_7\hat{C}^{(0,7)}\bar{u}_3 + \tilde{\omega}_v\bar{\omega}_7
\end{aligned} \tag{2.92}$$

The accelerations of the link origins are as follows

$$\begin{aligned}
\bar{a}_{O_v} &= \left(\dot{u} - rv + qw\right)\bar{u}_1 + \left(\dot{v} + ru - pw\right)\bar{u}_2 + \left(\dot{w} - qu + pv\right)\bar{u}_3 \\
\bar{a}_{O_1} &= \bar{a}_{O_v} + a_1\left[\tilde{\alpha}_v + \tilde{\omega}_v^2\right]\bar{u}_3 + \left[\tilde{\alpha}_v + \tilde{\omega}_v^2\right]\bar{p}_{O_v} + 2\tilde{\omega}_v\bar{v}_{O_v} \\
\bar{a}_{O_2} &= \bar{a}_{O_1} + a_2\left[\tilde{\alpha}_2 + \tilde{\omega}_2^2\right]\hat{C}^{(0,2)}\bar{u}_1 + \left[\tilde{\alpha}_v + \tilde{\omega}_v^2\right]\bar{p}_{O_1} + 2\tilde{\omega}_v\bar{v}_{O_1} \\
\bar{a}_{O_3} &= \bar{a}_{O_4} = \bar{a}_{O_2} + a_3\left[\tilde{\alpha}_3 + \tilde{\omega}_3^2\right]\hat{C}^{(0,3)}\bar{u}_1 + \left[\tilde{\alpha}_v + \tilde{\omega}_v^2\right]\bar{p}_{O_2} + 2\tilde{\omega}_v\bar{v}_{O_2} \\
\bar{a}_{O_5} &= \bar{a}_{O_4} + a_{45}\left[\tilde{\alpha}_5 + \tilde{\omega}_5^2\right]\hat{C}^{(0,4)}\bar{u}_3 + \left[\tilde{\alpha}_v + \tilde{\omega}_v^2\right]\bar{p}_{O_4} + 2\tilde{\omega}_v\bar{v}_{O_4} \\
\bar{a}_{O_6} &= \bar{a}_{O_5} + a_6\left[\tilde{\alpha}_6 + \tilde{\omega}_6^2\right]\hat{C}^{(0,6)}\bar{u}_1 + \left[\tilde{\alpha}_v + \tilde{\omega}_v^2\right]\bar{p}_{O_5} + 2\tilde{\omega}_v\bar{v}_{O_5} \\
\bar{a}_{O_7} &= \bar{a}_{O_6} + a_7\left[\tilde{\alpha}_7 + \tilde{\omega}_7^2\right]\hat{C}^{(0,7)}\bar{u}_3 + \left[\tilde{\alpha}_v + \tilde{\omega}_v^2\right]\bar{p}_{O_6} + 2\tilde{\omega}_v\bar{v}_{O_6} \\
\bar{a}_P &= \bar{a}_{O_7} + a_8\left[\tilde{\alpha}_8 + \tilde{\omega}_8^2\right]\hat{C}^{(0,8)}\bar{u}_3 + \left[\tilde{\alpha}_v + \tilde{\omega}_v^2\right]\bar{p}_{O_7} + 2\tilde{\omega}_v\bar{v}_{O_7}
\end{aligned} \tag{2.93}$$

In the equation group (2.94), the accelerations of the mass centers are given as

$$
\begin{aligned}
\bar{a}_{G_1} &= \bar{a}_{O_v} + \frac{a_1}{2}\left[\tilde{\alpha}_1 + \tilde{\omega}_1^2\right]\bar{u}_3 + \left[\tilde{\alpha}_v + \tilde{\omega}_v^2\right]\bar{p}_{O_v} + 2\tilde{\omega}_v\bar{v}_{O_v} \\
\bar{a}_{G_2} &= \bar{a}_{O_1} + \frac{a_2}{2}\left[\tilde{\alpha}_2 + \tilde{\omega}_2^2\right]\hat{C}^{(0,2)}\bar{u}_1 + \left[\tilde{\alpha}_v + \tilde{\omega}_v^2\right]\bar{p}_{O_1} + 2\tilde{\omega}_v\bar{v}_{O_1} \\
\bar{a}_{G_3} &= \bar{a}_{O_2} + \frac{a_3}{2}\left[\tilde{\alpha}_3 + \tilde{\omega}_3^2\right]\hat{C}^{(0,3)}\bar{u}_1 + \left[\tilde{\alpha}_v + \tilde{\omega}_v^2\right]\bar{p}_{O_2} + 2\tilde{\omega}_v\bar{v}_{O_2} \\
\bar{a}_{G_4} &= \bar{a}_{O_3} + \frac{a_4}{2}\left[\tilde{\alpha}_4 + \tilde{\omega}_4^2\right]\hat{C}^{(0,4)}\bar{u}_3 + \left[\tilde{\alpha}_v + \tilde{\omega}_v^2\right]\bar{p}_{O_3} + 2\tilde{\omega}_v\bar{v}_{O_3} \\
\bar{a}_{G_5} &= \bar{a}_{O_4} + \left(a_4 + \frac{a_5}{2}\right)\left[\tilde{\alpha}_5 + \tilde{\omega}_5^2\right]\hat{C}^{(0,4)}\bar{u}_3 + \left[\tilde{\alpha}_v + \tilde{\omega}_v^2\right]\bar{p}_{O_4} + 2\tilde{\omega}_v\bar{v}_{O_4} \\
\bar{a}_{G_6} &= \bar{a}_{O_5} + \frac{a_6}{2}\left[\tilde{\alpha}_6 + \tilde{\omega}_6^2\right]\hat{C}^{(0,6)}\bar{u}_1 + \left[\tilde{\alpha}_v + \tilde{\omega}_v^2\right]\bar{p}_{O_5} + 2\tilde{\omega}_v\bar{v}_{O_5} \\
\bar{a}_{G_7} &= \bar{a}_{O_6} + \frac{a_7}{2}\left[\tilde{\alpha}_7 + \tilde{\omega}_7^2\right]\hat{C}^{(0,7)}\bar{u}_3 + \left[\tilde{\alpha}_v + \tilde{\omega}_v^2\right]\bar{p}_{O_6} + 2\tilde{\omega}_v\bar{v}_{O_6} \\
\bar{a}_{G_8} &= \bar{a}_{O_7} + \frac{a_8}{2}\left[\tilde{\alpha}_8 + \tilde{\omega}_8^2\right]\hat{C}^{(0,8)}\bar{u}_3 + \left[\tilde{\alpha}_v + \tilde{\omega}_v^2\right]\bar{p}_{O_7} + 2\tilde{\omega}_v\bar{v}_{O_7}
\end{aligned}
\tag{2.94}
$$

During the simulation of the systems, all the above kinematic equations are converted into MATLAB® codes and written in m-files.

CHAPTER III

UVMS DYNAMICS

UVMS dynamics is highly nonlinear and coupled. In order to derive the dynamic equations of motion, several methods can be used such as the Newton–Euler method, the Lagrange method and the Kane's method. This study covers the Newton–Euler method because of two reasons. First, it is a commonly used approach in robotics since the derivation of the Newton–Euler equations of a system of bodies in the 3 dimensional space is rather simple, compared to other methods. Second, the equations of motion can be generated recursively and easily be extended to add new bodies to the system under consideration.

In the following parts, the dynamic models of the UVMSs are presented. First, the dynamic equations of motion of the AUV and the manipulator subsystems are derived one by one considering the coordinates expressed in the body fixed frames. Then, these two sets of equations are combined in order to obtain the final form of the equations of the entire system. Basic hydrodynamic forces that exert on the bodies working underwater are discussed. The hydrodynamic interaction between the bodies and the effect of the ocean currents on the systems are explained. The thruster model is introduced and its incorporation to the dynamic equations is clarified.

3.1 Underwater Vehicle Dynamics

3.1.1 Newton-Euler Equations for the AUV

The linear motion of the AUV can be expressed in its own frame using Newton's equation based on 2^{nd} law as

$$m_v \bar{a}_{G_v} = \sum \bar{F}_v \tag{3.1}$$

where

m_v is the mass of the AUV,

$\bar{F}_v \in \Re^{3x1}$ is the vector of external forces applied on the AUV.

External forces can be decomposed into reaction forces if connected by another rigid body, actuator forces, hydrostatic forces and hydrodynamic forces which will be explained in following sections.

Combining Equation (2.18) and Equation (3.1) gives

$$m_v \begin{bmatrix} \dot{u} - rv + qw - x_G(r^2 + q^2) + y_G(pq - \dot{r}) + z_G(pr + \dot{q}) \\ \dot{v} + ur - pw + x_G(pq + \dot{r}) - y_G(p^2 + r^2) + z_G(qr - \dot{p}) \\ \dot{w} - qu + pv + x_G(pr - \dot{q}) + y_G(qr + \dot{p}) - z_G(p^2 + q^2) \end{bmatrix} = \sum \bar{F}_v \tag{3.2}$$

The angular motion of the AUV, on the other hand, can be expressed about the origin of its own frame using Euler's equation as

$$\hat{J}_{O_v}^{(v)} \bar{\alpha}_{v/e}^{(v)} + \tilde{\omega}_{v/e}^{(v)} \hat{J}_{O_v}^{(v)} \bar{\omega}_{v/e}^{(v)} + m_v \tilde{r}_G^{(v)} \bar{a}_{O_v}^{(v)} = \sum \bar{M}_{O_v} \tag{3.3}$$

Substituting Equation (2.15) into Equation (3.3) gives

$$\hat{J}_{O_v}^{(v)} \bar{\alpha}_{v/e}^{(v)} + \tilde{\omega}_{v/e}^{(v)} \hat{J}_{O_v}^{(v)} \bar{\omega}_{v/e}^{(v)} + m_v \tilde{r}_G^{(v)} \left(\dot{\bar{v}}_{O_v}^{(v)} + \tilde{\omega}_{v/e}^{(v)} \bar{v}_{O_v}^{(v)} \right) = \sum \bar{M}_{O_v} \tag{3.4}$$

Inserting other relevant equations into Equation (3.4) yields

$$\hat{J}_{O_v}^{(v)} \begin{bmatrix} \dot{p} \\ \dot{q} \\ \dot{r} \end{bmatrix} + \ldots \tag{3.5}$$

$$\begin{bmatrix} (I_{zz}-I_{yy})qr + I_{yz}(r^2-q^2) + I_{xy}pr - I_{xz}pq + m_v[y_G(-qu+pv) - z_G(ru-pw)] \\ (I_{xx}-I_{zz})pr + I_{xz}(p^2-r^2) - I_{xy}qr + I_{yz}pq + m_v[z_G(-rv+qw) - x_G(-qu+pv)] \\ (I_{yy}-I_{xx})pq + I_{xy}(q^2-p^2) + I_{xz}qr - I_{yz}pr + m_v[x_G(ru-pw) - y_G(-rv+qw)] \end{bmatrix} = \sum \bar{M}_{O_v}$$

where $\hat{J}_{O_v}^{(v)} \in \Re^{3x3}$ moment of inertia matrix which is constant when expressed in $\Im_v$.

$$\hat{J}_{O_v}^{(v)} = \begin{bmatrix} I_{xx} & -I_{xy} & -I_{xz} \\ -I_{xy} & I_{yy} & -I_{yz} \\ -I_{xz} & -I_{yz} & I_{zz} \end{bmatrix} \tag{3.6}$$

External moments include reaction moments, reaction moments caused by the reaction forces, actuator torques, hydrostatic moments, hydrodynamic moments and the moments caused by the disturbance forces.

Final form of the equations of motion of the AUV expressed in $\Im_v$ can be written by combining Equation (3.2) and Equation (3.5) as below:

$$\hat{M}_v \dot{\bar{\eta}} + \bar{Q}_v = \bar{\tau}_v \tag{3.7}$$

$$\bar{\tau}_v = \hat{A}_v \bar{F}_{mv} + \hat{B}_v \bar{T}_v + \bar{F}_{hs_v} + \bar{F}_{hd_v} + \bar{F}_{ex_v}$$

where

$\hat{M}_v \in \Re^{6x6}$ is the generalized mass matrix of the vehicle,

$\bar{Q}_v \in \Re^{6x1}$ is the vector of velocity dependent terms,

$\bar{F}_{mv} \in \Re^{6x1}$ is the vector of reaction forces and moments applied on the vehicle by the manipulator,

$\bar{F}_{hs_v} \in \Re^{6x1}$ and $\bar{F}_{hd_v} \in \Re^{6x1}$ are the vectors of hydrostatic and hydrodynamic forces and moments applied on the vehicle,

$\bar{F}_{ex_v} \in \Re^{6x1}$ is the vector of external disturbance forces and moments,

$\bar{T}_v \in \Re^{6x1}$ is the vector of control forces and moments and

$\hat{A}_v \in \Re^{6x6}$ and $\hat{B}_v \in \Re^{6x6}$ are the influence coefficient matrices of the reaction forces and moments and the control forces and moments respectively.

The matrices in Equation (3.7) can be written explicitly as

$$\hat{M}_v = \begin{bmatrix} m_v \hat{I}_{3x3} & m_v \tilde{r}_{G_v} \\ m_v \tilde{r}_{G_v}^T & \hat{J}_{O_v} \end{bmatrix} \tag{3.8}$$

where

$\hat{I}_{3x3}$ is an identity matrix,

$$\bar{Q}_v = \begin{bmatrix} m_v\left[-rv + qw - x_G(r^2+q^2) + y_G(pq) + z_G(pr)\right] \\ m_v\left[ur - pw + x_G(pq) - y_G(p^2+r^2) + z_G(qr)\right] \\ m_v\left[-qu + pv + x_G(pr) + y_G(qr) - z_G(p^2+q^2)\right] \\ \left(I_{zz} - I_{yy}\right)qr + I_{yz}\left(r^2 - q^2\right) + I_{xy}pr - I_{xz}pq + m_v\left[y_G(pv-qu) - z_G(ru-pw)\right] \\ \left(I_{xx} - I_{zz}\right)pr + I_{xz}\left(p^2 - r^2\right) - I_{xy}qr + I_{yz}pq + m_v\left[z_G(qw-rv) - x_G(pv-qu)\right] \\ \left(I_{yy} - I_{xx}\right)pq + I_{xy}\left(q^2 - p^2\right) + I_{xz}qr - I_{yz}pr + m_v\left[x_G(ru-pw) - y_G(qw-rv)\right] \end{bmatrix} \tag{3.9}$$

and

$$\bar{F}_{mv} = -\begin{bmatrix} \bar{f}_{v1}^{(v)} \\ \bar{m}_{v1}^{(v)} \end{bmatrix} \tag{3.10}$$

where $\bar{f}_{v1}^{(v)} \in \Re^{3x1}, \bar{m}_{v1}^{(v)} \in \Re^{3x1}$ are reaction force and moment vectors respectively.

3.2 Manipulator Dynamics

As explained, the UVMSs under consideration are of two kinds regarding the manipulator system they have, i.e. regular manipulator and redundant manipulator. In

deriving dynamic equations of both types of manipulator systems, the body fixed frames are chosen as the frames of interest for each body. For this reason, the velocities and the accelerations obtained in Chapter-II are supposed to be pre-multiplied by the appropriate transformation matrices to change their resolution frames from $\Im_v$ to the relevant link frame.

3.2.1 Newton-Euler Equations for Regular Manipulator Subsystem

The regular manipulator subsystem is composed of 6 rigid bodies which are connected to each other by revolute joints. The Newton-Euler equations and the inertia tensors for all bodies are expressed about their mass centers. Therefore, the restoring moments created by the weights of the bodies disappear in the Euler equations. A total of 36 scalar equations belonging to these bodies are given in matrix form as below.

Body-1

$$m_1 \bar{a}_{G_1}^{(1)} = \hat{C}^{(1,0)} \bar{f}_{01}^{(0)} + \bar{f}_{21}^{(1)} + \bar{f}_{hs_1}^{(1)} + \bar{f}_{hd_1}^{(1)} + \bar{f}_{ex_1}^{(1)} \tag{3.11}$$

$$\hat{J}_{G_1}^{(1)} \bar{\alpha}_1^{(1)} + \tilde{\omega}_1^{(1)} \hat{J}_{G_1}^{(1)} \bar{\omega}_1^{(1)} = \hat{C}^{(1,0)} \bar{m}_{01}^{(0)} + \bar{m}_{21}^{(1)} - \frac{a_1}{2} \hat{C}^{(1,0)} \left[\tilde{u}_3^{(0)} \bar{f}_{01}^{(0)} \right] + \ldots$$

$$\frac{a_1}{2} \hat{C}^{(1,0)} \tilde{u}_3^{(0)} \left[\hat{C}^{(0,1)} \bar{f}_{21}^{(1)} \right] + \bar{m}_{hs_1}^{(1)} + \bar{m}_{hd_1}^{(1)} + \bar{m}_{ex_1}^{(1)}$$

Body-2

$$m_2 \bar{a}_{G_2}^{(2)} = -\hat{C}^{(2,1)} \bar{f}_{21}^{(1)} + \bar{f}_{32}^{(2)} + \bar{f}_{hs_2}^{(2)} + \bar{f}_{hd_2}^{(2)} + \bar{f}_{ex_2}^{(2)} \tag{3.12}$$

$$\hat{J}_{G_2}^{(2)} \bar{\alpha}_2^{(2)} + \tilde{\omega}_2^{(2)} \hat{J}_{G_2}^{(2)} \bar{\omega}_2^{(2)} = -\hat{C}^{(2,1)} \bar{m}_{21}^{(1)} + \bar{m}_{32}^{(2)} + \frac{a_2}{2} \tilde{u}_1^{(2)} \hat{C}^{(2,1)} \bar{f}_{21}^{(1)} + \frac{a_2}{2} \tilde{u}_1^{(2)} \bar{f}_{32}^{(2)} + \bar{m}_{hs_2}^{(2)} + \bar{m}_{hd_2}^{(2)} + \bar{m}_{ex_2}^{(2)}$$

Remark:

$$\tilde{u}_1^{(2)} = \hat{C}^{(2,0)} \tilde{u}_1^{(0)} \hat{C}^{(0,2)}$$

Body-3

$$m_3\bar{a}_{G_3}^{(3)} = -\hat{C}^{(3,2)}\bar{f}_{32}^{(2)} + \bar{f}_{43}^{(3)} + \bar{f}_{hs_3}^{(3)} + \bar{f}_{hd_3}^{(3)} + \bar{f}_{ex_3}^{(3)} \tag{3.13}$$

$$\hat{J}_{G_3}^{(3)}\bar{\alpha}_3^{(3)} + \tilde{\omega}_3^{(3)}\hat{J}_{G_3}^{(3)}\bar{\omega}_3^{(3)} = -\hat{C}^{(3,2)}\bar{m}_{32}^{(2)} + \bar{m}_{43}^{(3)} + \frac{a_3}{2}\tilde{u}_1^{(3)}\hat{C}^{(3,2)}\bar{f}_{32}^{(2)} + \frac{a_3}{2}\tilde{u}_1^{(3)}\bar{f}_{43}^{(3)} + \bar{m}_{hs_3}^{(3)} + \bar{m}_{hd_3}^{(3)} + \bar{m}_{ex_3}^{(3)}$$

Body-4

$$m_4\bar{a}_{G_4}^{(4)} = -\hat{C}^{(4,3)}\bar{f}_{43}^{(3)} + \bar{f}_{54}^{(4)} + \bar{f}_{hs_4}^{(4)} + \bar{f}_{hd_4}^{(4)} + \bar{f}_{ex_4}^{(4)} \tag{3.14}$$

$$\hat{J}_{G_4}^{(4)}\bar{\alpha}_4^{(4)} + \tilde{\omega}_4^{(4)}\hat{J}_{G_4}^{(4)}\bar{\omega}_4^{(4)} = -\hat{C}^{(4,3)}\bar{m}_{43}^{(3)} + \bar{m}_{54}^{(4)} + \frac{a_4}{2}\tilde{u}_1^{(4)}\hat{C}^{(4,3)}\bar{f}_{43}^{(3)} + \frac{a_4}{2}\tilde{u}_1^{(4)}\bar{f}_{54}^{(4)} + \bar{m}_{hs_4}^{(4)} + \bar{m}_{hd_4}^{(4)} + \bar{m}_{ex_4}^{(4)}$$

Body-5

$$m_5\bar{a}_{G_5}^{(5)} = -\hat{C}^{(5,4)}\bar{f}_{54}^{(4)} + \bar{f}_{65}^{(5)} + \bar{f}_{hs_5}^{(5)} + \bar{f}_{hd_5}^{(5)} + \bar{f}_{ex_5}^{(5)} \tag{3.15}$$

$$\hat{J}_{G_5}^{(5)}\bar{\alpha}_5^{(5)} + \tilde{\omega}_5^{(5)}\hat{J}_{G_5}^{(5)}\bar{\omega}_5^{(5)} = -\hat{C}^{(5,4)}\bar{m}_{54}^{(4)} + \bar{m}_{65}^{(5)} + \frac{a_5}{2}\tilde{u}_3^{(5)}\hat{C}^{(5,4)}\bar{f}_{54}^{(4)} + \frac{a_5}{2}\tilde{u}_3^{(5)}\bar{f}_{65}^{(5)} + \bar{m}_{hs_5}^{(5)} + \bar{m}_{hd_5}^{(5)} + \bar{m}_{ex_5}^{(5)}$$

Body-6

$$m_6\bar{a}_{G_6}^{(6)} = -\hat{C}^{(6,5)}\bar{f}_{65}^{(5)} + \bar{f}_{hs_6}^{(6)} + \bar{f}_{hd_6}^{(6)} + \bar{f}_{ex_6}^{(6)} \tag{3.16}$$

$$\hat{J}_{G_6}^{(6)}\bar{\alpha}_6^{(6)} + \tilde{\omega}_6^{(6)}\hat{J}_{G_6}^{(6)}\bar{\omega}_6^{(6)} = -\hat{C}^{(6,5)}\bar{m}_{65}^{(5)} + \frac{a_6}{2}\tilde{u}_3^{(6)}\hat{C}^{(6,5)}\bar{f}_{65}^{(5)} + \bar{m}_{hs_6}^{(6)} + \bar{m}_{hd_6}^{(6)} + \bar{m}_{ex_6}^{(6)}$$

Let $\bar{\theta} = [\theta_1, ..., \theta_6]^T$ be the vector of the joint variables of the manipulator subsystem. The equations of motion derived in Equations (3.11) – (3.16) can then be written in compact form as follows:

$$\hat{M}_{m\theta}\ddot{\bar{\theta}} + \hat{M}_{m\eta}\dot{\bar{\eta}} + \bar{Q}_m = \bar{\tau}_m \tag{3.17}$$

$$\bar{\tau}_m = \hat{A}_m \bar{F}_{vm} + \hat{B}_m \bar{T}_m + \bar{F}_{hs_m} + \bar{F}_{hd_m} + \bar{F}_{ex_m}$$

where

$\hat{M}_{m\theta} \in \Re^{36x6}$ and $\hat{M}_{m\eta} \in \Re^{36x6}$ are the generalized mass matrices of the manipulator,

$\bar{Q}_m \in \Re^{36x1}$ is the vector of velocity dependent terms,

$\bar{F}_{vm} \in \Re^{30x1}$ is the vector of reaction forces applied on the links by the AUV,

$\bar{F}_{hs_m} \in \Re^{36x1}$, $\bar{F}_{hd_m} \in \Re^{36x1}$ are the vectors of hydrostatic and hydrodynamic forces and moments applied on the links,

$\bar{F}_{ex_m} \in \Re^{36x1}$ is the vector of external disturbance forces and moments,

$\bar{T}_m \in \Re^{6x1}$ is the vector of generalized control forces and

$\hat{A}_m \in \Re^{36x30}$, $\hat{B}_m \in \Re^{36x6}$ are coefficient matrices of the reaction forces applied on the links of the manipulator and generalized control forces of the manipulator respectively.

The factorization can be performed symbolically using any of the commercial Symbolic Math software. In this study, the Symbolic Math Toolbox of MATLAB® is used to facilitate the solution. To achieve this, all of the equations are written in an m-file and *sym* command is utilized together with the *diff* command to factor out the generalized coordinates from the dynamic equations by taking their symbolic partial derivatives.

3.2.2 Newton-Euler Equations for Redundant Manipulator Subsystem

The redundant manipulator subsystem is composed of 8 rigid bodies which are connected to each other by revolute joints. Similarly, the Newton-Euler equations and the inertia tensors for all bodies are expressed about their mass centers resulting 48 scalar equations which are given in matrix form as below.

Body-1

$$m_1\bar{a}_{G_1}^{(1)} = \hat{C}^{(1,0)}\bar{f}_{01}^{(0)} + \bar{f}_{21}^{(1)} + \bar{f}_{hs_1}^{(1)} + \bar{f}_{hd_1}^{(1)} + \bar{f}_{ex_1}^{(1)} \tag{3.18}$$

$$\hat{J}_{G_1}^{(1)}\bar{\alpha}_1^{(1)} + \tilde{\omega}_1^{(1)}\hat{J}_{G_1}^{(1)}\bar{\omega}_1^{(1)} = \hat{C}^{(1,0)}\bar{m}_{01}^{(0)} + \bar{m}_{21}^{(1)} - \frac{a_1}{2}\hat{C}^{(1,0)}\left[\tilde{u}_3^{(0)}\bar{f}_{01}^{(0)}\right] + \ldots$$
$$\frac{a_1}{2}\hat{C}^{(1,0)}\tilde{u}_3^{(0)}\left[\hat{C}^{(0,1)}\bar{f}_{21}^{(1)}\right] + \bar{m}_{hs_1}^{(1)} + \bar{m}_{hd_1}^{(1)} + \bar{m}_{ex_1}^{(1)}$$

Body-2

$$m_2\bar{a}_{G_2}^{(2)} = -\hat{C}^{(2,1)}\bar{f}_{21}^{(1)} + \bar{f}_{32}^{(2)} + \bar{f}_{hs_2}^{(2)} + \bar{f}_{hd_2}^{(2)} + \bar{f}_{ex_2}^{(2)} \tag{3.19}$$

$$\hat{J}_{G_2}^{(2)}\bar{\alpha}_2^{(2)} + \tilde{\omega}_2^{(2)}\hat{J}_{G_2}^{(2)}\bar{\omega}_2^{(2)} = -\hat{C}^{(2,1)}\bar{m}_{21}^{(1)} + \bar{m}_{32}^{(2)} + \frac{a_2}{2}\tilde{u}_1^{(2)}\hat{C}^{(2,1)}\bar{f}_{21}^{(1)} + \frac{a_2}{2}\tilde{u}_1^{(2)}\bar{f}_{32}^{(2)} + \bar{m}_{hs_2}^{(2)} + \bar{m}_{hd_2}^{(2)} + \bar{m}_{ex_2}^{(2)}$$

Body-3

$$m_3\bar{a}_{G_3}^{(3)} = -\hat{C}^{(3,2)}\bar{f}_{32}^{(2)} + \bar{f}_{43}^{(3)} + \bar{f}_{hs_3}^{(3)} + \bar{f}_{hd_3}^{(3)} + \bar{f}_{ex_3}^{(3)} \tag{3.20}$$

$$\hat{J}_{G_3}^{(3)}\bar{\alpha}_3^{(3)} + \tilde{\omega}_3^{(3)}\hat{J}_{G_3}^{(3)}\bar{\omega}_3^{(3)} = -\hat{C}^{(3,2)}\bar{m}_{32}^{(2)} + \bar{m}_{43}^{(3)} + \frac{a_3}{2}\tilde{u}_1^{(3)}\hat{C}^{(3,2)}\bar{f}_{32}^{(2)} + \frac{a_3}{2}\tilde{u}_1^{(3)}\bar{f}_{43}^{(3)} + \bar{m}_{hs_3}^{(3)} + \bar{m}_{hd_3}^{(3)} + \bar{m}_{ex_3}^{(3)}$$

Body-4

$$m_4\bar{a}_{G_4}^{(4)} = -\hat{C}^{(4,3)}\bar{f}_{43}^{(3)} + \bar{f}_{54}^{(4)} + \bar{f}_{hs_4}^{(4)} + \bar{f}_{hd_4}^{(4)} + \bar{f}_{ex_4}^{(4)} \tag{3.21}$$

$$\hat{J}_{G_4}^{(4)}\bar{\alpha}_4^{(4)} + \tilde{\omega}_4^{(4)}\hat{J}_{G_4}^{(4)}\bar{\omega}_4^{(4)} = -\hat{C}^{(4,3)}\bar{m}_{43}^{(3)} + \bar{m}_{54}^{(4)} + \frac{a_4}{2}\tilde{u}_3^{(4)}\hat{C}^{(4,3)}\bar{f}_{43}^{(3)} + \frac{a_4}{2}\tilde{u}_3^{(4)}\bar{f}_{54}^{(4)} + \bar{m}_{hs_4}^{(4)} + \bar{m}_{hd_4}^{(4)} + \bar{m}_{ex_4}^{(4)}$$

Body-5

$$m_5\bar{a}_{G_5}^{(5)} = -\hat{C}^{(5,4)}\bar{f}_{54}^{(4)} + \bar{f}_{65}^{(5)} + \bar{f}_{hs_5}^{(5)} + \bar{f}_{hd_5}^{(5)} + \bar{f}_{ex_5}^{(5)} \tag{3.22}$$

$$\hat{J}_{G_5}^{(5)}\bar{\alpha}_5^{(5)} + \tilde{\omega}_5^{(5)}\hat{J}_{G_5}^{(5)}\bar{\omega}_5^{(5)} = -\hat{C}^{(5,4)}\bar{m}_{54}^{(4)} + \bar{m}_{65}^{(5)} + \frac{a_5}{2}\tilde{u}_3^{(5)}\hat{C}^{(5,4)}\bar{f}_{54}^{(4)} + \frac{a_5}{2}\tilde{u}_3^{(5)}\bar{f}_{65}^{(5)} + \bar{m}_{hs_5}^{(5)} + \bar{m}_{hd_5}^{(5)} + \bar{m}_{ex_6}^{(6)}$$

Body-6

$$m_6\bar{a}_{G_6}^{(6)} = -\hat{C}^{(6,5)}\bar{f}_{65}^{(5)} + \bar{f}_{76}^{(6)} + \bar{f}_{hs_6}^{(6)} + \bar{f}_{hd_6}^{(6)} + \bar{f}_{ex_6}^{(6)} \tag{3.23}$$

$$\hat{J}_{G_6}^{(6)}\bar{\alpha}_6^{(6)} + \tilde{\omega}_6^{(6)}\hat{J}_{G_6}^{(6)}\bar{\omega}_6^{(6)} = -\hat{C}^{(6,5)}\bar{m}_{65}^{(5)} + \bar{m}_{76}^{(6)} + \frac{a_6}{2}\tilde{u}_1^{(6)}\hat{C}^{(6,5)}\bar{f}_{65}^{(5)} + \frac{a_6}{2}\tilde{u}_1^{(6)}\bar{f}_{76}^{(6)} + \bar{m}_{hs_6}^{(6)} + \bar{m}_{hd_6}^{(6)} + \bar{m}_{ex_6}^{(6)}$$

Body-7

$$m_7\bar{a}_{G_7}^{(7)} = -\hat{C}^{(7,6)}\bar{f}_{76}^{(6)} + \bar{f}_{87}^{(7)} + \bar{f}_{hs_7}^{(7)} + \bar{f}_{hd_7}^{(7)} + \bar{f}_{ex_7}^{(7)} \tag{3.24}$$

$$\hat{J}_{G_7}^{(7)}\bar{\alpha}_7^{(7)} + \tilde{\omega}_7^{(7)}\hat{J}_{G_7}^{(7)}\bar{\omega}_7^{(7)} = -\hat{C}^{(7,6)}\bar{m}_{76}^{(6)} + \bar{m}_{87}^{(7)} + \frac{a_7}{2}\tilde{u}_3^{(7)}\hat{C}^{(7,6)}\bar{f}_{76}^{(6)} + \frac{a_7}{2}\tilde{u}_3^{(7)}\bar{f}_{87}^{(7)} + \bar{m}_{hs_7}^{(7)} + \bar{m}_{hd_7}^{(7)} + \bar{m}_{ex_7}^{(7)}$$

Body-8

$$m_8\bar{a}_{G_8}^{(8)} = -\hat{C}^{(8,7)}\bar{f}_{87}^{(7)} + \bar{f}_{hs_8}^{(8)} + \bar{f}_{hd_8}^{(8)} + \bar{f}_{ex_8}^{(8)} \tag{3.25}$$

$$\hat{J}_{G_8}^{(8)}\bar{\alpha}_8^{(8)} + \tilde{\omega}_8^{(8)}\hat{J}_{G_8}^{(8)}\bar{\omega}_8^{(8)} = -\hat{C}^{(8,7)}\bar{m}_{87}^{(7)} + \frac{a_8}{2}\tilde{u}_3^{(8)}\hat{C}^{(8,7)}\bar{f}_{87}^{(7)} + \bar{m}_{hs_8}^{(8)} + \bar{m}_{hd_8}^{(8)} + \bar{m}_{ex_8}^{(8)}$$

This time, let $\bar{\theta} = \left[\theta_1,...,\theta_8\right]^T$ be the vector of the joint variables of the redundant manipulator subsystem. The equations of motion can similarly be written in factored form as follows:

$$\hat{M}_{m\theta}\ddot{\bar{\theta}} + \hat{M}_{m\eta}\dot{\bar{\eta}} + \bar{Q}_m = \bar{\tau}_m \tag{3.26}$$

$$\bar{\tau}_m = \hat{A}_m \bar{F}_{vm} + \hat{B}_m \bar{T}_m + \bar{F}_{hs_m} + \bar{F}_{hd_m} + \bar{F}_{ex_m}$$

where

$\hat{M}_{m\theta} \in \Re^{48x8}$, $\hat{M}_{m\eta} \in \Re^{48x6}$ are the generalized mass matrices of the manipulator,

$\bar{Q}_m \in \Re^{48x1}$ is the vector of velocity dependent terms,

$\bar{F}_{vm} \in \Re^{40x1}$ is the vector of reaction forces applied on the links by the AUV,

$\bar{F}_{hs_m} \in \Re^{48x1}, \bar{F}_{hd_m} \in \Re^{48x1}$ are the vectors of hydrostatic and hydrodynamic forces applied on the links,

$\bar{F}_{ex_m} \in \Re^{48x1}$ is the vector of external disturbance forces and moments,

$\bar{T}_m \in \Re^{8x1}$ is the vector of generalized control forces and

$\hat{A}_m \in \Re^{48x40}, \hat{B}_m \in \Re^{48x8}$ are coefficient matrices of the reaction forces applied on the links of the manipulator and generalized control forces of the manipulator respectively.

3.3 Hydrostatic Forces and Moments

A fully submerged body in a fluid experiences some restoring effects under gravitational field due to the masses of itself and the surrounding fluid. These effects can be combined into resultant force vectors named as *gravitational force (i.e. weight)* and *buoyant force (i.e. buoyancy)*. The position vectors expressed in body reference frames as illustrated in Figure 3.3 defined respectively to the center of gravity (i.e. Point C_{G_i}) and the center of buoyancy (i.e. Point C_{B_i}) of the i^{th} rigid body from the origin of body fixed frame (i.e. Point O_i) can be written as

$$\bar{r}_{G_i}^{(i)} = \bar{r}_{G_i/O_i}^{(i)} = \begin{bmatrix} x_{G_i} \\ y_{G_i} \\ z_{G_i} \end{bmatrix} \tag{3.27}$$

$$\overline{r}_{B_i}^{(i)} = \overline{r}_{B_i/O_i}^{(i)} = \begin{bmatrix} x_{B_i} \\ y_{B_i} \\ z_{B_i} \end{bmatrix} \tag{3.28}$$

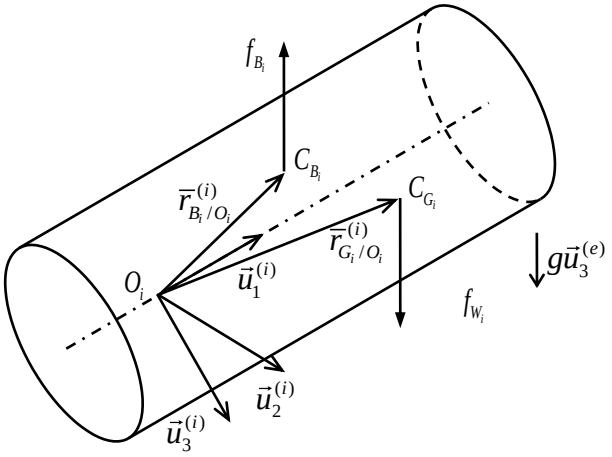

Figure 3.1 Hydrostatic Forces

It should be noted that the center of gravity is generally located below the center of buoyancy considering the static stability of the body.

$\therefore$ *Weight*

The weight of a rigid body totally submerged in a fluid can be expressed in inertial reference frame as

$$\overline{f}_{W_i}^{(e)} = \begin{bmatrix} 0 \\ 0 \\ m_i g \end{bmatrix} \tag{3.29}$$

where

m_i is the mass of the i^{th} body,

g is local gravitational acceleration which is taken to be 9.81 m/s^2.

$\therefore$ *Buoyancy*

The buoyancy force of a rigid body totally submerged in a fluid can be expressed in inertial reference frame as

$$\overline{f}_{B_i}^{(e)} = \begin{bmatrix} 0 \\ 0 \\ -\rho_w \upsilon_i g \end{bmatrix} \tag{3.30}$$

where

υ_i is the volume swept by the i^{th} body,

ρ_w is the sea water density which is taken to be 1020 kg/m^3.

Since Newton-Euler equations are derived in body fixed reference frames, total hydrostatic force applied on the i^{th} body as expressed in its own frame is formulated as below.

$$\overline{f}_{hs_i}^{(i)} = \overline{f}_{W_i}^{(i)} + \overline{f}_{B_i}^{(i)} = \hat{C}^{(i,e)} \left[\overline{f}_{W_i}^{(e)} + \overline{f}_{B_i}^{(e)} \right] \tag{3.31}$$

where $\hat{C}^{(i,e)}$ is the transformation matrix that transforms the coordinates expressed in $\Im_e$ to the ones in the i^{th} reference frame.

In a similar way, restoring moments corresponding to the restoring forces are obtained in body fixed frames as

$$\overline{m}_{hs_i}^{(i)} = \tilde{r}_{G_i} \overline{f}_{W_i}^{(i)} + \tilde{r}_{B_i} \overline{f}_{B_i}^{(i)} \tag{3.32}$$

Combining Equation (3.31) and Equation (3.32) gives consequent generalized hydrostatic force vector applied on the i^{th} rigid body as expressed in its own frame as

$$\overline{F}_{hs_i}^{(i)} = \begin{bmatrix} \overline{f}_{hs_i}^{(i)} \\ \overline{m}_{hs_i}^{(i)} \end{bmatrix} \tag{3.33}$$

3.4 Hydrodynamic Effects

Modeling effects due to motion underwater is a rather complex task. It is too hard to generate even a model for some of the hydrodynamic effects. In this study, the effects are modeled utilizing the efforts of researchers on the individual effects in the literature as well as the theory grounded in the context of aerodynamics. Therefore, the hydrodynamic forces acting on a fully submerged body due to its motion in the surrounding media are considered to be *the added mass/inertia forces* and *the damping forces*. These forces are expressed in the relevant body frames for both the AUV and the manipulator links as below:

$$\bar{F}_{hd}^{(i)} = \bar{F}_{A}^{(i)} + \bar{F}_{D}^{(i)} \tag{3.34}$$

In the following sections, these hydrodynamic forces acting on a rigid body moving in a fluid are discussed in detail.

3.4.1 Added Mass/Inertia Forces and Moments

When a body is accelerated through a fluid, some of the surrounding fluid is also accelerated with the body. A force is exerted on the surrounding fluid to achieve this acceleration, and the reaction force, which is equal in magnitude and opposite in direction, is exerted on the body. The latter is referred to as the added mass force [56]. This is a resulting fact that the density of the sea water is comparable to the density of the body itself. The forces and moments associated with this effect can be formulated as

$$\bar{F}_{A}^{(i)} = -\hat{M}_{A_i} \begin{bmatrix} \bar{a}_{O_i}^{(i)} \\ \bar{\alpha}_{i}^{(i)} \end{bmatrix} - \bar{C}_{A_i} \tag{3.35}$$

where

$\hat{M}_{A_i} \in \Re^{6x6}$ is the added mass matrix,

$\bar{C}_{A_i} \in \Re^{6x1}$ is the vector of Coriolis and centrifugal terms due to the added mass of the i^{th} rigid body.

The added mass coefficients which are the entries of these matrices depend on the geometry of the bodies. Considering a fully submerged body having a shape with three planes of symmetry and assuming that the velocity of the body is low, the cross flow added mass terms will then be equal to zero. In such a case, the $\hat{M}_{A_i}$ and $\bar{C}_{A_i}$ in Equation (3.35) will simply reduce to

$$\hat{M}_{A_i} = -diag[X_{a_{i_1}} \quad Y_{a_{i_2}} \quad Z_{a_{i_3}} \quad K_{\alpha_{i_1}} \quad M_{\alpha_{i_2}} \quad N_{\alpha_{i_3}}] \tag{3.36}$$

$$\bar{C}_{A_i} = \begin{bmatrix} 0 & 0 & 0 & 0 & -Z_{a_{i_3}} v_{i_3} & Y_{a_{i_2}} v_{i_2} \\ 0 & 0 & 0 & Z_{a_{i_3}} v_{O_{i_3}} & 0 & -X_{a_{i_1}} v_{O_{i_1}} \\ 0 & 0 & 0 & -Y_{a_{i_2}} v_{O_{i_2}} & X_{a_{i_1}} v_{O_{i_1}} & 0 \\ 0 & -Z_{a_{i_3}} v_{O_{i_3}} & Y_{a_{i_2}} v_{O_{i_2}} & 0 & -N_{\alpha_{i_3}} \omega_{i_3} & M_{\alpha_{i_2}} \omega_{i_2} \\ Z_{a_{i_3}} v_{O_{i_3}} & 0 & -X_{a_{i_1}} v_{O_{i_3}} & N_{\alpha_{i_3}} \omega_{i_3} & 0 & -K_{\alpha_{i_1}} \omega_{i_1} \\ -Y_{a_{i_2}} v_{O_{i_2}} & X_{a_{i_1}} v_{O_{i_1}} & 0 & -M_{\alpha_{i_2}} \omega_{i_2} & K_{\alpha_{i_1}} \omega_{i_1} & 0 \end{bmatrix} \begin{bmatrix} \bar{v}_{O_i}^{(i)} \\ \bar{\omega}_i^{(i)} \end{bmatrix} \tag{3.37}$$

The AUV of the UVMS has prolate spheroidal shape having three planes of symmetry. Let us consider an ellipsoid totally submerged with its origin at its geometric center which can be described as

$$\frac{x^2}{a^2} + \frac{y^2}{b^2} + \frac{z^2}{c^2} = 1 \tag{3.38}$$

where a, b and c are the semi axes.

By setting a>b=c, this ellipsoid turns out to be a prolate spheroid. The expressions for the added mass coefficients can be theoretically derived using the geometry of the body by applying the strip theory. The expressions obtained for the diagonal added mass coefficients of the AUV can be found in [51] as

$$\dot{X}_{v_1} = -\frac{\alpha_0}{2-\alpha_0} m_v \tag{3.39}$$

$$\dot{Y}_{v_2} = \dot{Z}_{v_3} = -\frac{\beta_0}{2-\beta_0} m_v \tag{3.40}$$

$$\dot{K}_{\omega_1} = 0 \tag{3.41}$$

$$\dot{N}_{\omega_2} = \dot{M}_{\omega_3} = -\frac{1}{5} \frac{\left(b^2 - a^2\right)^2 \left(\alpha_0 - \beta_0\right)}{2\left(b^2 - a^2\right) + \left(b^2 + a^2\right)\left(\beta_0 - \alpha_0\right)} m_v \tag{3.42}$$

where the mass of the AUV is calculated using

$$m_v = \frac{4}{3} \pi a b^2 \rho_v \tag{3.43}$$

Let us define the eccentricity as

$$e = 1 - \left(\frac{b}{a}\right)^2 \tag{3.44}$$

The constants α_0 and β_0 that appear in Equations (3.39), (3.40) and (3.42) are calculated in terms of the eccentricity as below.

$$\alpha_0 = \frac{2\left(1-e^2\right)}{e^3} \left(\frac{1}{2} \ln \frac{1+e}{1-e} - e\right) \tag{3.45}$$

$$\beta_0 = \frac{1}{e^2} - \frac{1-e^2}{2e^3} \ln \frac{1+e}{1-e} \tag{3.46}$$

The links of the manipulator subsystem, on the other hand, have cylindrical geometry. Considering a link having mass m_i, density ρ_i, length l_i and radius r_i, the expressions for the diagonal added mass coefficients are given in [49] as

$$\dot{X}_{v_{1_i}} = -0.1 m_i \tag{3.47}$$

$$\dot{Y}_{v_{2_i}} = \dot{Z}_{v_{3_i}} = -\pi \rho_i r_i^2 l_i \tag{3.48}$$

$$\dot{K}_{\omega_{1_i}} = 0 \tag{3.49}$$

$$\dot{N}_{\omega_{2_i}} = \dot{M}_{\omega_{3_i}} = -\frac{1}{12} \pi \rho_i r_i^2 l_i^3 \tag{3.50}$$

3.4.2 Damping Forces and Moments

3.4.2.1 Damping Forces

The damping forces acting on a fully submerged body take place due to the viscosity of the fluid. All fluids possess viscosity which is defined to be the measure of the fluid's resistance to flow. As the definition implies, these forces act along axes parallel and perpendicular to the direction of flow. These axes along which the damping forces act form a frame called *current frame* which is shown in Figure 3.2.

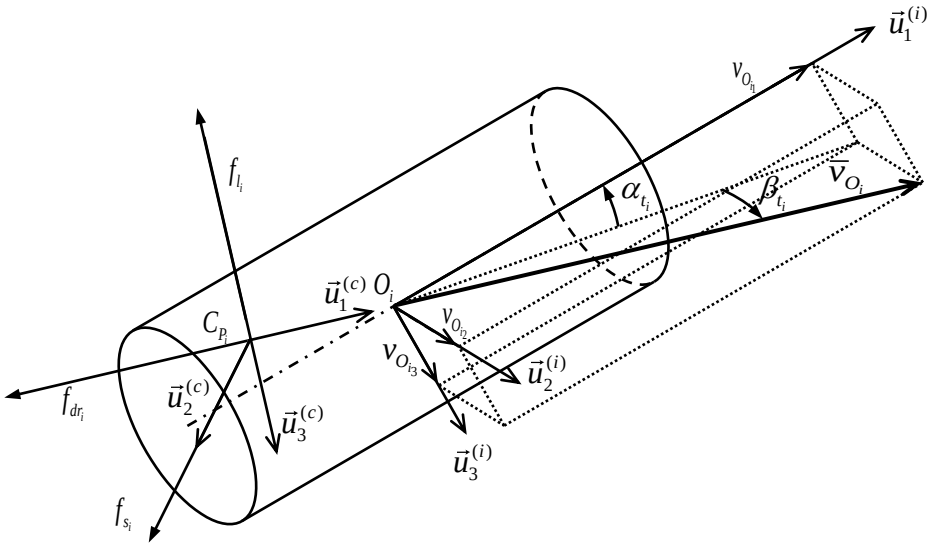

Figure 3.2 Damping Forces & Current Frame

In Figure 3.2, $\vec{u}_i^{(c)}$, $i = 1,2,3.$ denote the unit vectors of the current frame. The damping forces can be decomposed into *drag force* $\bar{f}_{D_i}$, *lift force* $\bar{f}_{L_i}$ and *side force* $\bar{f}_{S_i}$

in the current frame and are assumed to act at a point which is called the *hydrodynamic center of pressure* of the body (i.e. Point C_{P_i}). This decomposition is analogous to the one in aerodynamics.

In addition to above definitions, the angle between the relative flow velocity vector and the surge velocity vector of the body is called *the angle of attack* α_t and is defined in terms of the velocity components as

$$\alpha_t = tg^{-1}\left[\frac{v_{O_{i3}}}{v_{O_{i1}}}\right] \tag{3.51}$$

and the angle between the relative flow velocity vector and the resultant velocity vector formed by surge and heave components of the body is called *the sideslip angle* β_t and is formulated as

$$\beta_t = \sin^{-1}\left[\frac{v_{O_{i2}}}{|\bar{v}_{O_i}|}\right] \tag{3.52}$$

where the norm of the relative velocity vector is

$$|\bar{v}_{O_i}| = \sqrt{\left(v_{O_{i1}}\right)^2 + \left(v_{O_{i2}}\right)^2 + \left(v_{O_{i3}}\right)^2}\,. \tag{3.53}$$

3.4.2.1.1 Drag Forces

The drag forces are generally decomposed into the pressure drag and shear drag constituents. They oppose the direction of the velocity of the body and can be expressed in current frame as

$$\bar{f}_{D_i} = -f_{dr_i}\bar{u}_1^{(c)} \tag{3.54}$$

The magnitude of the drag force can be formulated as

$$f_{dr_i} = C_{D_i} q_{\infty_i} S_i \tag{3.55}$$

In Equation (3.55), C_{D_i} is the drag coefficient, q_{∞_i} is the dynamic pressure of the i^{th} body written in terms of the sea water density ρ_w and the velocity of the body $\left|\overline{v}_{O_i}\right|$ as

$$q_{\infty_i} = \frac{1}{2}\rho_w \left|\overline{v}_{O_i}\right|^2 \tag{3.56}$$

and S_i is the frontal area of the i^{th} body which can be obtained as

$$S_i = \frac{\pi}{4} d_i^2 \tag{3.57}$$

The drag coefficient can be calculated as described in [52] as

$$C_{D_i} = \left[C_{f_i} \left(1 + \frac{60 d_i^3}{l_i^3} + 0.0025 \frac{l_i}{d_i} \right) \frac{4 S_{p_i}}{\pi d_i^2} + C_{D_{b_i}} \right] \frac{\pi d_i^2}{4 l_i^2} \tag{3.58}$$

$$C_{D_{b_i}} = \frac{0.029}{\sqrt{C_{f_i} \left(1 + \frac{60 d_i^3}{l_i^3} + 0.0025 \frac{l_i}{d_i} \right) \frac{4 S_{p_i}}{\pi d_i^2}}} \left(\frac{d_{b_i}}{d_i} \right)^3 \tag{3.59}$$

In Equations (3.58) and (3.59),

C_{f_i} is the skin friction coefficient,

$C_{D_{b_i}}$ is the base drag coefficient,

l_i is the characteristic length,

d_i is the maximum diameter,

d_{b_i} is the base diameter,

S_{p_i} is the peripheral area of the i^{th} body.

The skin friction coefficient can be estimated as

$$C_{f_i} = \frac{0.075}{\left[log(Re) - 2\right]^2} \tag{3.60}$$

where *Re* is the Reynolds number.

3.4.2.1.2 Lift Forces

The lift forces take place due to the pressure difference arising when a rigid body moves with an angle of attack α_t. These forces act perpendicularly to horizontal plane of the body fixed frame tilted by the angle α_t opposing the direction of the relative flow and are expressed in the current frame as

$$\overline{f}_{L_i} = -f_{l_i}\overline{u}_3^{(c)} \tag{3.61}$$

The magnitude of the lift force can be formulated as

$$f_{l_i} = C_{L_i} q_{\infty_i} S_i \tag{3.62}$$

where C_{L_i} is the lift coefficient of the i^{th} body.

The lift coefficient can be calculated as

$$C_{L_i} = C_{L\alpha_i}\alpha_{t_i} + C_{Lq_i}\frac{d_i}{2\left|\overline{v}_{O_i}\right|}\omega_{i_2} \tag{3.63}$$

Here, $C_{L\alpha_i}$ and C_{Lq_i} are called the hydrodynamic derivatives that defines the change in the lift coefficient C_{L_i} with respect to the angle of attack α_{t_i} and the second component of the angular velocity of the i^{th} body, i.e. ω_{i_2}. As Equation (3.63) reveals, the lift forces can be small and neglected at small values of the angle of attack. However, they become significant at higher angles of attack and should be taken into account. These hydrodynamic derivatives can be computed using the formulas derived in [52] as

$$C_{L\alpha_i} = \frac{2(k_2 - k_1)S_i}{l_i^2} \tag{3.64}$$

where $(k_2 - k_1)$ is the apparent mass factor developed by [53] as given in Figure 3.3 as a function of the fineness ratio of the body.

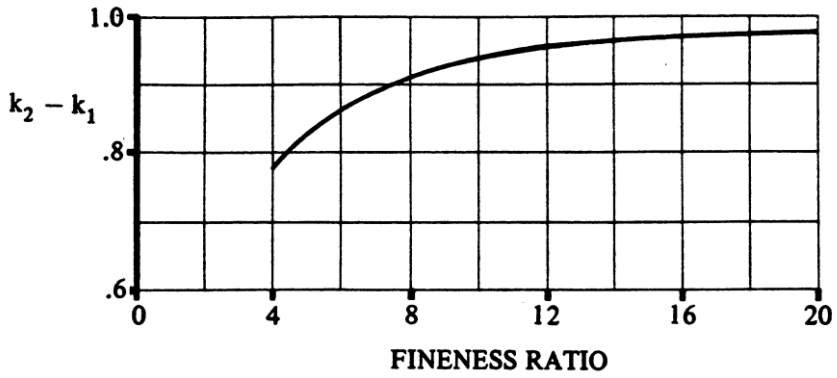

Figure 3.3 Apparent Mass Factor [53]

It should be noted that the body fineness ratio is defined as the ratio of the length of the body and to its diameter as below.

$$fr_i = \frac{l_i}{d_i} \tag{3.65}$$

On the other hand, the derivative C_{Lq_i} is calculated as

$$C_{Lq_i} = 2C_{L\alpha_i}\left(1-\frac{x_{n_i}}{l_i}\right)\frac{S_i}{l_i^2} \tag{3.66}$$

where x_{n_i} is the longitudinal distance from the body nose to the origin of the body fixed frame. The Equation (3.66) is simply reduced to the following expression since the origins of the AUV and the links are selected to be at their geometric centers, i.e. $x_{n_i} = l_i/2$.

$$C_{Lq_i} = C_{L\alpha_i}\frac{S_i}{l_i^2} \tag{3.67}$$

A more detailed theoretical and experimental discussion on the lift and drag forces can be obtained in [54-57].

3.4.2.1.3 Side Forces

The side forces take place due to the pressure difference arising when a rigid body moves with a side-slip angle. These forces act perpendicularly to the plane of the lift and drag forces and are expressed in the current frame as

$$\overline{f}_{S_i} = f_{s_i}\overline{u}_2^{(c)} \tag{3.68}$$

The magnitude of the side force can be formulated as

$$f_{s_i} = C_{S_i}\, q_{\infty_i}\, S_i \tag{3.69}$$

where C_{S_i} is the side coefficient of the i^{th} body.

In a similar fashion, the side coefficient can be decomposed as

$$C_{S_i} = C_{S\beta_i}\,\beta_{t_i} + C_{Sr_i}\frac{d_i}{2\left|\overline{v}_{O_i}\right|}\omega_{i_3} \tag{3.70}$$

Here, $C_{S\beta_i}$ and C_{Sr_i} are defined as the changes in the side coefficient C_{S_i} with respect to the angle of attack β_{t_i} and the third component of the angular velocity of the i^{th} body, i.e. ω_{i_3}.

The estimation of the side force acting on a submerged body is studied by various authors as explained in [58]. Most of the results in these studies are based on measuring the data obtained by testing the wires used in fishing gears as shown in Figure 3.4.

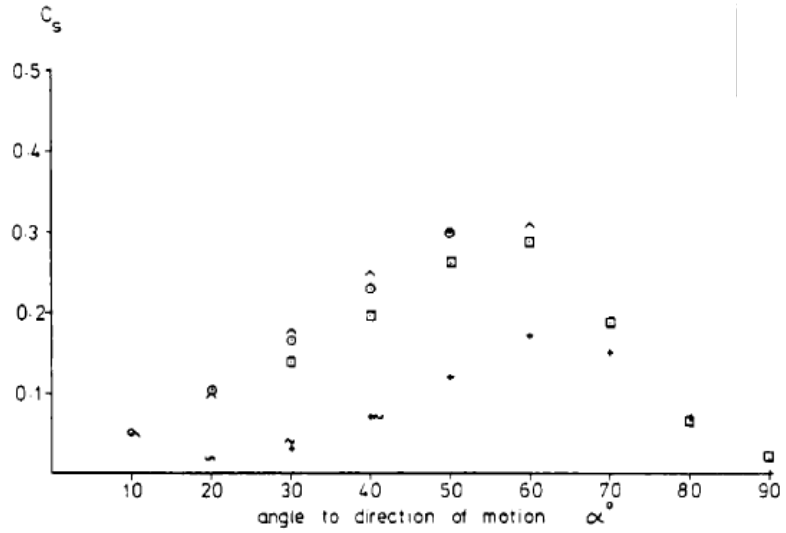

Figure 3.4 The Side Force Coefficient Variations [58]

Therefore, the side coefficient C_{S_i} with respect to the angle of attack β_{t_i} can be obtained using upper and lower limits of the angles by interpolation given in Equation (3.71).

$$C_{S\beta} = C_{S\beta}(\beta_l) + \frac{\beta - \beta_l}{\beta_u - \beta_l}\left[C_{S\beta}(\beta_u) - C_{S\beta}(\beta_l)\right] \tag{3.71}$$

Substitution yields

$$C_{S\beta}\,\beta = \begin{cases} 0.344\beta & 0 \le \beta < 50^o \\ 0.675 - 0.428\beta & 50 \le \beta \le 90^o \end{cases} \tag{3.72}$$

Similarly, C_{Sr_i} can be derived as in Equation (3.73) as

$$C_{Sr_i} = C_{S\beta_i} \frac{S_i}{l_i^2} \tag{3.73}$$

Having completed the effect of the individual forces on the body, total hydrodynamic force vector can be expressed in the current axis system as

$$\overline{f}_{d_i}^{(c)} = \begin{bmatrix} -f_{dr_i} \\ f_{s_i} \\ -f_{l_i} \end{bmatrix} \tag{3.74}$$

In order to plug these forces into the system dynamic equations, one needs to transform the vector of damping forces expressed in the current frame into the ones expressed in the body frame. Let the current frame be denoted as $\Im_c$. The forces of the body in $\Im_c$ can be transformed into the body fixed frame of the i^{th} body $\Im_i$ by using the following sequence.

$$\Im_c \xrightarrow[\vec{u}_3^{(c)}=\vec{u}_3^{(m)}]{-\beta_t} \Im_m \xrightarrow[\vec{u}_2^{(m)}=\vec{u}_2^{(i)}]{\alpha_t} \Im_i$$

where $\Im_m$ stands for the intermediate frame.

In order to find coordinate transformation matrix $\hat{C}^{(c,i)}$, elementary rotation matrices are used as in the following equations.

$$\hat{C}^{(c,i)} = \hat{C}^{(c,m)} \hat{C}^{(m,i)} \tag{3.75}$$

where

$$\hat{C}^{(c,m)} = e^{\tilde{u}_3 - \beta_t} = \begin{bmatrix} c\beta_t & s\beta_t & 0 \\ -s\beta_t & c\beta_t & 0 \\ 0 & 0 & 1 \end{bmatrix} \tag{3.76}$$

$$\hat{C}^{(m,i)} = e^{\tilde{u}_2 \alpha_t} = \begin{bmatrix} c\alpha_t & 0 & s\alpha_t \\ 0 & 1 & 0 \\ -s\alpha_t & 0 & c\alpha_t \end{bmatrix} \tag{3.77}$$

Substituting Equation (3.76) and Equation (3.77) into Equation (3.75) gives the transformation matrix as

$$\hat{C}^{(c,i)} = \begin{bmatrix} c\alpha_t c\beta_t & s\beta_t & s\alpha_t c\beta_t \\ -c\alpha_t s\beta_t & c\beta_t & -s\alpha_t s\beta_t \\ -s\alpha_t & 0 & c\alpha_t \end{bmatrix} \tag{3.78}$$

where $s(.) = \sin(.)$ & $c(.) = \cos(.)$.

In order to obtain the damping forces vector $\overline{f}_{d_i}^{(i)}$ exerted on the i^{th} body which is expressed in $\Im_i$, the following equation can be used.

$$\overline{f}_{d_i}^{(i)} = \left[\hat{C}^{(c,i)}\right]^T \overline{f}_{d_i}^{(c)} \tag{3.79}$$

Let f_{d_x}, f_{d_y} and f_{d_z} be the components of the damping forces vector $\overline{f}_{d_i}^{(i)}$. By substituting Equation (3.74) and Equation (3.78) into Equation (3.79) gives the following relations

$$f_{d_x} = -f_{dr_i} c\alpha_t c\beta_t - f_{s_i} c\alpha_t s\beta_t + f_{l_i} s\alpha_t \tag{3.80}$$

$$f_{d_y} = -f_{dr_i} s\beta_t + f_{s_i} c\beta_t \tag{3.81}$$

$$f_{d_z} = -f_{dr_i} s\alpha_t c\beta_t - f_{s_i} s\alpha_t s\beta_t - f_{l_i} c\alpha_t \tag{3.82}$$

As seen from Equations (3.80)–(3.82), all three forces have contributions to the force components in surge and heave directions. However, the lift force does not have any effect on the force component in sway direction.

3.4.2.2 Damping Moments

The damping moments are caused by the damping forces acting at the hydrodynamic center of pressure of the body and the relative angular velocities of the body itself. These moments are rolling, pitching and yawing moments along the axes of the current frame and they can be expressed in vectorial form as

$$\bar{m}_{d_i}^{(c)} = \begin{bmatrix} m_{r_i} \\ m_{p_i} \\ m_{y_i} \end{bmatrix} \tag{3.83}$$

These components are generally expressed in terms of the dynamic pressure q_{∞_i}, frontal area S_i and the diameter d_i of the body as

$$m_{r_i} = C_{l_i} q_{\infty_i} S_i d_i \tag{3.84}$$

$$m_{p_i} = C_{m_i} q_{\infty_i} S_i d_i \tag{3.85}$$

$$m_{y_i} = C_{n_i} q_{\infty_i} S_i d_i \tag{3.86}$$

where $C_{l_i}, C_{m_i}, C_{n_i}$ are the moment coefficients of the i^{th} body.

The moment coefficients are composed of the individual effects that are due to the center of pressure offset and the angular velocities of the body and can be expressed as in the following relations.

$$C_{l_i} = C_{l\beta_i} \beta_{t_i} + C_{lp_i} \frac{d_i}{2\left|\bar{v}_{O_i}\right|} \omega_{i_1} \tag{3.87}$$

$$C_{m_i} = C_{m\alpha_i} \alpha_{t_i} + C_{mq_i} \frac{d_i}{2\left|\bar{v}_{O_i}\right|} \omega_{i_2} \tag{3.88}$$

$$C_{n_i} = C_{n\beta_i}\,\beta_{t_i} + C_{nr_i}\,\frac{d_i}{2\left|\bar{v}_{O_i}\right|}\,\omega_{i_3} \tag{3.89}$$

For the symmetric bodies, however, the center of pressure can be considered to be coincident with the buoyancy center of the body. If the origin of the body fixed frame is selected as the buoyancy center, then the moment contribution due to the pressure offset can be neglected. Therefore, it is sufficient to calculate the velocity related coefficients C_{lp}, C_{mq} and C_{nr} to obtain the total damping moments acting on the body. These coefficients can be calculated using the formulas derived in [64].

In order to obtain the damping moments vector $\bar{m}_{d_i}^{(i)}$ exerted on the i^{th} body which is expressed in its own frame, the following transformation is needed.

$$\bar{m}_{d_i}^{(i)} = \left[\hat{C}^{(c,i)}\right]^T \bar{m}_{d_i}^{(c)} \tag{3.90}$$

Consequently, the generalized hydrodynamic damping force vector $\bar{F}_D^{(i)}$ applied on the i^{th} rigid body as expressed in its own frame can be obtained by combining Equation (3.79) and Equation (3.90) as

$$\bar{F}_{D_i}^{(i)} = \begin{bmatrix} \bar{f}_{d_i}^{(i)} \\ \bar{m}_{d_i}^{(i)} \end{bmatrix} \tag{3.91}$$

3.4.3 The Shadowing Effect

When the relative velocity vector of a body is directed toward the others, it prevents some part of the hydrodynamic force acting on them. This phenomenon can be called as *the shadowing effect*. The shadowed area cannot contribute to the total hydrodynamic force acting on that body and the magnitude of the velocity vector decreases due to the velocity of the body to which it is connected. Therefore, it is highly important to include the shadowing effects of bodies in the calculation of the hydrodynamic forces in order to create more realistic models.

For the sake of simplicity and convenience, let us consider two links connected to each other as shown in Figure 3.5 and denote their relative velocities by $\overline{v}_{O_i}$ and $\overline{v}_{O_{i+1}}$ respectively.

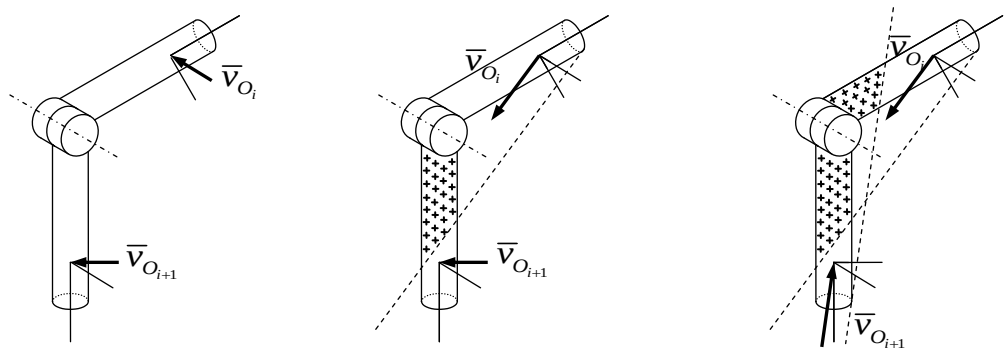

Figure 3.5 Shadowing Effects

The first case is a simple illustration that there is no shadowing effect between the links. The second case shows when one of the links affects the other link. In such a situation, the velocity and peripheral area of the affected link are recalculated as

$$\overline{v}^*_{O_{i+1}} = \overline{v}_{O_{i+1}} - \hat{C}^{(i+1,i)}\overline{v}_{O_i} \tag{3.92}$$

$$S^*_{p_{i+1}} = d_{i+1}\left(l_{i+1} - \overline{u}_1^t \hat{C}^{(i+1,i)} l_i \overline{u}_1\right) \tag{3.93}$$

where $\hat{C}^{(i+1,i)}$ is the transformation matrix that transforms the coordinates expressed in i^{th} frame to ones in $(i+1)^{th}$ frame.

The third case demonstrating the condition where two links affect each other necessitates the following additional recalculations.

$$\overline{v}^*_{O_i} = \overline{v}_{O_i} - \hat{C}^{(i,i+1)}\overline{v}_{O_{i+1}} \tag{3.94}$$

$$S^*_{p_i} = d_i\left(l_i - \overline{u}_1^t \hat{C}^{(i,i+1)} l_{i+1} \overline{u}_1\right) \tag{3.95}$$

The starred quantities are taken as the new values in computing only the hydrodynamic forces on the rigid bodies.

3.4.4 The Effect of Ocean Currents

The ocean currents are mainly caused by tidal movement, the atmospheric wind system over the sea surface, the heat exchange at the sea surface, the changes in the salinity of the sea water and the Coriolis force due to Earth's rotation [49].

Although there are various approaches in modeling the ocean current, in this study, however, it is considered to be as an external disturbance which is expressed as a randomly changing force exerted on all bodies of the system in the y direction of the Earth-fixed frame.

$$\overline{f}_{ex}^{(e)} = \begin{bmatrix} 0 \\ f_c \\ 0 \end{bmatrix} \tag{3.96}$$

Fossen [49] used a first order Gauss-Markov process to model the ocean current velocity. Here, the ocean current is assumed to induce a disturbing force $f_c(t)$ of similar nature. Thus, it is modeled according to the following differential equation.

$$\dot{f}_c(t) + 0.1 f_c(t) = n(t) \tag{3.97}$$

where *n(t)* is a zero mean Gaussian white noise.

This process should be limited such that $f_{c_{\min}}(t) \le f_c(t) \le f_{c_{\max}}(t)$ by taking the initial value as the mean value of the upper and lower limits to create a realistic ocean current effect. In order to obtain the disturbance force on each body of the UVMS as expressed in their own frames, one needs to transform $f_c(t)$ in proportion to the masses of the AUV and the manipulator links as defined below:

$$\overline{f}_{ex_i}^{(i)} = \frac{m_i}{m_t} \hat{C}^{(i,e)} \overline{f}_{ex}^{(e)} \tag{3.98}$$

where m_t is the total mass of the UVMS. By presuming that the current is irrotational and that the point of application of this force is the center of buoyancy of the i^{th} body, the moments can be calculated as

$$\bar{m}_{ex_i}^{(i)} = \tilde{r}_{B_i}^{(i)} \bar{f}_{ex_i}^{(i)} \tag{3.99}$$

Though, the moments induced by the current on the manipulator links can be neglected, i.e. $\bar{m}_{ex_i}^{(i)} = \bar{0}$, $i = 1,...,6$.

Consequently, the generalized external force vector $\bar{F}_{ex_i}^{(i)}$ applied on the i^{th} rigid body as expressed in its own frame can be obtained by combining Equation (3.98) and Equation (3.99) as

$$\bar{F}_{ex_i}^{(i)} = \begin{bmatrix} \bar{f}_{ex_i}^{(i)} \\ \bar{m}_{ex_i}^{(i)} \end{bmatrix} \tag{3.100}$$

3.5 Thruster Dynamics

Underwater vehicles are generally actuated by electrical motors that drive the propellers of the thrusters. The torques generated by these motors create the actual thrust forces. The thruster dynamics have great influence on the overall dynamics of the UVMS. There are many studies given in [59-63] addressing the problem of the influence of thruster dynamics on overall system behavior and the importance of its incorporation into control system design.

Yoerger *et al.* [60] indicated that neglecting this dynamics may result in a limited bandwidth controller with limit cycle instability and developed a simple thruster model as given in Figure 3.6. Under the assumption that the thruster dynamics have much smaller time constants than the vehicle dynamics, a simple thruster model can be described by using the following equations.

$$\dot{\Omega}_k + \alpha_{t_k} |\Omega_k| \Omega_k = \beta_{t_k} \tau_k$$
$$f_{th_k} = C_{t_k} |\Omega_k| \Omega_k \tag{3.101}$$

where

Ω_k is the angular velocity of the k^{th} propeller,

τ_k is the motor torque provided by the k^{th} thruster,

$\alpha_{t_k}, \beta_{t_k}, C_{t_k}$ are the constant model parameters.

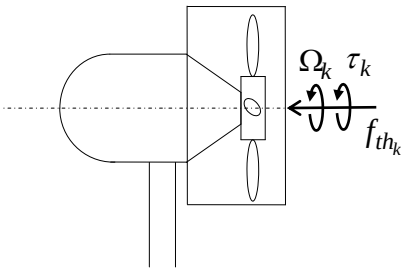

Figure 3.6 Thruster Model [60]

The model parameters given in [60] are the functions of the propeller efficiency υ_{t_k}, the sea water density ρ_w, the propeller pitch p_{t_k}, the area A_{t_k} and the volume V_{t_k} are

$$\alpha_{t_k} = \frac{\upsilon_{t_k} p_{t_k} A_{t_k}}{2V_{t_k}} \tag{3.102}$$

$$\beta_{t_k} = \frac{1}{V_{t_k} \rho_w \upsilon_{t_k}^2 p_{t_k}^2} \tag{3.103}$$

$$C_{t_k} = A_{t_k} \rho_w \upsilon_{t_k}^2 p_{t_k}^2 \tag{3.104}$$

The fully actuated AUV is actuated by six thrusters which are controlled independently to supply the desired thrust forces to the systems. The thrusters considered for all three types of the systems, i.e. UVMS, u-UVMS and u-UVRMS are configured as in Figure 3.7.

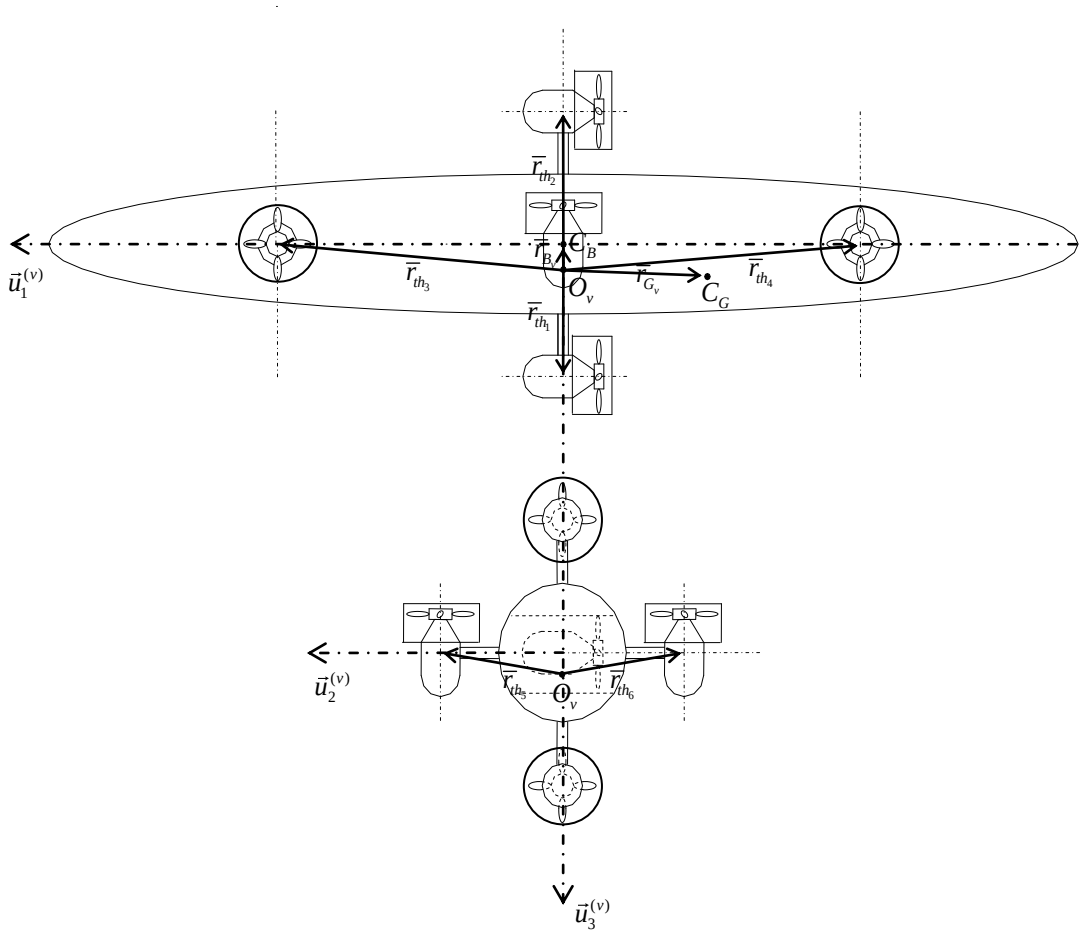

Figure 3.7 Thrusters' Configuration

Since the origin of the body fixed frame of the AUV is selected to be coincident with the center of buoyancy, the first and the second thrusters are used to provide thrust forces in surge and pitch motions. As the third and the fourth thrusters generate thrust forces in sway and yaw motions, the fifth and the sixth ones supply thrust forces to move in heave and roll motions as formulated below.

$$\bar{X}_{th} = \left(f_{th_1} + f_{th_2} \right) \bar{u}_1 \tag{3.105}$$

$$\bar{Y}_{th} = \left(f_{th_3} + f_{th_4} \right) \bar{u}_2 \tag{3.106}$$

$$\bar{Z}_{th} = \left(f_{th_5} + f_{th_6} \right) \bar{u}_3 \tag{3.107}$$

$$\bar{K}_{th} = \left(\tilde{r}_{th_5} f_{th_5} + \tilde{r}_{th_6} f_{th_6} \right) \bar{u}_3 \tag{3.108}$$

$$\bar{M}_{th} = \left(\tilde{r}_{th_1} f_{th_1} + \tilde{r}_{th_2} f_{th_2} \right) \bar{u}_1 \tag{3.109}$$

$$\bar{N}_{th} = \left(\tilde{r}_{th_3} f_{th_3} + \tilde{r}_{th_4} f_{th_4} \right) \bar{u}_2 \tag{3.110}$$

where

f_{th_k} show the thrust force generated by the k^{th} thruster,

$\bar{r}_{th_k}$ denote the position vector of the k^{th} thruster defined with respect to the origin of the body fixed frame of the vehicle O_v.

Therefore, the vector of generalized control forces $\bar{T}_v$ can be related to the thrust forces vector $\bar{F}_{th}$ by the following equation:

$$\bar{T}_v = \hat{\mu} \bar{F}_{th} \tag{3.111}$$

where

$\bar{F}_{th} \in \Re^{6x1}$ is the vector of thrust forces,

$\hat{\mu} \in \Re^{6x6}$ is the thruster configuration matrix as defined below.

$$\hat{\mu} = \begin{bmatrix} 1 & 1 & 0 & 0 & 0 & 0 \\ 0 & 0 & 1 & 1 & 0 & 0 \\ 0 & 0 & 0 & 0 & 1 & 1 \\ 0 & 0 & 0 & 0 & \bar{u}_1^t \tilde{r}_{th_5} \bar{u}_3 & \bar{u}_1^t \tilde{r}_{th_6} \bar{u}_3 \\ \bar{u}_2^t \tilde{r}_{th_1} \bar{u}_1 & \bar{u}_2^t \tilde{r}_{th_2} \bar{u}_1 & 0 & 0 & 0 & 0 \\ 0 & 0 & \bar{u}_3^t \tilde{r}_{th_3} \bar{u}_2 & \bar{u}_3^t \tilde{r}_{th_4} \bar{u}_2 & 0 & 0 \end{bmatrix} \tag{3.112}$$

When it comes to an underactuated AUV which is actuated by four thrusters with a lack of actuation in sway and yaw motions, i.e. the third and the fourth thrusters, the vector of thrust forces is $\bar{F}_{th} \in \Re^{4x1}$ and the thruster configuration matrix is $\hat{\mu} \in \Re^{6x4}$ derived as

$$\hat{\mu} = \begin{bmatrix} 1 & 1 & 0 & 0 \\ 0 & 0 & 0 & 0 \\ 0 & 0 & 1 & 1 \\ 0 & 0 & \bar{u}_1^t \tilde{r}_{th_3} \bar{u}_3 & \bar{u}_1^t \tilde{r}_{th_4} \bar{u}_3 \\ \bar{u}_2^t \tilde{r}_{th_2} \bar{u}_1 & \bar{u}_2^t \tilde{r}_{th_2} \bar{u}_1 & 0 & 0 \\ 0 & 0 & 0 & 0 \end{bmatrix} \tag{3.113}$$

3.6 Underwater Vehicle Regular Manipulator System Dynamics

The system dynamic equations (see Figure 2.3) can be derived by combining dynamic equations of the AUV given in Equation (3.7) and those of the manipulator subsystem stated in Equation (3.17) as

$$\begin{bmatrix} \hat{M}_{v_{6x6}} & \hat{0} \\ \hat{M}_{m_{\eta 36x6}} & \hat{M}_{m_{\theta 36x6}} \end{bmatrix} \begin{bmatrix} \dot{\bar{\eta}}_{6x1} \\ \ddot{\bar{\theta}}_{6x1} \end{bmatrix} + \begin{bmatrix} \bar{Q}_{v_{6x1}} \\ \bar{Q}_{m_{36x1}} \end{bmatrix} = \begin{bmatrix} \hat{A}_{v_{6x30}} \\ \hat{A}_{m_{36x30}} \end{bmatrix} \begin{bmatrix} \bar{f}_{r_{18x1}} \\ \bar{m}_{r_{12x1}} \end{bmatrix} + \begin{bmatrix} \hat{B}_{v_{6x6}} & \hat{0} \\ \hat{0} & \hat{B}_{m_{36x6}} \end{bmatrix} \begin{bmatrix} \bar{T}_{v_{6x1}} \\ \bar{T}_{m_{6x1}} \end{bmatrix} \cdots + \begin{bmatrix} \bar{F}_{hs_{v_{6x1}}} \\ \bar{F}_{hs_{m_{36x1}}} \end{bmatrix} + \begin{bmatrix} \bar{F}_{hd_{v_{6x1}}} \\ \bar{F}_{hd_{m_{36x1}}} \end{bmatrix} + \begin{bmatrix} \bar{F}_{ex_{v_{6x1}}} \\ \bar{F}_{ex_{m_{36x1}}} \end{bmatrix} \tag{3.114}$$

The system equations can be rewritten in compact form as follows:

$$\hat{M}\bar{\alpha} + \bar{Q} = \hat{A}\bar{F}_r + \hat{B}\bar{T} + \bar{F}_{hs} + \bar{F}_{hd} + \bar{F}_{ex} \tag{3.115}$$

$$\bar{\alpha} = \begin{bmatrix} \dot{\bar{\eta}} \\ \ddot{\bar{\theta}} \end{bmatrix}$$

where

$\hat{M} \in \Re^{42x12}$ is the generalized mass matrix including the added mass and the added rotational inertia,

$\bar{\alpha} \in \Re^{12x1}$ is the vector of generalized accelerations expressed in the body fixed frames,

$\bar{Q} \in \Re^{42x1}$ is the vector consisting of Coriolis and centrifugal terms including the added mass and the added rotational inertia,

$\hat{A} \in \Re^{42x30}$ is the coefficient matrix of the generalized reaction forces,

$\bar{F}_r \in \Re^{30x1}$ is vector of the generalized reaction forces,

$\hat{B} \in \Re^{42x12}$ is the coefficient matrix of the generalized control forces,

$\bar{T} \in \Re^{12x1}$ is the vector of the generalized control forces and

$\bar{F}_{hs}, \bar{F}_{hd}, \bar{F}_{ex} \in \Re^{42x1}$ are the vectors of hydrostatic, hydrodynamic and external disturbance forces respectively.

The system equations are 42 dimensional and have a total of 42 unknowns consisting of 12 system accelerations, 18 reaction forces and 12 reaction moments as given in Table 3.1.

Table 3.1 UVMS Unknowns

Types of unknowns	Names of unknowns	# of unknowns
System Accelerations	$\dot{u}, \dot{v}, \dot{w}, \dot{p}, \dot{q}, \dot{r}$ $\ddot{\theta}_1, \ddot{\theta}_2, \ddot{\theta}_3, \ddot{\theta}_4, \ddot{\theta}_5, \ddot{\theta}_6$	12
Reaction Forces	$\bar{f}_{01}^{(0)}, \bar{f}_{21}^{(1)}, \bar{f}_{32}^{(2)},$ $\bar{f}_{43}^{(3)}, \bar{f}_{54}^{(4)}, \bar{f}_{65}^{(5)}$	18
Reaction Moments	$m_{011}^{(0)}, m_{012}^{(0)}, m_{211}^{(1)}, m_{212}^{(1)}, m_{321}^{(2)}, m_{322}^{(2)},$ $m_{431}^{(3)}, m_{432}^{(3)}, m_{541}^{(4)}, m_{542}^{(4)}, m_{651}^{(5)}, m_{652}^{(5)}$	12

3.6.1 The Elimination of the Generalized Constraint Forces

There are several methods in the literature to eliminate the generalized constraint forces, i.e. the reaction forces and moments in the dynamic equations of the systems. By utilizing *the matrix inversion method* for example, 12 unknown acceleration components and 30 reaction force and moment components of the Equation (3.115) can be solved by making the following rearrangement:

$$\left[\hat{M}\bar{\alpha} - \hat{A}\bar{F}_r\right] + \left[\bar{Q} - \bar{F}_{hs} - \bar{F}_{hd} - \bar{F}_{ex}\right] = \hat{B}\bar{T} \tag{3.116}$$

The Equation (3.116) is rewritten in compact form as

$$\hat{D}\begin{bmatrix}\bar{\alpha}\\ \bar{F}_r\end{bmatrix} + \bar{P} = \hat{B}\bar{T} \tag{3.117}$$

leading to the following 12 dimensional equation in which the generalized reaction force vector is eliminated by a proper partitioning of the coefficient matrix $\hat{D}$.

$$\hat{M}^*\bar{\alpha} + \bar{Q}^* = \hat{B}^*\bar{T} \tag{3.118}$$

where

$$\hat{M}^* = \left[\hat{D}_{11} - \hat{D}_{12}\hat{D}_{22}^{-1}\hat{D}_{21}\right] \tag{3.119}$$

$$\bar{Q}^* = \left[\bar{P}_1 - \hat{D}_{12}\hat{D}_{22}^{-1}\bar{P}_2\right] \tag{3.120}$$

$$\hat{B}^* = \left[\hat{B}_1 - \hat{D}_{12}\hat{D}_{22}^{-1}\hat{B}_2\right] \tag{3.121}$$

In Equations (3.119)-(3.121), $\hat{D}_{11} \in \Re^{12x12}, \hat{D}_{12} \in \Re^{12x30}, \hat{D}_{21} \in \Re^{30x12}, \hat{D}_{22} \in \Re^{30x30}$ are the sub-matrices of the coefficient matrix-$\hat{D}$ and $\bar{P}_1 \in \Re^{12x1}, \bar{P}_2 \in \Re^{30x1}$ are the sub-vectors of the vector-$\bar{P}$. As a result, the reaction forces and the reaction moments in the dynamic equations have been removed and the forward dynamics solution can be achieved by means of the following equation.

$$\bar{\alpha} = \hat{M}^{*-1}\left[\hat{B}^*\bar{T} - \bar{Q}^*\right] \tag{3.122}$$

There is a crucial point, however, in the derivation of these expressions. It is more likely to experience singularity if the partitioning is not made properly. Therefore, in

order to guarantee a non-singular $\hat{D}_{22}$ matrix, some rows of the primary coefficient matrix $\hat{D}$ may be interchanged together with consistent changes in the right hand side of Equation (3.117) as well as in the vector $\overline{P}$ [66,67]. Besides that, the solving for the motion variables takes long time due to the inversion of $\hat{D}_{22}$ matrix which is needed at each time step during the forward dynamics solution. Consequently, this method is assessed to be less useful and time consuming since it brings additional computational complexity.

Another method which is much more commonly used in the literature [68,69] is called *the embedding technique*. In this method, the reaction forces and moments are also eliminated in the dynamic equations of motion and the dimensions of the corresponding matrices are reduced.

To apply this method, let the accelerations of the AUV and the manipulator subsystems represented by the Equation (2.15) and Equation (2.85) be factored in the following form.

$$\overline{a}_{sys} = \hat{H}\begin{bmatrix} \dot{\overline{\eta}} \\ \ddot{\overline{\theta}} \end{bmatrix} + \overline{v}_{sys} \tag{3.123}$$

where

$\overline{a}_{sys} \in \Re^{42x1}$ is the vector of linear and angular accelerations of the AUV and the links of the manipulator of the UVMS.

$\hat{H} \in \Re^{42x12}$ is the coefficient matrix of the system accelerations.

$\overline{v}_{sys} \in \Re^{42x1}$ is the bias vector consisting of the velocity terms.

This factorization can be performed easily by using the Symbolic Math Toolbox of MATLAB. Having obtained the matrix $\hat{H}$, the system equations of motion can be re-expressed by pre-multiplying the Equation (3.116) on both sides by $\hat{H}^T$ as

$$\hat{M}^{*}\bar{\alpha}+\bar{Q}^{*}=\hat{H}^{T}\hat{A}\bar{F}_{r}+\hat{B}^{*}\bar{T} \tag{3.124}$$

where

$$\hat{M}^{*}=\hat{H}^{T}\hat{M} \tag{3.125}$$

$$\bar{Q}^{*}=\hat{H}^{T}\left(\bar{Q}-\bar{F}_{hs}-\bar{F}_{hd}-\bar{F}_{ex}\right) \tag{3.126}$$

$$\hat{B}^{*}=\hat{H}^{T}\hat{B} \tag{3.127}$$

The sizes of the matrices that appear in Equations (3.125) – (3.127) are reduced to the number of system accelerations as $\hat{M}^{*}\in\Re^{12x12}$, $\bar{Q}^{*}\in\Re^{12x1}$ and $\hat{B}^{*}\in\Re^{12x12}$ which require only arithmetic operations of summation or multiplication rather than the matrix inversion. The term regarding the constraint forces, on the other hand, in Equation (3.124) cancels, that is,

$$\hat{H}^{T}\hat{A}\bar{F}_{r}=\bar{0} \tag{3.128}$$

Because it can be shown that $\hat{H}$ and $\hat{A}$ are orthogonal complement matrices of each other [68,69]. Hence, the final form yields to be as

$$\hat{M}^{*}\bar{\alpha}+\bar{Q}^{*}=\hat{B}^{*}\bar{T} \tag{3.129}$$

leading to the forward dynamic solution given in Equation (3.122). The main benefit of this method is that it greatly reduces the computational load. As a result of this, the time that it takes to compute the system accelerations decreases.

3.7 Underwater Vehicle Redundant Manipulator System Dynamics

In a similar way, the dynamic equations of the system having redundant manipulator illustrated in Figure 2.4 can be obtained by combining dynamic equations of the

AUV given in Equation (3.7) and those of the manipulator subsystem stated in Equation (3.26) as

$$\begin{bmatrix} \hat{M}_{v_{6x6}} & \hat{0} \\ \hat{M}_{m_{\eta 48x6}} & \hat{M}_{m_{\theta 48x8}} \end{bmatrix} \begin{bmatrix} \dot{\bar{\eta}}_{6x1} \\ \ddot{\bar{\theta}}_{8x1} \end{bmatrix} + \begin{bmatrix} \bar{Q}_{v_{6x1}} \\ \bar{Q}_{m_{48x1}} \end{bmatrix} = \begin{bmatrix} \hat{A}_{v_{6x40}} \\ \hat{A}_{m_{48x40}} \end{bmatrix} \begin{bmatrix} \bar{f}_{r_{24x1}} \\ \bar{m}_{r_{16x1}} \end{bmatrix} + \begin{bmatrix} \hat{B}_{v_{6x4}} & \hat{0} \\ \hat{0} & \hat{B}_{m_{48x8}} \end{bmatrix} \begin{bmatrix} \bar{T}_{v_{4x1}} \\ \bar{T}_{m_{8x1}} \end{bmatrix} \cdots + \begin{bmatrix} \bar{F}_{hs_{v_{6x1}}} \\ \bar{F}_{hs_{m_{48x1}}} \end{bmatrix} + \begin{bmatrix} \bar{F}_{hd_{v_{6x1}}} \\ \bar{F}_{hd_{m_{48x1}}} \end{bmatrix} + \begin{bmatrix} \bar{F}_{ex_{v_{6x1}}} \\ \bar{F}_{ex_{m_{48x1}}} \end{bmatrix} \quad (3.130)$$

The system equations given in Equation (3.130) can be rewritten in compact form as follows:

$$\hat{M}\bar{\alpha} + \bar{Q} = \hat{A}\bar{F}_r + \hat{B}\bar{T} + \bar{F}_{hs} + \bar{F}_{hd} + \bar{F}_{ex} \quad (3.131)$$

where

$\hat{M} \in \Re^{54x14}$ is the generalized mass matrix including the added mass and the added rotational inertia,

$\bar{\alpha} \in \Re^{14x1}$ is the vector of generalized accelerations expressed in the body fixed frames,

$\bar{Q} \in \Re^{54x1}$ is the vector consisting of Coriolis and centrifugal terms including the added mass and the added rotational inertia,

$\hat{A} \in \Re^{54x40}$ is the coefficient matrix of the generalized reaction forces,

$\bar{F}_r \in \Re^{40x1}$ is vector of the generalized reaction forces,

$\hat{B} \in \Re^{54x12}$ is the coefficient matrix of the generalized control forces,

$\bar{T} \in \Re^{12x1}$ is the vector of the generalized control forces and

$\bar{F}_{hs}, \bar{F}_{hd}, \bar{F}_{ex} \in \Re^{54x1}$ are the vectors of hydrostatic, hydrodynamic and external disturbance forces respectively.

This time, the system equations are 54 dimensional and have a total of 54 unknowns consisting of 14 system accelerations, 24 reaction forces and 16 reaction moments as given in Table 3.2.

Table 3.2 UVRMS Unknowns

Types of unknowns	Names of unknowns	# of unknowns
System Accelerations	$\dot{u}, \dot{v}, \dot{w}, \dot{p}, \dot{q}, \dot{r}$ $\ddot{\theta}_1, \ddot{\theta}_2, \ddot{\theta}_3, \ddot{\theta}_4, \ddot{\theta}_5, \ddot{\theta}_6, \ddot{\theta}_7, \ddot{\theta}_8$	14
Reaction Forces	$\overline{f}_{01}^{(0)}, \overline{f}_{21}^{(1)}, \overline{f}_{32}^{(2)}, \overline{f}_{43}^{(3)}$ $\overline{f}_{54}^{(4)}, \overline{f}_{65}^{(5)}, \overline{f}_{76}^{(6)}, \overline{f}_{87}^{(7)}$	24
Reaction Moments	$m_{011}^{(0)}, m_{012}^{(0)}, m_{211}^{(1)}, m_{212}^{(1)},$ $m_{321}^{(2)}, m_{322}^{(2)}, m_{431}^{(3)}, m_{432}^{(3)},$ $m_{541}^{(4)}, m_{542}^{(4)}, m_{651}^{(5)}, m_{652}^{(5)},$ $m_{761}^{(6)}, m_{762}^{(6)}, m_{871}^{(7)}, m_{872}^{(7)}$	16

In the same way, the Equation (3.123) can be utilized to apply the embedding technique in order to get the final form of the dynamic equations of the UVRMS as in the form of that of Equation (3.129). The sizes of the matrices alter as $\hat{H} \in \Re^{54x14}$, $\hat{M}^* \in \Re^{14x14}$, $\overline{Q}^* \in \Re^{14x1}$ and $\hat{B}^* \in \Re^{14x12}$.

CHAPTER IV

TRAJECTORY PLANNING AND CONTROLLER DESIGN

This chapter mainly covers the inverse dynamics control methods developed for tracking the desired trajectories of the UVMSs as well as the thrusters. The task equations are formulated and the expressions relating the task variables to the joint variables are explained. Trajectories for both of the AUV and the end-effector of the manipulator subsystem are defined for typical underwater missions like mine detection and geological sampling. The position error dynamics of the systems under consideration are formulated.

4.1 Task Equations

The control methods to be used for the systems are based on getting a relationship between the inputs and the outputs. The inputs are the joint torques for the manipulator and the thrust forces for the AUV. The aim of the control system is to make both the AUV and the end-effector move sufficiently close to desired motions specified for them with respect to the *Earth-fixed reference frame*, $\Im_e$. Hence, the outputs of the system are taken as the position variables of the vehicle and the end-effector.

4.1.1 Position Level Equations

The end-effector and the AUV trajectories prescribed in $\Im_e$ represent the tasks of the UVMS. Reminding that x_v, y_v, z_v and ϕ_i (for $i=1,2,3$) denote the position and orientation variables of the AUV in the task space which are put together into the

vector $\bar{\zeta}$, the relationship between $\bar{\zeta}$ and $\bar{\eta}$ is expressed at the acceleration level as in Equation (2.50). Let also x_P, y_P, z_P and ψ_i (for $i=1,2,3$) denote the position and orientation variables of the tip point of the end-effector in the task space. Let them be jointly denoted by the vector $\bar{\zeta}_{ee}$,i.e.

$$\bar{\zeta}_{ee}=\left[\bar{\zeta}_{ee_L}^T \vdots \bar{\zeta}_{ee_A}^T\right]^T=\left[x_P \quad y_P \quad z_P \vdots \psi_1 \quad \psi_2 \quad \psi_3\right]^T \tag{4.1}$$

In order to express position, velocity and acceleration relations of the tip point of the end-effector in terms of Earth fixed coordinates, one needs to transform the kinematic equations from $\Im_v$ to $\Im_e$. Using Equation (2.23), the position of the tip point of the end-effector in $\Im_e$ can be obtained as

$$\bar{\zeta}_{ee_L}=\hat{C}^{(e,v)}\bar{p}_P \tag{4.2}$$

The orientation of the end-effector of the UVMS relative to the task reference frame can be described using Rotated Frame Based 323 (azimuth, declination, twist) Euler angle sequence which is more commonly used in robotic applications as shown below

$$\Im_e \xrightarrow[\vec{u}_3^{(e)}=\vec{u}_3^{(m)}]{\psi_1} \Im_m \xrightarrow[\vec{u}_2^{(m)}=\vec{u}_2^{(n)}]{\psi_2} \Im_n \xrightarrow[\vec{u}_3^{(n)}=\vec{u}_3^{(6)}]{\psi_3} \Im_6$$

where $\Im_6$ stand for the frame attached to the end effector. The orientation of the end-effector is illustrated in Figure 4.1.

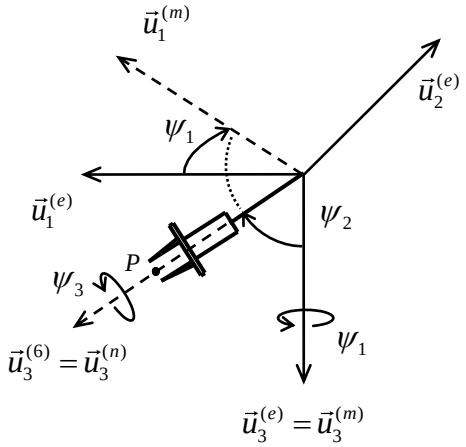

Figure 4.1 End-effector Orientation

The coordinate transformation matrix of the end-effector is obtained by using elementary rotation matrices as in the following.

$$\hat{C}^{(e,6)} = \hat{C}^{(e,m)}\hat{C}^{(m,n)}\hat{C}^{(n,6)} \tag{4.3}$$

where

$$\hat{C}^{(e,m)} = e^{\tilde{u}_3\psi_1} = \begin{bmatrix} c\psi_1 & -s\psi_1 & 0 \\ s\psi_1 & c\psi_1 & 0 \\ 0 & 0 & 1 \end{bmatrix} \tag{4.4}$$

$$\hat{C}^{(m,n)} = e^{\tilde{u}_2\psi_2} = \begin{bmatrix} c\psi_2 & 0 & s\psi_2 \\ 0 & 1 & 0 \\ -s\psi_2 & 0 & c\psi_2 \end{bmatrix} \tag{4.5}$$

$$\hat{C}^{(n,6)} = e^{\tilde{u}_3\psi_3} = \begin{bmatrix} c\psi_3 & -s\psi_3 & 0 \\ s\psi_3 & c\psi_3 & 0 \\ 0 & 0 & 1 \end{bmatrix} \tag{4.6}$$

and in compact form

$$\hat{C}^{(e,6)} = \begin{bmatrix} c\psi_1 c\psi_2 c\psi_3 - s\psi_1 s\psi_3 & -c\psi_3 s\psi_1 - c\psi_2 c\psi_1 s\psi_3 & s\psi_2 c\psi_1 \\ c\psi_2 c\psi_3 s\psi_1 + c\psi_1 s\psi_3 & c\psi_1 c\psi_3 - c\psi_2 s\psi_1 s\psi_3 & s\psi_2 s\psi_1 \\ -s\psi_2 c\psi_3 & s\psi_2 s\psi_3 & c\psi_2 \end{bmatrix} \tag{4.7}$$

where $s\psi_i = \sin\psi_i$ & $c\psi_i = \cos\psi_i$ $i=1,2,3.$ and ψ_i $i=1,2,3.$ are the Euler angles of the azimuth, declination, twist of the end-effector. Since the coordinate transformation matrix is computed using following relation

$$\hat{C}^{(e,6)} = \hat{C}^{(e,v)}\hat{C}^{(v,6)} \tag{4.8}$$

the Euler angles can be calculated using the following equations

$$\psi_1 = \text{atan2}\left(c_{23}, c_{13}\right) \tag{4.9}$$

$$\psi_2 = \text{atan2}\left(\sqrt{1-c_{33}^2}, c_{33}\right) \tag{4.10}$$

$$\psi_3 = \text{atan2}\left(c_{32}, -c_{31}\right) \tag{4.11}$$

where c_{ij} is the entry of the transformation matrix $\hat{C}^{(e,6)}$ in the i^{th} row and j^{th} column.

4.1.2 Velocity Level Equations

The velocity of the Point-P of the end-effector given in Equation (2.81) can be rewritten in factored form as

$$\overline{v}_{P/O_e}^{(v)} = \hat{J}_{\theta_1}\dot{\overline{\theta}} + \hat{J}_{\eta_1}\overline{\eta} \tag{4.12}$$

where the Jacobian matrices $\hat{J}_{\theta_1}, \hat{J}_{\eta_1} \in \Re^{3x6}$ are

$$\hat{J}_{\theta_1} = \begin{bmatrix} \overline{J}_{\theta_{11}} & \overline{J}_{\theta_{12}} & \dots & \overline{J}_{\theta_{1i}} \end{bmatrix} \tag{4.13}$$

$$\overline{J}_{\theta_{1i}} = \frac{\partial \overline{v}_{P/O_e}^{(0)}}{\partial \theta_i} \tag{4.14}$$

$$\hat{J}_{\eta_1} = \begin{bmatrix} \overline{J}_{\eta_{11}} & \overline{J}_{\eta_{12}} & \dots & \overline{J}_{\eta_{1i}} \end{bmatrix} \tag{4.15}$$

$$\overline{J}_{\eta_{1i}} = \frac{\partial \overline{v}_{P/O_e}^{(0)}}{\partial \eta_i} \tag{4.16}$$

The angular velocity of the end-effector given in Equation (2.80) can be rewritten in factored form as

$$\overline{\omega}_{6/e}^{(v)} = \hat{J}_{\theta_2}\dot{\overline{\theta}} + \hat{J}_{\eta_2}\overline{\eta} \tag{4.17}$$

where the Jacobian matrices $\hat{J}_{\theta_2}, \hat{J}_{\eta_2} \in \Re^{3x6}$ are

$$\hat{J}_{\theta_2} = \begin{bmatrix} \overline{J}_{\theta_{21}} & \overline{J}_{\theta_{22}} & \dots & \overline{J}_{\theta_{2i}} \end{bmatrix} \tag{4.18}$$

$$\bar{J}_{\theta_{2i}} = \frac{\partial \bar{\omega}_{6/e}^{(0)}}{\partial \theta_i} \tag{4.19}$$

$$\hat{J}_{\eta_2} = \begin{bmatrix} \bar{J}_{\eta_{21}} & \bar{J}_{\eta_{22}} & \ldots & \bar{J}_{\eta_{2i}} \end{bmatrix} \tag{4.20}$$

$$\bar{J}_{\eta_{2i}} = \frac{\partial \bar{\omega}_{6/e}^{(0)}}{\partial \eta_i} \tag{4.21}$$

Therefore, combining Equation (4.12) and Equation (4.17) gives the augmented form as

$$\begin{bmatrix} \bar{v}_{P/O}^{(v)} \\ \bar{\omega}_{6/e}^{(v)} \end{bmatrix} = \hat{J}_\theta \dot{\bar{\theta}} + \hat{J}_\eta \bar{\eta} \tag{4.22}$$

where $\hat{J}_\theta$, $\hat{J}_\eta \in \Re^{6x6}$

$$\hat{J}_\theta = \begin{bmatrix} \hat{J}_{\theta_1} \\ \hat{J}_{\theta_2} \end{bmatrix} \tag{4.23}$$

$$\hat{J}_\eta = \begin{bmatrix} \hat{J}_{\eta_1} \\ \hat{J}_{\eta_2} \end{bmatrix} \tag{4.24}$$

The velocities expressed in $\Im_v$ are transformed to those expressed in $\Im_e$ using the following relationship.

$$\dot{\bar{\zeta}}_{ee_L} = \hat{C}^{(e,v)} \bar{v}_{P/O}^{(v)} \tag{4.25}$$

where

$$\dot{\bar{\zeta}}_{ee_L} = \begin{bmatrix} \dot{x}_P \\ \dot{y}_P \\ \dot{z}_P \end{bmatrix} \tag{4.26}$$

The angular velocity of the end-effector can be expressed in terms of the Euler angles as

$$\bar{\omega}_{6/e}^{(6)} = \dot{\psi}_1 \bar{u}_3^{(e)} + \dot{\psi}_2 \bar{u}_2^{(m)} + \dot{\psi}_3 \bar{u}_3^{(n)} = \hat{C}^{(6,v)} \bar{\omega}_{6/e}^{(v)} \tag{4.27}$$

which can also be expressed as

$$\dot{\bar{\zeta}}_{ee_A} = \hat{E}_m^{-1} \hat{C}^{(6,v)} \bar{\omega}_{6/e}^{(v)} \tag{4.28}$$

where $\hat{E}_m(\psi) \in \Re^{3x3}$ is obtained as

$$\hat{E}_m = \begin{bmatrix} -s\psi_2 c\psi_3 & s\psi_3 & 0 \\ s\psi_2 s\psi_3 & c\psi_3 & 0 \\ c\psi_2 & 0 & 1 \end{bmatrix} \tag{4.29}$$

and $\dot{\bar{\zeta}}_{ee_A}(\dot{\psi}) \in \Re^{3x1}$ consists of the Euler rates as below

$$\dot{\bar{\zeta}}_{ee_A} = \begin{bmatrix} \dot{\psi}_1 \\ \dot{\psi}_2 \\ \dot{\psi}_3 \end{bmatrix} \tag{4.30}$$

In Equation (4.28), $\hat{E}_m$ is called the rotation matrix of the end effector. It should be noted that $\det(\hat{E}_m) = 0$ when $s\psi_2 = 0$. That means singularity takes place when the intermediate angle $\psi_2 = 0, \pm\pi$.

Finally, taking both of the linear and angular coordinate transformations into account and combining Equation (4.25) and Equation (4.28) in augmented form yields

$$\dot{\bar{\zeta}}_{ee} = \hat{J}_m \begin{bmatrix} \bar{v}_{P/O}^{(v)} \\ \bar{\omega}_{6/e}^{(v)} \end{bmatrix} \tag{4.31}$$

where $\dot{\bar{\zeta}}_{ee} \in \Re^{6x1}$

$$\dot{\bar{\zeta}}_{ee} = \begin{bmatrix} \dot{\bar{\zeta}}_{ee_L} \\ \dot{\bar{\zeta}}_{ee_A} \end{bmatrix} \tag{4.32}$$

and $\hat{J}_m \in \Re^{6x6}$ is the Jacobian matrix of the end-effector and can be written as

$$\hat{J}_m = \begin{bmatrix} \hat{C}^{(e,v)} & \hat{0}_{3x3} \\ \hat{0}_{3x3} & \hat{E}_m^{-1}\hat{C}^{(6,v)} \end{bmatrix} \tag{4.33}$$

Finally putting Equation (4.22) and Equation (4.31) together gives

$$\dot{\bar{\zeta}}_{ee} = \hat{J}_m \left(\hat{J}_\theta \dot{\bar{\theta}} + \hat{J}_\eta \bar{\eta} \right) \tag{4.34}$$

4.1.3 Acceleration Level Equations

Let the acceleration expression given in Equation (2.84) be written in factored form as

$$\bar{a}_{P/O_e}^{(v)} = \hat{J}_{\theta_1} \ddot{\bar{\theta}} + \hat{J}_{\eta_1} \dot{\bar{\eta}} + \bar{J}_{L_{b,ee}} \tag{4.35}$$

where $\bar{J}_{L_{b,ee}} = \bar{J}_{L_{b,ee}}(\bar{\theta}, \dot{\bar{\theta}}, \bar{\eta}_A, \bar{\eta}_L) \in \Re^{3x1}$.

Let also the angular acceleration expression given in Equation (2.83) be written in factored form as

$$\bar{\alpha}_{6/e}^{(v)} = \hat{J}_{\theta_2} \ddot{\bar{\theta}} + \hat{J}_{\eta_2} \dot{\bar{\eta}} + \bar{J}_{A_{b,ee}} \tag{4.36}$$

where $\bar{J}_{A_{b,ee}} = \bar{J}_{A_{b,ee}}(\bar{\theta}, \dot{\bar{\theta}}, \bar{\eta}_A) \in \Re^{3x1}$.

Combining the Equation (4.35) and the Equation (4.36) yields

$$\begin{bmatrix} \bar{a}_{P/O_e}^{(v)} \\ \bar{\alpha}_{6/e}^{(v)} \end{bmatrix} = \hat{J}_{\theta}\ddot{\bar{\theta}} + \hat{J}_{\eta}\dot{\bar{\eta}} + \bar{J}_{b,m} \tag{4.37}$$

where $\bar{J}_{b,m}\left(\bar{\theta}, \dot{\bar{\theta}}, \bar{\eta}\right) \in \Re^{6x1}$

$$\bar{J}_{b,m} = \begin{bmatrix} \bar{J}_{L_{b,ee}} \\ \bar{J}_{A_{b,ee}} \end{bmatrix} \tag{4.38}$$

The acceleration expressions expressed in $\Im_v$ is transformed to the one expressed in $\Im_e$ using the following relationship.

$$\ddot{\bar{\zeta}}_{ee_L} = \hat{C}^{(e,v)}\bar{a}_{P/O_e}^{(v)} \tag{4.39}$$

where

$$\ddot{\bar{\zeta}}_{ee_L} = \begin{bmatrix} \ddot{x}_P \\ \ddot{y}_P \\ \ddot{z}_P \end{bmatrix} \tag{4.40}$$

On the other hand, the angular acceleration expressions can be obtained by differentiating Equation (4.28) and written in expanded form as

$$\alpha_{6_1} = -\ddot{\psi}_1 s\psi_2 c\psi_3 + \ddot{\psi}_2 s\psi_3 - \dot{\psi}_1\left(\dot{\psi}_2 c\psi_2 c\psi_3 - \dot{\psi}_3 s\psi_2 s\psi_3\right) + \dot{\psi}_2\dot{\psi}_3 c\psi_3 \tag{4.41}$$

$$\alpha_{6_2} = \ddot{\psi}_1 s\psi_2 s\psi_3 + \ddot{\psi}_2 c\psi_3 + \dot{\psi}_1\left(c\psi_2\dot{\psi}_2 s\psi_3 + s\psi_2 c\psi_3\dot{\psi}_3\right) - \dot{\psi}_2\dot{\psi}_3 s\psi_3 \tag{4.42}$$

$$\alpha_{6_3} = \ddot{\psi}_1 c\psi_2 + \ddot{\psi}_3 - s\psi_2\dot{\psi}_2\dot{\psi}_1 \tag{4.43}$$

Equations (4.41) – (4.43) can be written in compact form as

$$\bar{\alpha}_{6/e}^{(6)} = \hat{E}_m \ddot{\bar{\zeta}}_{ee_A} + \hat{E}_2 = \hat{C}^{(6,v)} \bar{\alpha}_{6/e}^{(v)} \tag{4.44}$$

where $\hat{E}_2\left(\psi, \dot{\psi}\right) \in \Re^{3x1}$ is obtained as

$$\hat{E}_2 = \begin{bmatrix} \dot{\psi}_1 \dot{\psi}_3 s\psi_2 s\psi_3 + \dot{\psi}_2\left(\dot{\psi}_3 - \dot{\psi}_1 c\psi_2\right) c\psi_3 \\ \dot{\psi}_1 \dot{\psi}_3 s\psi_2 c\psi_3 - \dot{\psi}_2\left(\dot{\psi}_3 - \dot{\psi}_1 c\psi_2\right) s\psi_3 \\ -\dot{\psi}_1 \dot{\psi}_2 s\psi_2 \end{bmatrix} \tag{4.45}$$

and

$$\ddot{\bar{\zeta}}_{ee_A} = \begin{bmatrix} \ddot{\psi}_1 \\ \ddot{\psi}_2 \\ \ddot{\psi}_3 \end{bmatrix} \tag{4.46}$$

In the next step, combining Equations (4.39) and (4.44) gives

$$\ddot{\bar{\zeta}}_{ee} = \hat{J}_m \begin{bmatrix} \bar{a}_{P/O_e}^{(v)} \\ \bar{\alpha}_{6/e}^{(v)} \end{bmatrix} + \bar{T}_{b,m} \tag{4.47}$$

where $\ddot{\bar{\zeta}}_{ee} \in \Re^{6x1}$

$$\ddot{\bar{\zeta}}_{ee} = \begin{bmatrix} \ddot{\bar{\zeta}}_{ee_L} \\ \ddot{\bar{\zeta}}_{ee_A} \end{bmatrix} \tag{4.48}$$

and $\bar{T}_{b,m}\left(\psi, \dot{\psi}\right) \in \Re^{6x1}$

$$\bar{T}_{b,m} = \begin{bmatrix} 0 \\ -\hat{E}_m^{-1} \bar{E}_2 \end{bmatrix} \tag{4.49}$$

Consequently, the following acceleration relationship is obtained utilizing Equation (4.37) and Equation (4.47) as

$$\ddot{\bar{\zeta}}_{ee} = \hat{J}_m \hat{J}_\theta \ddot{\bar{\theta}} + \hat{J}_m \hat{J}_\eta \dot{\bar{\eta}} + \bar{a}_{b_m} \tag{4.50}$$

where acceleration bias vector for the manipulator $\bar{a}_{b_m}$ is expressed as

$$\bar{a}_{b_m} = \hat{J}_m \bar{J}_{b,m} + \bar{T}_{b,m} \tag{4.51}$$

The acceleration equation that relates the task space accelerations and the body fixed accelerations of the UVMS can be obtained by augmenting Equation (2.50) written for the AUV and Equation (4.50) written for the 6-DOF manipulator as

$$\ddot{\bar{\xi}} = \hat{J}_{sys} \bar{\alpha} + \bar{a}_b \tag{4.52}$$

where the UVMS Jacobian matrix $\hat{J}_{sys} \in \Re^{12x12}$ is

$$\hat{J}_{sys} = \begin{bmatrix} \hat{J}_v & \hat{0} \\ \hat{J}_m \hat{J}_\eta & \hat{J}_m \hat{J}_\theta \end{bmatrix} \tag{4.53}$$

the Earth-fixed acceleration vector of the system $\ddot{\bar{\xi}} \in \Re^{12x1}$ is

$$\ddot{\bar{\xi}} = \begin{bmatrix} \ddot{\bar{\zeta}} \\ \ddot{\bar{\zeta}}_{ee} \end{bmatrix} \tag{4.54}$$

the acceleration bias vector of the system $\bar{a}_b \in \Re^{12x1}$ is

$$\bar{a}_b = \begin{bmatrix} \bar{a}_{b_v} \\ \bar{a}_{b_m} \end{bmatrix} \tag{4.55}$$

The detailed derivation of the UVMS Jacobian matrices are given in Appendix-A.

4.2 Inverse Dynamics Controller Design for Fully Actuated UVMS

The proposed *inverse dynamics controller* utilizes the full nonlinear model of the UVMS and consists of a linearizing control law that uses the feedback of positions and velocities of the outputs in order to cancel off the nonlinearities of the system. The PD control is applied after this complicated feedback linearization process. It should be noted that the control method is not based on the usage of linearized approximations to the nonlinear dynamic equations about certain operating points. On the other hand, it is a challenging task to control the underwater vehicle especially having small mass equipped with manipulator due to the significance of the coupled effects between the two subsystems. In order to minimize the interaction between the subsystems and to resolve the kinematic redundancy of the whole system, the method should be applied to the system of equations defined in $\Im_e$ by assigning separate tasks to both the AUV and the end-effector of the manipulator subsystem. That means the system accelerations vector defined in body frames $\overline{\alpha}$ is supposed to be eliminated in Equation (3.129) by using Equation (4.52). This manipulation gives the relation between the inputs $\overline{T}$ and the outputs $\overline{\xi}$ as below

$$\hat{M}^{**}\ddot{\overline{\xi}} + \overline{Q}^{**} = \hat{B}^{*}\overline{T} \tag{4.56}$$

where the system mass matrix $\hat{M}^{**} \in \Re^{12x12}$ and the system vector containing velocity dependent terms $\overline{Q}^{**} \in \Re^{12x1}$ are

$$\hat{M}^{**} = \hat{M}^{*}\hat{J}_{sys}^{-1} \tag{4.57}$$

$$\overline{Q}^{**} = \overline{Q}^{*} - \hat{M}^{*}\hat{J}_{sys}^{-1}\overline{a}_b \tag{4.58}$$

Equation (4.56) shows that the generalized control forces have an instantaneous effect on the system accelerations. The inverse dynamics control law can then be formulated which computes the necessary driving input $\overline{T}$ as follows:

$$\overline{T} = \hat{B}^{*-1}\left[\hat{M}_{est}^{**}\overline{u} + \overline{Q}_{est}^{**}\right] \tag{4.59}$$

where the subscript "*est*" indicates *estimated* values due to parametric uncertainty, $\bar{u} \in \Re^{12x1}$ is the control input vector that represents the collection of the *commanded* accelerations to be generated for the system by the inverse dynamics controller. Note that the coefficient matrix $\hat{B}^*$ does not contain any uncertain value. The inverse dynamics control law expressed by Equation (4.59) has a linearizing effect in the sense that it reduces Equation (4.56) simply to

$$\ddot{\bar{\xi}} = \hat{E}\bar{u} - (\hat{M}^{**})^{-1}\bar{Q}_{err} \tag{4.60}$$

where

$$\bar{Q}_{err} = \bar{Q}^{**} - \bar{Q}^{**}_{est} \tag{4.61}$$

$$\hat{E} = (\hat{M}^{**})^{-1}\hat{M}^{**}_{est} \tag{4.62}$$

The mass matrix of any realistic mechanical system happens to be positive definite, so is its inverse. With a proper estimate of the mass matrix, the matrix $\hat{E}$ defined in Equation (4.60) comes out to be a positive definite matrix, too. On the other hand, it should be noted that $\hat{E} \approx \hat{I}$ provided that $\hat{M}^{**}_{est} \approx \hat{M}^{**}$.

Based on Equation (4.60), the following type of multi-variable PD control law which is also valid in the presence of modeling error can be proposed:

$$\bar{u} = \ddot{\bar{\xi}}^d + \hat{K}_v\left(\dot{\bar{\xi}}^d - \dot{\bar{\xi}}\right) + \hat{K}_p\left(\bar{\xi}^d - \bar{\xi}\right) \tag{4.63}$$

Here, the superscript "*d*" is used for the *desired* values. As for $\hat{K}_v$ and $\hat{K}_p$, they are the feedback gain matrices, which are normally taken to be diagonal. By defining the error vector as $\bar{e}_p = \bar{\xi}^d - \bar{\xi}$, Equation (4.63) leads to the following linear second order error dynamics

$$\ddot{\bar{e}}_p + \hat{E}\hat{K}_v\dot{\bar{e}}_p + \hat{E}\hat{K}_p\bar{e}_p = \bar{\delta} \tag{4.64}$$

where the deflector $\bar{\delta}$ is obtained as

$$\bar{\delta} = (\hat{I} - \hat{E})\ddot{\bar{\xi}}^d + (\hat{M}^{**})^{-1}\bar{Q}_{err} \tag{4.65}$$

As mentioned above, $\hat{E}$ is positive definite and $\hat{E} \approx \hat{I}$. Therefore, the asymptotic stability of the system can be achieved by generating the position and velocity feedback gain matrices simply as

$$\hat{K}_p = diag\left(\omega_1^2, \omega_2^2, ..., \omega_{12}^2\right) \tag{4.66}$$

$$\hat{K}_v = diag\left(2\varsigma_1\omega_1, 2\varsigma_2\omega_2, ..., 2\varsigma_{12}\omega_{12}\right) \tag{4.67}$$

where ω_i>0 and ς_i>0, i=1,2,...,12. Hence, by choosing ω_i large enough for all i, $\left|\bar{e}_p\right|$ can be reduced. This is because, in a practical situation, $\left|\bar{\delta}\right|$ varies much more slowly (i.e. it is almost constant) with respect to a sinusoidal function even for the smallest one of $\omega_1, \omega_2, ..., \omega_{12}$. Therefore, after the transient phase, the error converges to the value given in Equation (4.68), which gets smaller as the elements of $\hat{K}_p$ increase.

$$\bar{e}_p^* = \hat{K}_p^{-1}\hat{E}^{-1}\bar{\delta} \tag{4.68}$$

The feedback gains are selected by using *pole placement technique* either by using performance criteria like ITAE, ISE etc. or by self-tuning the values of ω_i>0 and ς_i>0, i=1,2,...,12. depending on the desired specifications of the response. The performance criterion called integral of time multiplied by the absolute value of error, i.e. ITAE for instance, defines $\varsigma_i = 0.707$ for a second order system. However, for a critically damped closed loop response, the damping ratio should be set to unity, i.e. $\varsigma_i = 1.0$.

Consequently, the control forces/torques which are obtained from Equation (4.59) *simultaneously* for both of the subsystems are applied to the system represented by Equation (3.122) for the forward dynamics solution. The necessary measurements for the calculation of the control torques and forces that appear in the control law are the positions and velocities of the actuated joints, i.e. $\bar{\theta}$, $\dot{\bar{\theta}}$ of the manipulator and the translational acceleration and the angular velocity components of the AUV.

The angular velocity components p, q and r of the AUV are measured by the onboard rate gyros. The Euler angle rates corresponding to the angular velocity components are obtained by using the Equation (2.29). The Euler angles are then calculated by numerical integration. The components of acceleration vector $\bar{a}_{O_v} = \bar{a}^{(v)}_{O_v/O_e}$ of the AUV, on the other hand, are measured by using the onboard accelerometers. The rates of the velocities of the point O_v are then calculated by using the following equation together with the angular velocity measurements.

$$\begin{bmatrix} \dot{u} \\ \dot{v} \\ \dot{w} \end{bmatrix} = \begin{bmatrix} a_{O_{v_1}} \\ a_{O_{v_2}} \\ a_{O_{v_3}} \end{bmatrix} - \begin{bmatrix} -rv + qw \\ ur - pw \\ -qu + pv \end{bmatrix} \tag{4.69}$$

The velocity components u , v and w are then calculated by numerical integration. The corresponding velocity vector defined in $\Im_e$ is obtained by using Equation (2.25). By using the measured values of the joint variables and their rates, the tip point coordinates and the Euler angles of the end-effector are calculated using kinematic equations given in Sections 4.1.1–4.1.3.

4.3 Inverse Dynamics Controller Design for Underactuated UVMS

The UVMS consisting of the AUV having 4 thrusters and a 6-DOF manipulator with 6 actuators is called underactuated UVMS, i.e. u-UVMS. Differing from a fully actuated UVMS, the AUV of this system is not controlled in *sway* and *yaw*

directions. Hence, the relation between the body-fixed and task space accelerations given in Equation (4.52) should be modified. Let $\hat{\lambda} \in \Re^{10x12}$ denote the coefficient matrix that eliminates the accelerations in the uncontrolled motions in $\Im_v$. In such a case, reduced the body fixed accelerations vector $\bar{\alpha}_r \in \Re^{10x1}$ is obtained by using Equation (4.52) as

$$\bar{\alpha}_r = \hat{\lambda}\bar{\alpha} = \hat{\lambda}\hat{J}_{sys}^{-1}\ddot{\bar{\xi}} - \hat{\lambda}\hat{J}_{sys}^{-1}\bar{a}_b \tag{4.70}$$

and by using Equation (3.129) as

$$\bar{\alpha}_r = \hat{\lambda}\bar{\alpha} = \hat{\lambda}\left(\hat{M}^*\right)^{-1}\left(\hat{B}^*\bar{T} - \bar{Q}^*\right) \tag{4.71a}$$

where

$\hat{B}^* \in \Re^{12x10}$ is the coefficient matrix of the actuating forces and torques,

$\bar{T} \in \Re^{10x1}$ is the vector of actuating forces and torques and

$$\hat{\lambda} = \begin{bmatrix} 1 & 0 & 0 & 0 & 0 & 0 & 0 & 0 & 0 & 0 & 0 & 0 \\ 0 & 0 & 1 & 0 & 0 & 0 & 0 & 0 & 0 & 0 & 0 & 0 \\ 0 & 0 & 0 & 1 & 0 & 0 & 0 & 0 & 0 & 0 & 0 & 0 \\ 0 & 0 & 0 & 0 & 1 & 0 & 0 & 0 & 0 & 0 & 0 & 0 \\ 0 & 0 & 0 & 0 & 0 & 0 & 1 & 0 & 0 & 0 & 0 & 0 \\ 0 & 0 & 0 & 0 & 0 & 0 & 0 & 1 & 0 & 0 & 0 & 0 \\ 0 & 0 & 0 & 0 & 0 & 0 & 0 & 0 & 1 & 0 & 0 & 0 \\ 0 & 0 & 0 & 0 & 0 & 0 & 0 & 0 & 0 & 1 & 0 & 0 \\ 0 & 0 & 0 & 0 & 0 & 0 & 0 & 0 & 0 & 0 & 1 & 0 \\ 0 & 0 & 0 & 0 & 0 & 0 & 0 & 0 & 0 & 0 & 0 & 1 \end{bmatrix} \tag{4.71b}$$

The inverse dynamics law can be re-formulated by combining the Equation (4.70) and Equation (4.71) as

$$\bar{T} = \hat{M}_{est}^{**}\bar{u} + \bar{Q}_{est}^{**} \tag{4.72}$$

where

$$\hat{M}_{est}^{**} = \left[\hat{\lambda} \left(\hat{M}_{est}^{*} \right)^{-1} \hat{B}^{*} \right]^{-1} \hat{\lambda} \hat{J}_{sys}^{-1} \tag{4.73}$$

$$\bar{Q}_{est}^{**} = \left[\hat{\lambda} \left(\hat{M}_{est}^{*} \right)^{-1} \hat{B}^{*} \right]^{-1} \left[\hat{\lambda} \left(\hat{M}_{est}^{*} \right)^{-1} \bar{Q}_{est}^{*} - \hat{\lambda} \hat{J}_{sys}^{-1} \bar{a}_{b} \right] \tag{4.74}$$

and $\bar{u} \in \Re^{12x1}$ is the control input vector that represents the collection of the commanded accelerations. The coefficient matrix $\hat{B}^{*}$ is known exactly and does not contain any uncertain value.

There is a crucial point that 12 task equations defined in task space is reduced 10 task equations by the inclusion of $\hat{\lambda}$ seen in Equation 4.70. Besides that, 12-DOF u-UVMS is driven by a total of 10 actuating forces and torques. In addition to this, in the calculation of the control torques and forces, the pseudo-inversion operation which can be the case in non-regular dynamic systems is unnecessary since the term to be inverted $\hat{\lambda} \left(\hat{M}_{est}^{*} \right)^{-1} \hat{B}^{*}$ in Equations (4.73), (4.74) turns out to be a square matrix as well as the system Jacobian matrix.

4.4 Inverse Dynamics Controller Design for Underactuated UVRMS

The UVMS consisting of the AUV having 4 thrusters and a 8-DOF manipulator with 8 actuators is called underactuated UVRMS, i.e. u-UVRMS. The AUV of this system is not controlled in *sway* and *yaw* directions likewise. This time, a total of 14-DOF system is controlled by 12 actuating forces and torques and the uncontrolled motions of the AUV are desired to be controlled dynamically as much as possible. Hence, the relation between the body-fixed and task space accelerations given in Equation () should be modified.

$$\ddot{\bar{\xi}} = \hat{J}_{sys} \bar{\alpha} + \bar{a}_{b} \tag{4.75}$$

where

$\hat{J}_{sys} \in \Re^{12x14}$ is the u-UVMS Jacobian matrix,

$\bar{a}_b \in \Re^{12x1}$ is the acceleration bias vector of the u-UVMS.

The detailed derivation of the u-UVRMS Jacobian matrices are given in Appendix-A.

Let $\hat{\lambda} \in \Re^{12x14}$ denote the coefficient matrix that eliminates the accelerations in the uncontrolled motions in $\Im_v$. The reduced the body fixed accelerations vector $\bar{\alpha}_r \in \Re^{12x1}$ is obtained by using Equation (4.75) as

$$\bar{\alpha}_r = \hat{\lambda}\bar{\alpha} = \hat{\lambda}\hat{J}_{sys}^{\#}\ddot{\bar{\xi}} - \hat{\lambda}\hat{J}_{sys}^{\#}\bar{a}_b \tag{4.76}$$

where $\hat{J}_{sys}^{\#} \in \Re^{14x12}$ is the pseudo-inverse of the system Jacobian matrix

and by using Equation (3.129) as

$$\bar{\alpha}_r = \hat{\lambda}\bar{\alpha} = \hat{\lambda}\left(\hat{M}^*\right)^{-1}\left(\hat{B}^*\bar{T} - \bar{Q}^*\right) \tag{4.77a}$$

where

$\hat{B}^* \in \Re^{14x12}$ is the coefficient matrix of the actuating forces and torques,

$\bar{T} \in \Re^{12x1}$ is the vector of actuating forces and

$$\hat{\lambda} = \begin{bmatrix} 1 & 0 & 0 & 0 & 0 & 0 & 0 & 0 & 0 & 0 & 0 & 0 & 0 & 0 \\ 0 & 0 & 1 & 0 & 0 & 0 & 0 & 0 & 0 & 0 & 0 & 0 & 0 & 0 \\ 0 & 0 & 0 & 1 & 0 & 0 & 0 & 0 & 0 & 0 & 0 & 0 & 0 & 0 \\ 0 & 0 & 0 & 0 & 1 & 0 & 0 & 0 & 0 & 0 & 0 & 0 & 0 & 0 \\ 0 & 0 & 0 & 0 & 0 & 0 & 1 & 0 & 0 & 0 & 0 & 0 & 0 & 0 \\ 0 & 0 & 0 & 0 & 0 & 0 & 0 & 1 & 0 & 0 & 0 & 0 & 0 & 0 \\ 0 & 0 & 0 & 0 & 0 & 0 & 0 & 0 & 1 & 0 & 0 & 0 & 0 & 0 \\ 0 & 0 & 0 & 0 & 0 & 0 & 0 & 0 & 0 & 1 & 0 & 0 & 0 & 0 \\ 0 & 0 & 0 & 0 & 0 & 0 & 0 & 0 & 0 & 0 & 1 & 0 & 0 & 0 \\ 0 & 0 & 0 & 0 & 0 & 0 & 0 & 0 & 0 & 0 & 0 & 1 & 0 & 0 \\ 0 & 0 & 0 & 0 & 0 & 0 & 0 & 0 & 0 & 0 & 0 & 0 & 1 & 0 \\ 0 & 0 & 0 & 0 & 0 & 0 & 0 & 0 & 0 & 0 & 0 & 0 & 0 & 1 \end{bmatrix} \tag{4.77b}$$

The inverse dynamics law can similarly be re-formulated by combining the Equation (4.76) and Equation (4.77) as

$$\bar{T} = \hat{M}^{**}_{est}\bar{u} + \bar{Q}^{**}_{est} \tag{4.78}$$

where

$$\hat{M}^{**}_{est} = \left[\hat{\lambda}\left(\hat{M}^{*}_{est}\right)^{-1}\hat{B}^{*}\right]^{-1}\hat{\lambda}\hat{J}^{\#}_{sys} \tag{4.79}$$

$$\bar{Q}^{**}_{est} = \left[\hat{\lambda}\left(\hat{M}^{*}_{est}\right)^{-1}\hat{B}^{*}\right]^{-1}\left[\hat{\lambda}\left(\hat{M}^{*}_{est}\right)^{-1}\bar{Q}^{*}_{est} - \hat{\lambda}\hat{J}^{\#}_{sys}\bar{a}_{b}\right] \tag{4.80}$$

Here, $\bar{u} \in \Re^{12x1}$ is the control input vector and the coefficient matrix $\hat{B}^{*}$ is known exactly and does not contain any uncertain value.

4.5 Thruster Controller Design

As discussed in Section 3.6, the thruster model is based on the fact that the generated thrust force is proportional to the square of the propeller speed. In order to control the propeller speeds, the same kind of inverse dynamics control law can be formulated. For this purpose, the driving torque input τ_k of the k^{th} thruster can be generated as follows:

$$\tau_k = \beta^{-1}_{k_{est}}\left[u_k + Q_{th_{k_{est}}}\right] \tag{4.81}$$

where u_k is the control input that represents the command acceleration of the k^{th} propeller.

The inverse dynamics control law for the thruster expressed by Equation (4.81) has a linearizing effect in the sense that it reduces Equation (3.101) to

$$\dot{\Omega}_k = E'_k u_k + \left(E'_k - 1\right)Q_{th_{est_k}} - Q_{th_{err_k}} \tag{4.82}$$

where

$$E_k^{'} = \beta_k \beta_{k_{est}}^{-1} \tag{4.83}$$

$$Q_{th_{err_k}} = Q_{th_k} - Q_{th_{est_k}} \tag{4.84}$$

Based on Equation (4.82), the command accelerations of the propellers are computed by the feedback of angular velocities using the following type of P control law which can be effectively used to drive propellers of the thrusters as desired:

$$u_k = \dot{\Omega}_k^d + K_{pt_k}\left(\Omega_k^d - \Omega_k\right) \tag{4.85}$$

Here, K_{pt_k} is the feedback gain of the k^{th} thruster. In order to obtain desired angular velocity of the propellers, the desired thrust forces, which are the computed control thrust forces of the UVMS, are used as inputs using Equation (3.101b).

$$\Omega_k^d = C_{t_k}^{-0.5}\left| f_{th_k}^d \right|^{0.5} \mathrm{sgn}(f_{th_k}^d) \tag{4.86}$$

Note that the desired angular acceleration $\dot{\Omega}_k^d$ in Equation (4.85) can be obtained by differentiating the desired angular velocity Ω_k^d expressed in Equation (4.86). However, this operation unnecessarily creates errors due to the numerical differentiation of $f_{th_k}^d$. Therefore, such errors are avoided by the compromise of taking $\dot{\Omega}_k^d = 0$ for all *k*.

By defining the error as $e_{p_t} = \left(\Omega_k^d - \Omega_k\right)$, Equation (4.85) leads to the following linear and first order error dynamics

$$\dot{e}_{p_t} + E_k^{'} K_{pt_k} e_{p_t} = \delta_k^{'} \tag{4.87}$$

where the deflector is obtained as

$$\delta_k^{'} = \left(1 - E_k^{'}\right)\dot{\Omega}_k^d + Q_{th_{k_{err}}} + \left(1 - E_k^{'}\right)Q_{th_{k_{est}}} \tag{4.88}$$

Because of a reasoning which is similar to that explained for Equation (4.64), $\left|e_{p_t}\right|$ can be reduced either by a proper estimation of the propeller efficiency which makes $E_k^{'} \approx 1$ and $Q_{th_{err_k}} \approx 0$ or by choosing K_{pt_k} large enough. The motor torques so computed are then fed back to the thruster dynamic model described by Equation (3.101) in order to find the actual thrust forces required to drive the AUV as desired.

4.6 Trajectory Planning

Trajectory planning is one of the essential aspects in robotics. As explained in the previous sections, the AUV and/or the end-effector of the manipulator can come across with some positions where there is no distinguishable solution and the control inputs shoot to infinity. In addition to these, the manipulator links can face with singular positions during motion when the manipulator Jacobian matrix has less than full rank corresponding to the situations where the joints are aligned in such a way that there is at least one direction of motion that physically cannot be achieved due to the extended or folded positions of the links. Some of these singular configurations of the UVMS having a 6-DOF manipulator subsystem are illustrated in Figure 4.2.

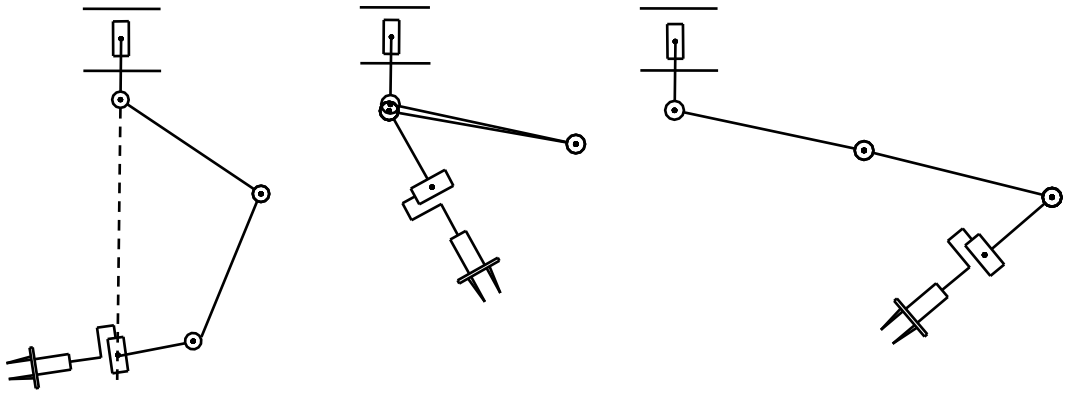

Figure 4.2 Singular Configurations

Therefore, tasks should be carefully planned by taking possible singular positions of the system into account. In this study, the end-effector of the UVMS is required to track a specified motion while the AUV is required to remain fixed at a specified location and orientation. To realize this, two different trajectory profiles are defined in which the singularities are avoided: namely, circular trajectory and straight line trajectory. The circular trajectory represents a typical mine detection mission while the straight line trajectory characterizes a geological sampling mission.

The specified circular motion of the tip point of the end-effector is described by the following equation.

$$\bar{\zeta}_{ee_L}^{d} = \begin{bmatrix} x_{P_0}^{d} + R\cos(\beta - 1) \\ y_{P_0}^{d} + R\sin(\beta) \\ z_{P_0}^{d} \end{bmatrix} \text{m} \tag{4.89}$$

where

$$\beta = \pi\left[1 - \cos\left(\frac{\pi t}{T}\right)\right],$$

T is the period of the motion,

R is the radius of the circle.

The specified cycloidal deployment motions of the tip point coordinates of the end-effector are described by the following equations.

$$x_P^d = \begin{cases} x_{P_0}^{d} + \dfrac{\Delta x_P}{T}\left[t - \dfrac{T}{2\pi}\sin\left(\dfrac{2\pi t}{T}\right)\right] \text{m} & 0 \le t \le T \\ \left[x_{P_0}^{d} + \Delta x_P\right] \text{m} & t > T \end{cases} \tag{4.90}$$

$$y_P^d = \begin{cases} y_{P_0}^{d} + \dfrac{\Delta y_P}{T}\left[t - \dfrac{T}{2\pi}\sin\left(\dfrac{2\pi t}{T}\right)\right] \text{m} & 0 \le t \le T \\ \left[y_{P_0}^{d} + \Delta y_P\right] \text{m} & t > T \end{cases} \tag{4.91}$$

$$z_P^d = \begin{cases} z_{P_0}^d + \dfrac{\Delta z_P}{T}\left[t - \dfrac{T}{2\pi}\sin\left(\dfrac{2\pi t}{T}\right)\right] \text{ m} & 0 \le t \le T \\ \left[z_{P_0}^d + \Delta z_P \right] \text{ m} & t > T \end{cases} \tag{4.92}$$

where $\Delta x_P, \Delta y_P, \Delta z_P$ are the changes in the tip point coordinates.

The specified angular motions of the end-effector in both missions are desired to be the following deployment motion:

$$\psi_i^d = \begin{cases} \psi_{i_0} + \dfrac{\Delta\psi_i}{T}\left(t - \dfrac{T}{2\pi}\sin\dfrac{2\pi t}{T}\right) \text{deg} & 0 \le t \le T \\ \left(\psi_{i_0} + \Delta\psi_i\right) \text{deg} & t > T \end{cases} \tag{4.93}$$

where $\{\Delta\psi_i : i = 1,2,3\}$ are the amounts of change in the Euler angles of the end-effector. It should be reminded that the desired change in $\Delta\psi_2$ should be carefully selected since there exists singularity when the intermediate angle $\psi_2 = 0, \pm\pi$.

CHAPTER V

CONTROL SIMULATIONS

In this chapter, the effectiveness of the control methods explained in Chapter IV is tested in MATLAB/Simulink environment and the results are presented for all three types of systems considered throughout the thesis: namely UVMS, u-UVMS and u-UVRMS. Firstly, the Simulink models which make use of the kinematic and dynamic equations of each body given in Chapter II and Chapter III that are converted into codes using m-files are developed in order to generate the system equations of motion by first producing relevant matrices and vectors and then to apply the control algorithm at each sampling time. Finally, the simulation results of the systems are compared with each other in terms of their closed loop responses and the errors. The main advantages and disadvantages are discussed in detail.

5.1 Simulink Model

The Simulink® models consist of some levels in hierarchy. These are arranged from the lower levels to upper ones. Some of the Simulink blocks create sub-models and these sub-models form another sub-model at one step upper level. This goes on till all of the sub-models constitute the main model of the system at the top level. The main model of the system developed in Simulink consisting of the sub-models together with their feedback lines are illustrated in Figure 5.1. These sub-models can be named as *trajectory generator*, *UVMS dynamics and controller* and *thruster dynamics and controller*. The simulation starts with generating trajectories of the AUV and the manipulator subsystems defined in task space by using the trajectory generator blocks.

These blocks contain *MATLAB function blocks* that use the m-files by utilizing the Equation (4.88) and Equation (4.92) in which the simulation time is generated by the *Clock* block. In the next step, the commanded acceleration inputs are produced which are defined by the Equation (4.63) for both of the subsystems of the UVMSs via the feedback gains. As the inputs of the computed torque block, all of the command accelerations are used to compute the desired thrust forces of the AUV and the actuator torques of the joints by employing the inverse dynamic control algorithm as explained in Sections 4.2–4.4 in a separate m-file in the MATLAB function block. As the actuating torques of the joints are fed to the UVMS dynamics model, i.e. the plant, the desired thrust forces are sent to the thruster controller block to compute the desired torques that drive the propellers of the thrusters using the algorithm explained in Section 4.5. It should be reminded that the angular velocities of the propellers are aimed to be controlled in this block. The motor torques for the propellers so computed become as a vector signal input to compute the actual thrust forces in the thruster dynamics block. Moreover, the current disturbance if ever exists can be another input to the plant. In the formation of the current block in the model, two different Simulink blocks are used, namely *Gaussian noise generator block* which generates Gaussian distributed noise with given mean and variance values to represent a random current force and *Saturation block* to limit the output signal to the upper and lower saturation values.

Similarly, there are also m-files embedded in the MATLAB function block of the UVMS plant for the forward dynamics solution. The m-files representing Newton-Euler equations for both subsystems produce the rates of the velocities of the AUV as well as the joint accelerations using the input vectors: the actuating thrust forces of the AUV, the actuating torques of the joints, the linear velocities of the origin of the body-fixed frame of the AUV, the angular body-fixed velocities of the AUV, the angular displacements and the angular velocities of the joints. In these m-files, the matrices $\hat{M}^*$, $\bar{Q}^*$ and $\hat{B}^*$ explained in Chapter III are generated and the matrix $\hat{H}$ is obtained via Symbolic Math Toolbox of MATLAB in order to eliminate the reaction forces and moments at each sampling time.

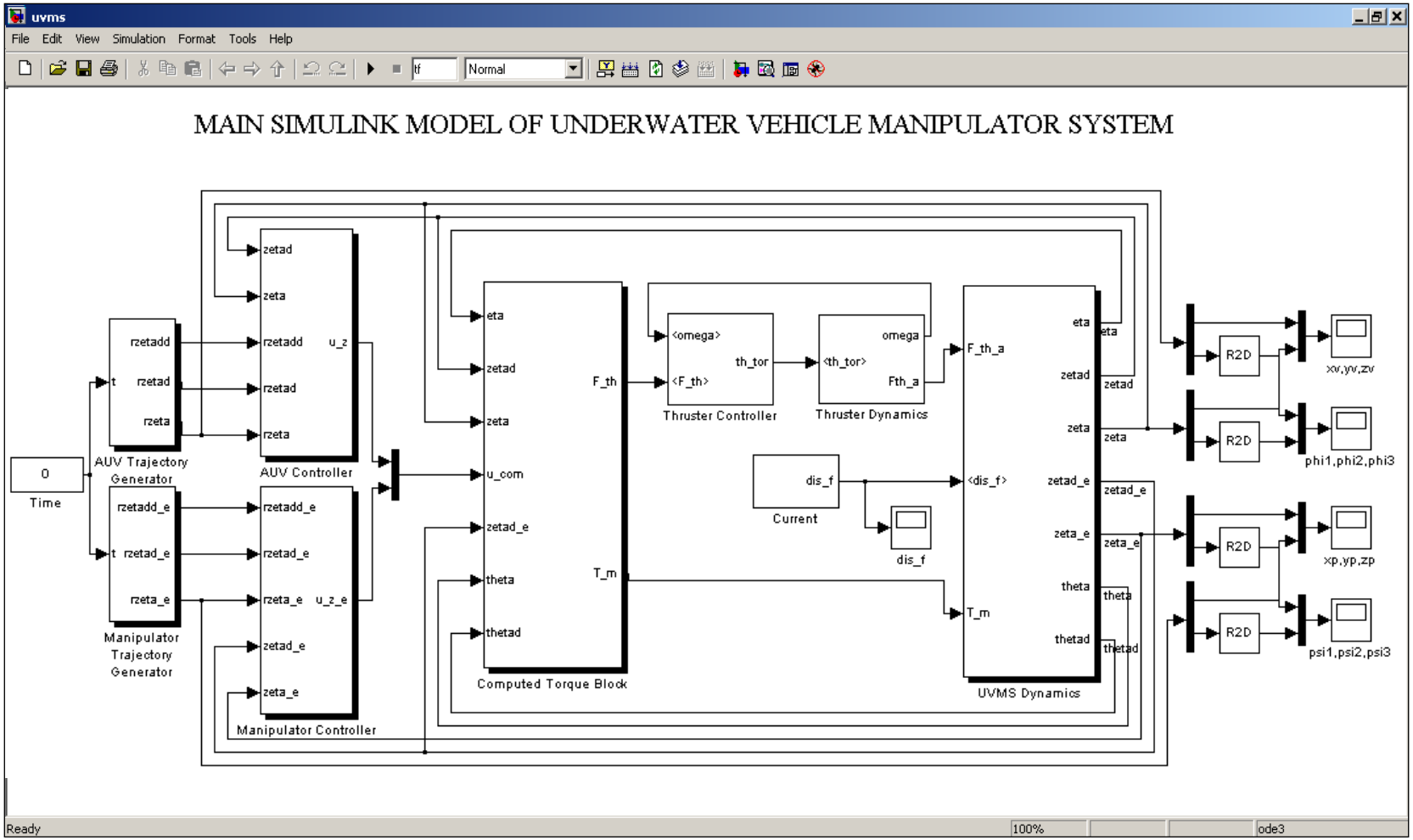

Figure 5.1 UVMS Simulink Model

Having obtained the rates of the velocities of the AUV and the joint accelerations, the position and velocity related variables are obtained by numerical integration to be taken as the measured quantities by using the initial conditions of the AUV and the joints in the integration block of the model. The computed values of the velocities of the AUV together with the joint positions and velocities feed the forward kinematics block of the model to work out the kinematic expressions given in Chapter II.

Hence, all of the kinematic information about the AUV and the links of the manipulator subsystem expressed in the task space is figured out. That gives opportunity to visualize the motion by creating 3-D plots at each sampling time and to monitor the responses of the UVMSs using the *Scope blocks*. Moreover, the task space position and velocity signals are fed back to the UVMS inverse dynamics controller to generate the command inputs for the next time step of the simulation.

Before the simulation starts, some parameters should be necessarily introduced, namely *the constant parameters* like the initial conditions, the geometric and mass properties of the UVMS, the model parameters of the thrusters etc. and *the configuration parameters* consisting of the parameters required for Simulink itself like solver options and simulation time. In all of the simulations, ode3 (Bogacki-Shampine) solver which is one of the fixed-step type solvers is used with a sampling frequency of 100 Hz (i.e. a sampling time t=10 ms).

5.2 Simulation Results

After constructing the system model and setting the initial conditions, the computer simulations are carried out for all three types of the systems which are

- fully actuated UVMS,
- underactuated UVMS,
- underactuated UVRMS.

Although the some of the parameters of the systems are given in relevant parts, the hydrodynamic added mass and added inertia coefficients and the changes in damping force/moment coefficients are given in Appendix-B.

All of the simulations are performed under two test scenarios for two different missions (see Section 4.6) corresponding to four test conditions as given in Table 5.1.

Table 5.1 Test Scenarios and Missions

Mission	**Scenario**	**Condition**
Mine Detection	Initial error	C1
	Initial error, modeling error & disturbance	C2
Geological Sampling	Initial error	C3
	Initial error, modeling error & disturbance	C4

In the first test scenario, the motions of the systems are tested in the presence of position errors in the tip point coordinates of the end-effector, i.e. the initial coordinates are different than the initial task coordinates.

The second test scenario corresponds to a case where there exist parametric uncertainties in both the constant model parameters of the propeller efficiency of the thrusters and the hydrodynamic coefficients of the AUV and the manipulator links such as lift, drag, side force / moment and added mass coefficients. In the series of simulations,

- the propeller efficiency is taken to be 20% smaller,
- the hydrodynamic coefficients of the vehicle are taken to be 20% smaller and 20% larger,
- the hydrodynamic coefficients of the manipulator links are taken to be 40% smaller and 40% larger as tabulated in Table 5.2.

Among the combinations of uncertainty, the worst case performance is spotted.

Table 5.2 Parametric Uncertainty Combinations

Uncertain Parameters	Case-1	Case-2	Case-3	Case-4
AUV: Added mass coefficients Added inertia coefficients Damping force/moment coefficients	20%	-20%	20%	-20%
Propeller efficiency (nominal value= 0.30)	-20%	-20%	-20%	-20%
Manipulator: Added mass coefficients Added inertia coefficients Damping force/moment coefficients	40%	40%	-40%	-40%

In addition to initial and modeling errors, the effects of the ocean currents are analyzed in the second test scenario as well. The systems are further enforced to work in the presence of nonzero mean current forces in order to emphasize the effectiveness of the control methods.

To demonstrate the control performance, the following graphs are plotted:

- Closed loop responses of the AUV and the manipulator subsystems
- Position errors of the AUV and the manipulator subsystems
- Control thrust forces of the AUV
- Control motor torques of the joints
- Angular displacements of the joints
- Control motor torques of the propellers
- Angular velocity responses of the thrusters

5.2.1 Fully Actuated UVMS Results

The fully actuated UVMS has a 6-DOF spatial manipulator and AUV having a prolate spheroidal shape. It is modeled as a *neutrally buoyant* system meaning that

total buoyant force is equal to total gravitational force acting on the system. However, the AUV and manipulator links are not neutrally buoyant individually as specified in Table 5.3. In the calculation of the masses, the specific weight of the aluminum is taken as $\rho_{al} = 2700\ kg/m^3$ and the density of the sea water is taken as $\rho_w = 1020\ kg/m^3$. The centers of gravity and buoyancy of the manipulator links are coincident due to their symmetrical homogeneous shapes. That means the moments created by the hydrostatic forces disappear in the dynamic equations since they are derived with respect to the mass centers of the links.

Table 5.3 UVMS Mass and Geometry Properties

	Length (m)	**Radius (m)**	**Volume (m^3)**	**Mass (kg)**	**Buoyancy (N)**	**Weight (N)**
AUV	2.000	0.125	0.0654	60.2	654.9	590.7
Link-1	0.500	0.020	0.0006	1.7	6.3	16.6
Link-2	0.900	0.020	0.0011	3.1	11.3	30.0
Link-3	1.200	0.020	0.0015	4.1	15.1	39.9
Link-4	0.250	0.020	0.0003	0.8	3.1	8.3
Link-5	0.150	0.020	0.0002	0.5	1.9	5.0
Link-6	0.100	0.020	0.0001	0.3	1.3	3.3

In order to design the UVMS as a neutral buoyant system, the mass of the AUV is calculated as $m_v = 60.2$ kg after the calculation of the masses of the links and the total buoyant force acting on the system. Therefore, the ratio of the masses of two subsystems are computed as

$$\frac{m_v}{m_m} = 5.72 \tag{5.1}$$

The position vector of the center of gravity of the AUV is given as

$$\bar{r}_{G_v} = \begin{bmatrix} -0.5 \\ 0 \\ 0.03 \end{bmatrix} \tag{5.2}$$

The system is assumed to be at rest initially with its configuration given in Figure 5.2. The initial location and orientation of the AUV are specified as

$$x_{v_0} = 3.00\,\text{m}, y_{v_0} = 2.00\,\text{m}, \; z_{v_0} = 1.00\,\text{m}; \tag{5.3}$$

$$\phi_{1_0} = \phi_{2_0} = \phi_{3_0} = 0^o \tag{5.4}$$

The initial joint angles of the manipulator are specified as

$$\begin{aligned} \theta_{1_0} &= 0^\circ \\ \theta_{2_0} &= 30^\circ \\ \theta_{3_0} &= 120^\circ \\ \theta_{4_0} &= -30^\circ \\ \theta_{5_0} &= 90^\circ \\ \theta_{6_0} &= 0^\circ \end{aligned} \tag{5.5}$$

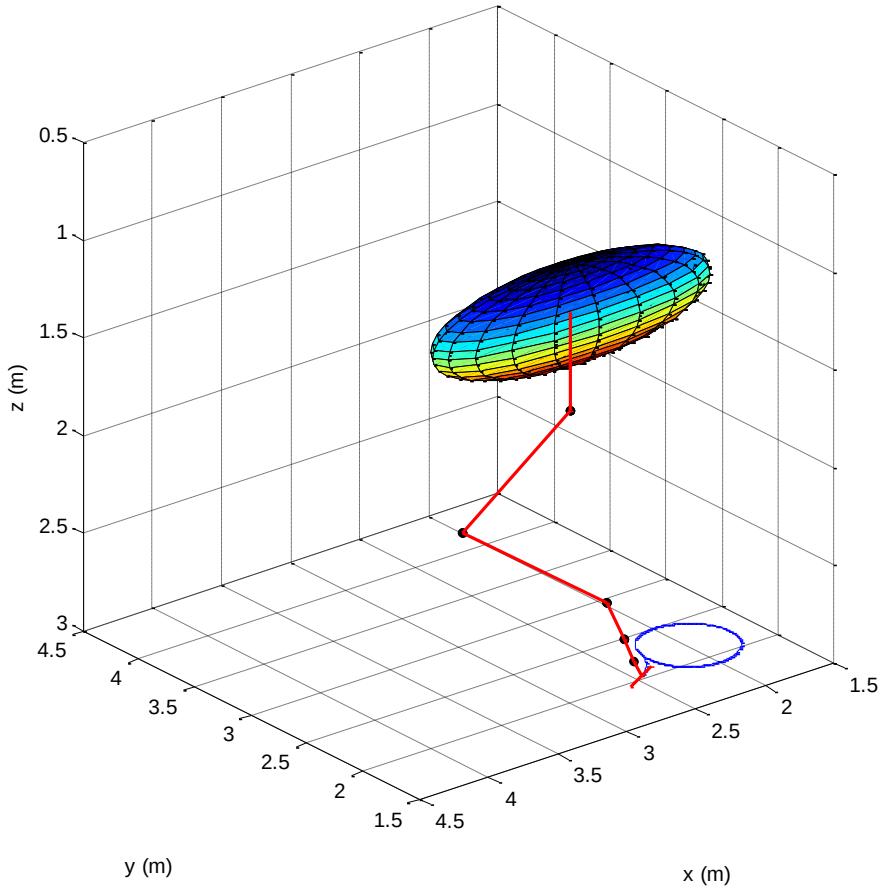

Figure 5.2 UVMS Initial Configuration

The initial location and orientation of the end-effector corresponding to the initial AUV position and the initial joint angles are obtained as

$$x_{P_0} = 2.49\,\text{m},\ y_{P_0} = 2.00\,\text{m},\ z_{P_0} = 2.98\,\text{m} \tag{5.6}$$

$$\psi_{1_0} = 180^o,\ \psi_{2_0} = 30^o,\ \psi_{3_0} = -90^o \tag{5.7}$$

However, the initial desired coordinates of the tip point of the end-effector which is shown in Figure 5.2 by a circle are specified as

$$x_{P_0}^d = 2.45\,\text{m},\ y_{P_0}^d = 2.00\,\text{m},\ z_{P_0}^d = 2.90\,\text{m}. \tag{5.8}$$

which means there exists initial position error.

The specified angular motions of the end-effector are desired to be as in Equation (5.9) with the following amounts of change in the Euler angles

$$\Delta\psi_1 = -60^0,\ \Delta\psi_2 = 0^0,\ \Delta\psi_3 = 0^0 \tag{5.9}$$

Since, the initial desired Euler angles of the end-effector are taken as the same as their initial values, initial orientation errors does not exist.

The thrusters are configured in such a way that their position vectors are

$$\bar{r}_{th_1} = -\bar{r}_{th_2} = \begin{bmatrix} 0 \\ 0 \\ 4b_v \end{bmatrix} \tag{5.10}$$

$$\bar{r}_{th_3} = -\bar{r}_{th_4} = \begin{bmatrix} a_v/2 \\ 0 \\ 0 \end{bmatrix} \tag{5.11}$$

$$\bar{r}_{th_5} = -\bar{r}_{th_6} = \begin{bmatrix} 0 \\ 2b_v \\ 0 \end{bmatrix} \tag{5.12}$$

where a_v and b_v are the semi-axes of the AUV.

The thruster parameters as well as the parameters given in Equation (3.102) through Equation (3.104) are taken as in Table 5.4.

Table 5.4 Thruster Parameters

Parameter	Value
Nozzle diameter	8.22 [inch]
Nozzle length	3.58 [inch]
Propeller efficiency	0.30 [-]
Pitch angle	30 [deg]
α_t	0.8660 [-]
β_t	10.4023 [$(Nm)^{-1}$ s^{-2}]
C_t	0.9613 [Ns^2]

The velocity and position feedback gain diagonal matrices $\hat{K}_v, \hat{K}_p$ are chosen to have a smooth critically damped transition (i.e. ς_j=1.0) from the actual to the desired trajectory as

$$K_{v_{jj}} = 2\omega_j,\ K_{p_{jj}} = \omega_j^2 \ \text{ for all } \ j = 1,...,12. \tag{5.13}$$

After lots of trials, the constant control parameter set

$$\{\omega_i = 10 \text{ rad/s} : i = 1,...,6\} \tag{5.14}$$

for the AUV and the time-varying control parameter set

$$\{\omega_i(\mathrm{t}) = \begin{cases} \dfrac{\omega_i^u - \omega_i^l}{e^{t_s} - 1} e^t + \left(\omega_i^l - \dfrac{\omega_i^u - \omega_i^l}{e^{t_s} - 1} \right) \text{ rad/s} & 0 < \mathrm{t} \le \mathrm{t_s} : i = 7,8,9\} \\ \omega_i^u \text{ rad/s} & \mathrm{t_s} \le \mathrm{t} \end{cases} \tag{5.15}$$

$$\{\omega_i(\mathrm{t}) = \begin{cases} \dfrac{3}{2}\left[\dfrac{\omega_i^u - \omega_i^l}{e^{t_s} - 1} e^t + \left(\omega_i^l - \dfrac{\omega_i^u - \omega_i^l}{e^{t_s} - 1} \right) \right] \text{ rad/s} & 0 < \mathrm{t} \le \mathrm{t_s} : i = 10,11,12\} \\ \omega_i^u \text{ rad/s} & \mathrm{t_s} \le \mathrm{t} \end{cases} \tag{5.16}$$

for the manipulator are observed to yield satisfactory closed loop responses which are illustrated in Figure 5.3 and Figure 5.4. In Equations (5.15) and (5.16), t_s is the settling time of the closed loop response and ω_i^l, ω_i^u are the lower and upper values of $\omega_i(\mathrm{t})$ which are taken respectively as 20 rad/s and 60 rad/s. The reason for choosing variable feedback gains for the manipulator is due to the need for decreasing the initial control torques that are caused by the initial position errors.

Meanwhile, the proportional feedback gains of the thrusters to control the angular speeds of the propellers are taken as

$$K_{pt_j} = 80 \text{ for } j = 1,...,6. \tag{5.17}$$

Since large values of the feedback gain K_{pt} increase the initial control thrust forces, the saturator blocks are used to limit the excessive amount of the forces which cause overshoots in the closed loop responses.

The radius of the circle is taken as $R = 0.30\,\mathrm{m}$ by taking some singular positions into account. It is concluded that increasing the radius of the circle has an increasing effect on the control torques of the joints of the manipulator subsystem. In addition to this, increasing the radius more than a certain value causes the system being out of its workspace boundary although the feedback gains of AUV subsystem are high enough.

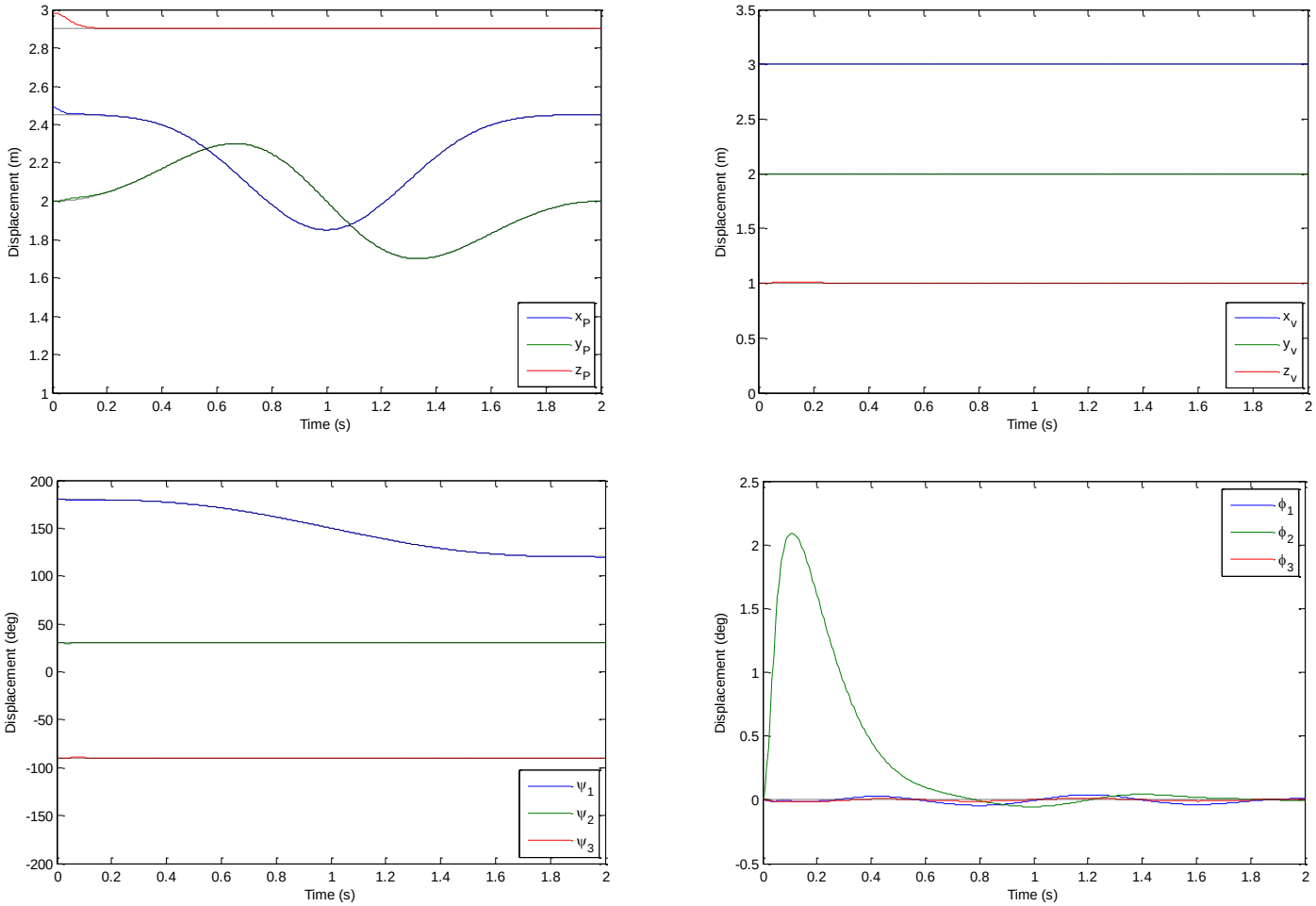

Figure 5.3 UVMS Closed Loop Responses (C1) (--- Desired, —Response)

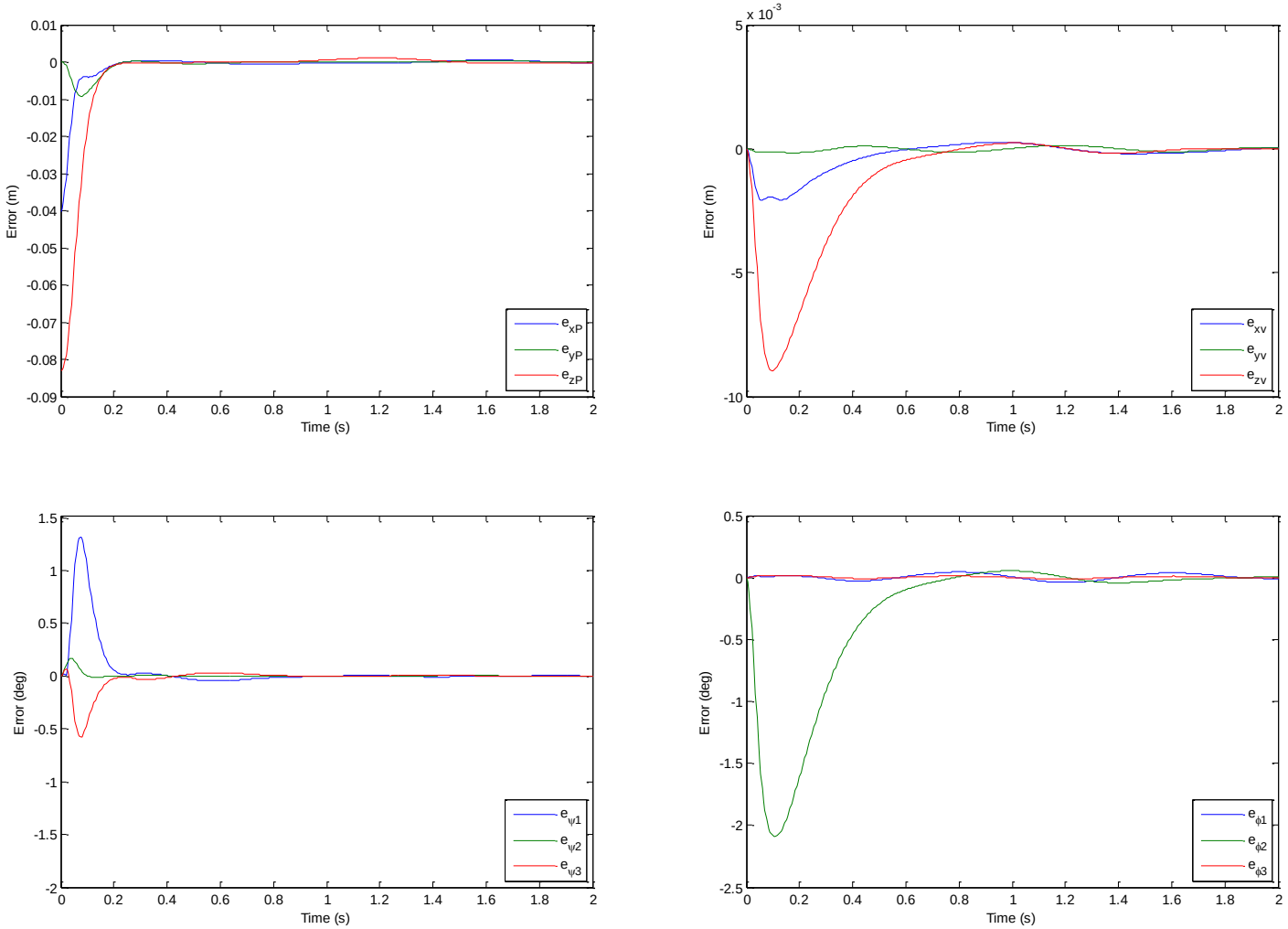

Figure 5.4 UVMS Position Errors (C1)

The results showed that good tracking properties are achieved for all task variables. The steady state and tracking errors are in negligible levels for such a system working in underwater environment. The motor control torques of the joints and the resulting forces of the thrusters are displayed in Figure 5.5.

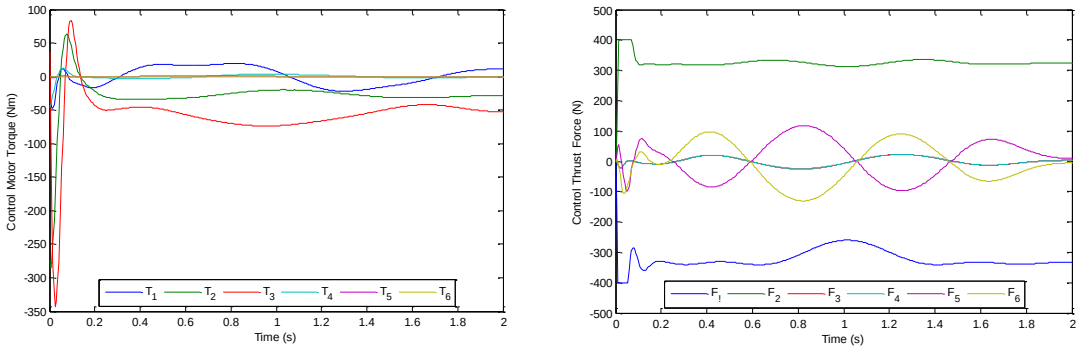

Figure 5.5 UVMS Control Forces and Torques (C1)

It is observed that the initial errors cause larger initial torques and larger tracking errors during motion. As ω_i's increase without altering the simulation conditions, the tracking errors tend to decrease to the cost of large initial control forces and torques to be applied by the thrusters and actuators. The upper and lower bounds on the control inputs of thrusters are 400 N. The corresponding angular displacements of the joints are given in Figure 5.6

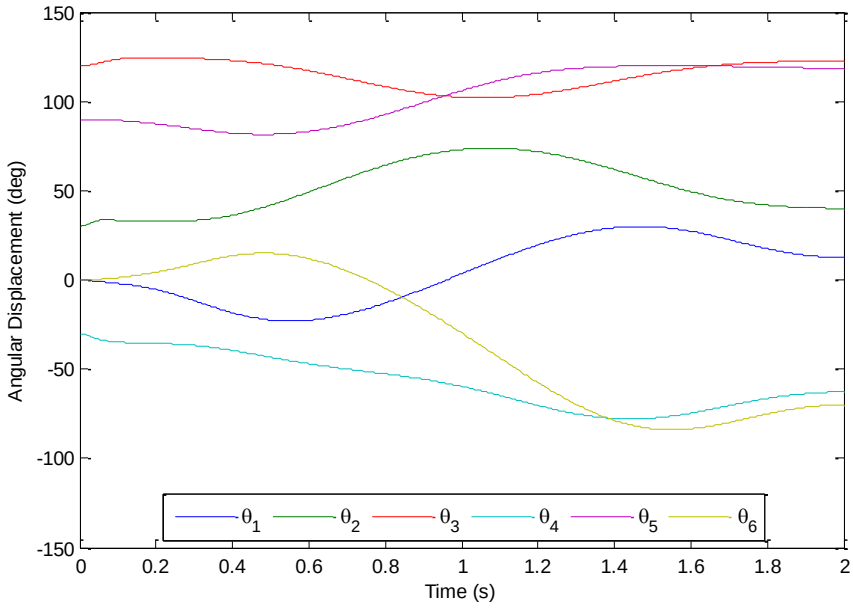

Figure 5.6 UVMS Joint Displacements (C1)

To disturb the system more and see the effects of modeling error in addition to initial error, the closed loop system is simulated under the parametric uncertainty combinations defined in Table 5.2. When the control simulations are performed using the previously defined feedback gains, it is observed that the worst case performance corresponds to Case-4 with the resulting motor control torques of the joints and control forces of the thrusters displayed in Figure 5.7.

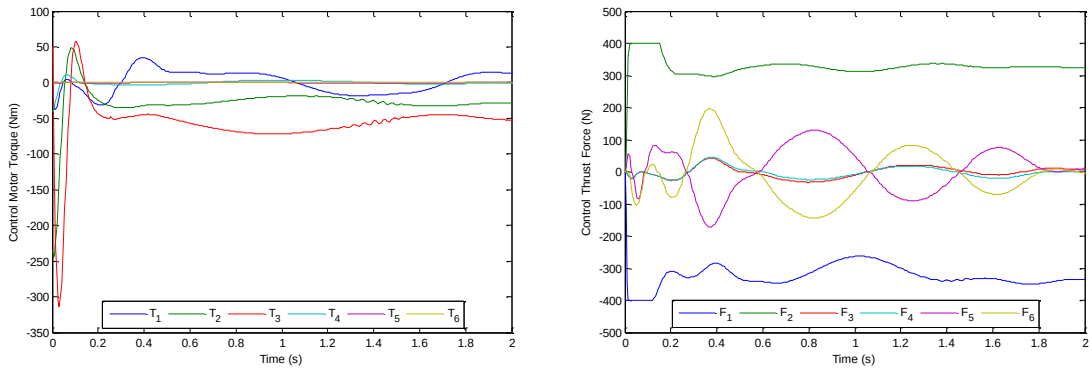

Figure 5.7 UVMS Control Forces and Torques (C2)

The angular velocity responses of the thrusters are depicted in Figure 5.8 while the closed loop responses and the errors in the presence of modeling error and disturbance are obtained as shown in Figure 5.9 and Figure 5.10 respectively.

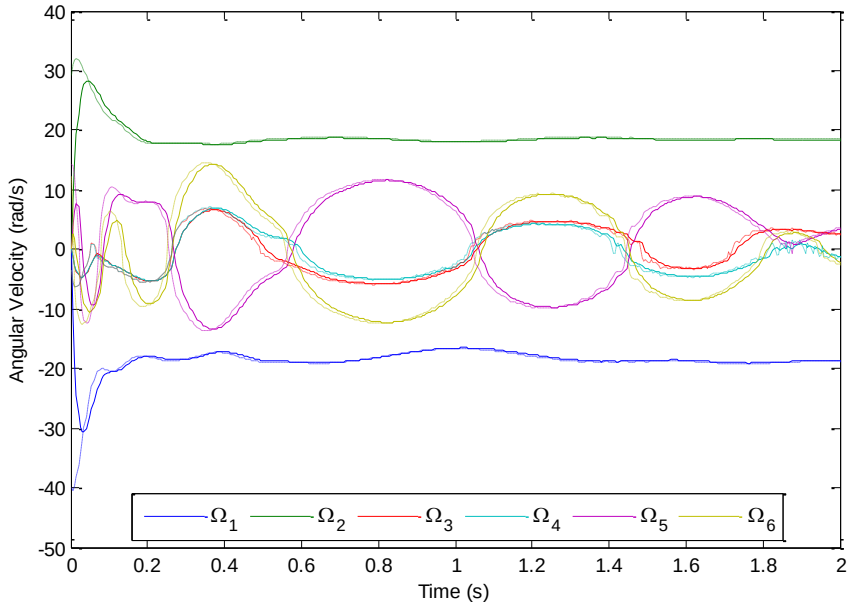

Figure 5.8 UVMS Propeller Speed Responses (C2) (--- Desired, — Response)

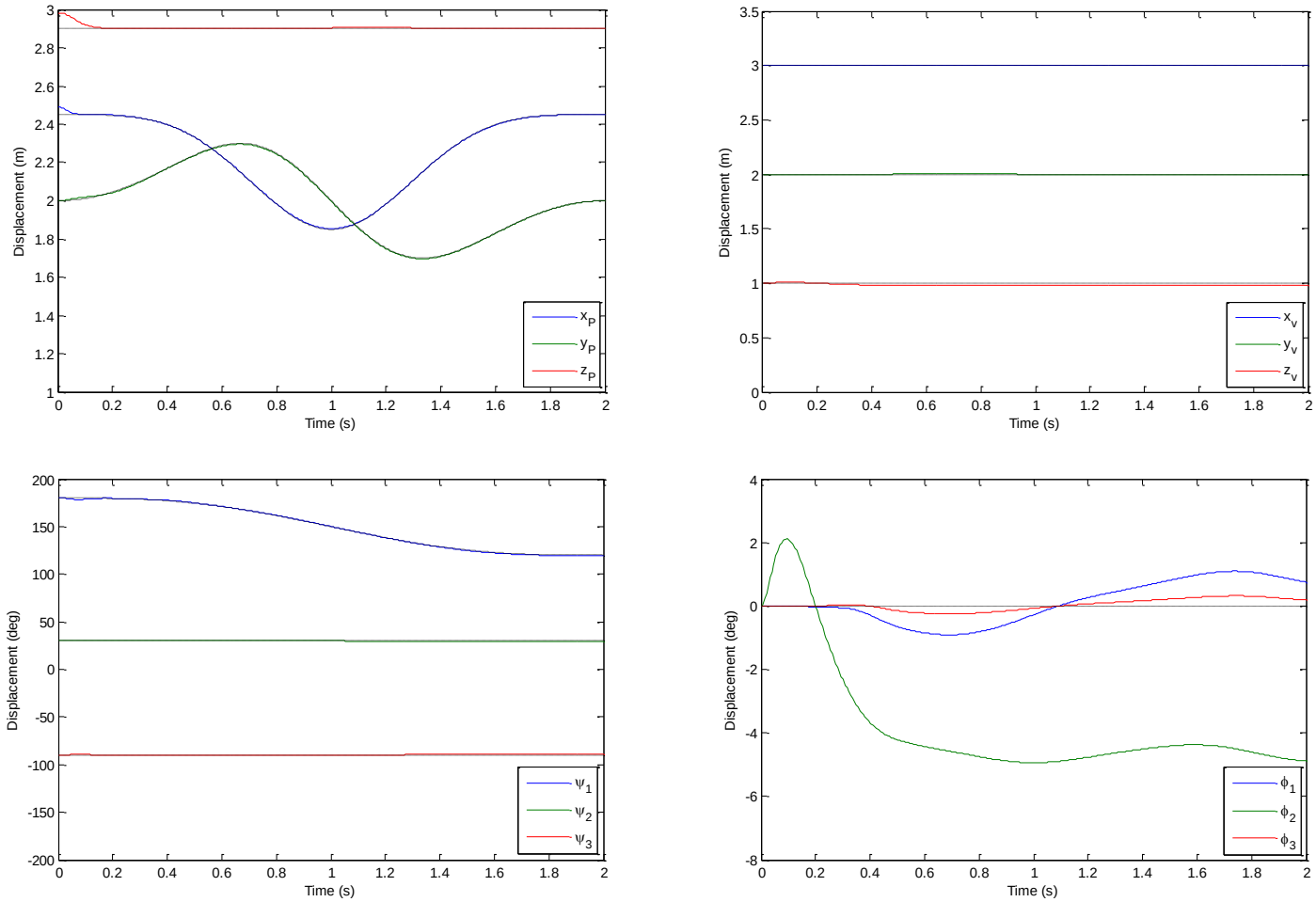

Figure 5.9 UVMS Closed Loop Responses (C2) (--- Desired, ─ Response)

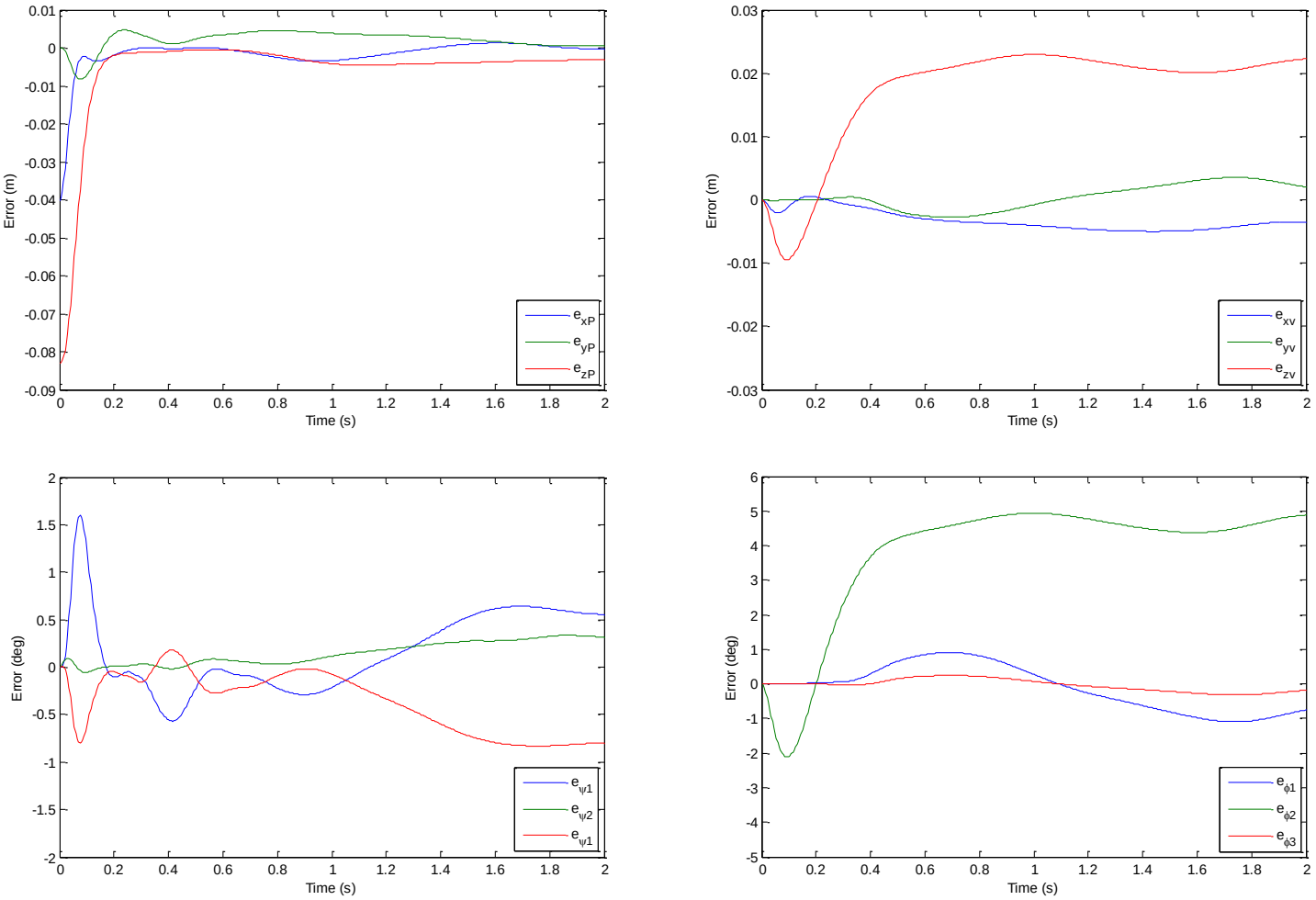

Figure 5.10 UVMS Position Errors (C2)

The results in Figure 5.10 showed that angular velocities of the propellers are controlled effectively and the errors are in negligible levels. However, by increasing the proportional gain in Equation (5.17) further causes increase in the torques that are applied by the motors of the propellers presented in Figure 5.11. The upper and lower bounds on the control inputs of motors are 60 Nm.

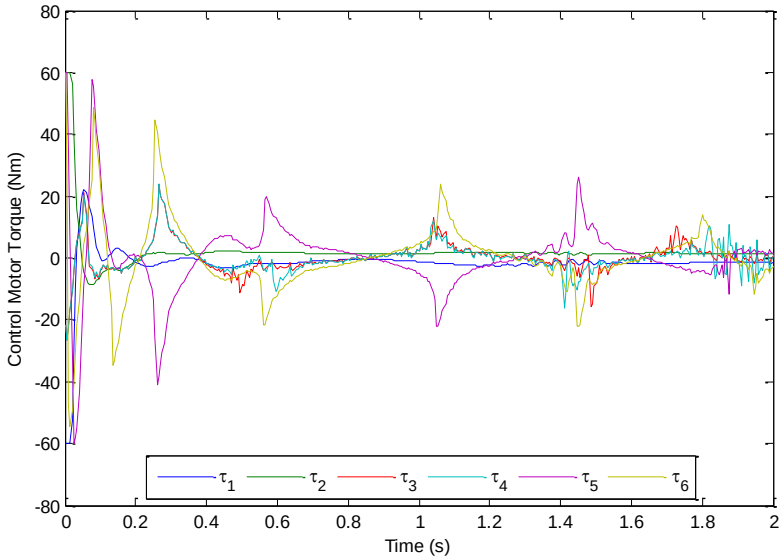

Figure 5.11 UVMS Thruster Motor Control Torques (C2)

In conclusion, the results showed that the tracking performance of the system is still quite satisfactory even in the presence of the external disturbance together with the parametric uncertainty. It is also observed that the steady state errors are small and tracking errors increase but they remain in acceptable levels even in the worst case. The errors of the end-effector variables, on the other hand, can be reduced further to the expense of larger control torques and the increase in the tracking errors of the AUV by increasing ω_i values of the manipulator subsystem. The control forces and torques to be supplied by the actuators and the thrusters increase slightly as far as Figure 5.5 and Figure 5.9 are concerned. Besides that, it is also inferred that the position and velocity feedback gain matrices which are chosen according to the ITAE criterion i.e. $\varsigma_i = 0.705$ cause overshoots yielding higher tracking errors as illustrated as an example in Figure 5.12 for the response of z_P coordinate of the tip point.

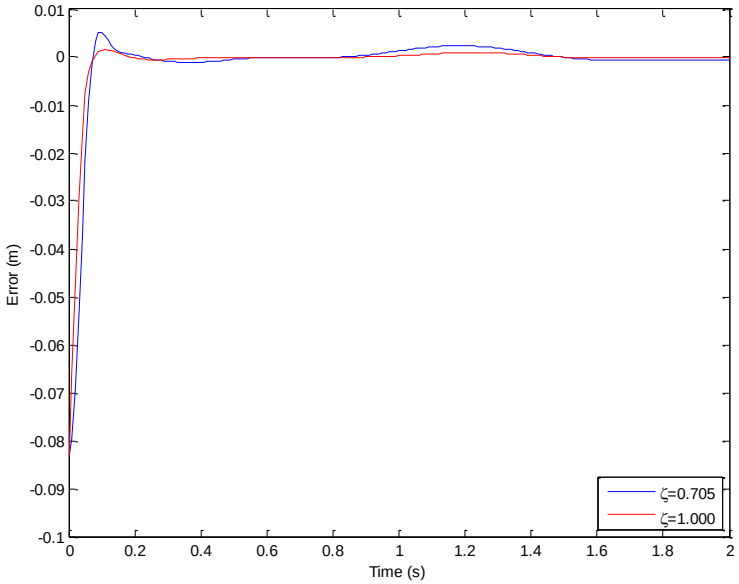

Figure 5.12 Effect of Damping Ratio on Responses

Since it is aimed to perform the underwater manipulation as slow but as accurate as possible in this study, all of the feedback gains are selected in such a way that the responses obey a smooth critically damped transition as much as possible, i.e. $\varsigma_i = 1.0$ for all *i*. In the simulations, the period the deployment motion is taken as $T = 2\text{s}$. As a general rule, increasing this parameter has a decreasing effect on the errors of task variables of both subsystems. Conversely, selecting the period of time below a certain value may cause instability and divergence in the controlled parameters.

5.2.2 Underactuated UVMS Results

The fully actuated system discussed in the previous section is reduced to an underactuated one by leaving thrusters in sway directions uncontrolled (see Figure 3.7). This creates the lack of actuation not only in sway direction but also in yaw direction of the AUV. The reason for doing this is to analyze the effectiveness of the developed control method for the underactuated system and to minimize the total energy required for the system to some certain extent. Having assigned the same initial joint space and task space variables and the feedback gains as in the previous

case, the closed loop responses and the errors are obtained as in Figure 5.13 and Figure 5.14, respectively.

The following statements can be listed as compared to the UVMS C1 results:

- The tracking errors of the AUV increase and the deviations are observed in the uncontrolled DOF's up to 4 centimeters in sway and 3 degrees in yaw.
- The tracking errors of the end-effector of the manipulator subsystem increase due to the uncontrolled AUV motion.
- The angular velocities and the torques provided by the motors of the thrusters do not have significant changes during motion.

In the second group of simulations, u-UVMS is tested in the presence of parametric uncertainty and the disturbing ocean current. In such a condition, the closed loop responses and the errors illustrated in Figure 5.15 and Figure 5.16 reveal that

- The tracking errors of the AUV increase especially in heave and pitch motions and the deviations are observed in the uncontrolled DOF's up to 8 centimeters in sway and 2 degrees in yaw.
- The tracking errors of the end-effector of the manipulator subsystem increase more due to the uncontrolled AUV motion.
- The control forces/torques supplied to the system increase slightly while the angular speeds remain almost the same as depicted in Figures 5.17-5.19.

When the results are compared with those of UVMS C2, it can be expressed that tracking errors of the tip point coordinates of the end-effector are higher especially in the second half of the motion. This is due to the fact that the disturbing force becomes dominant in negative sense such that the end-effector motion is much more affected by the uncontrolled motion of the AUV. This, in turn, causes the steady state errors to be high as well. However, these errors are still assessed to be acceptable as far as the energy minimization is concerned.

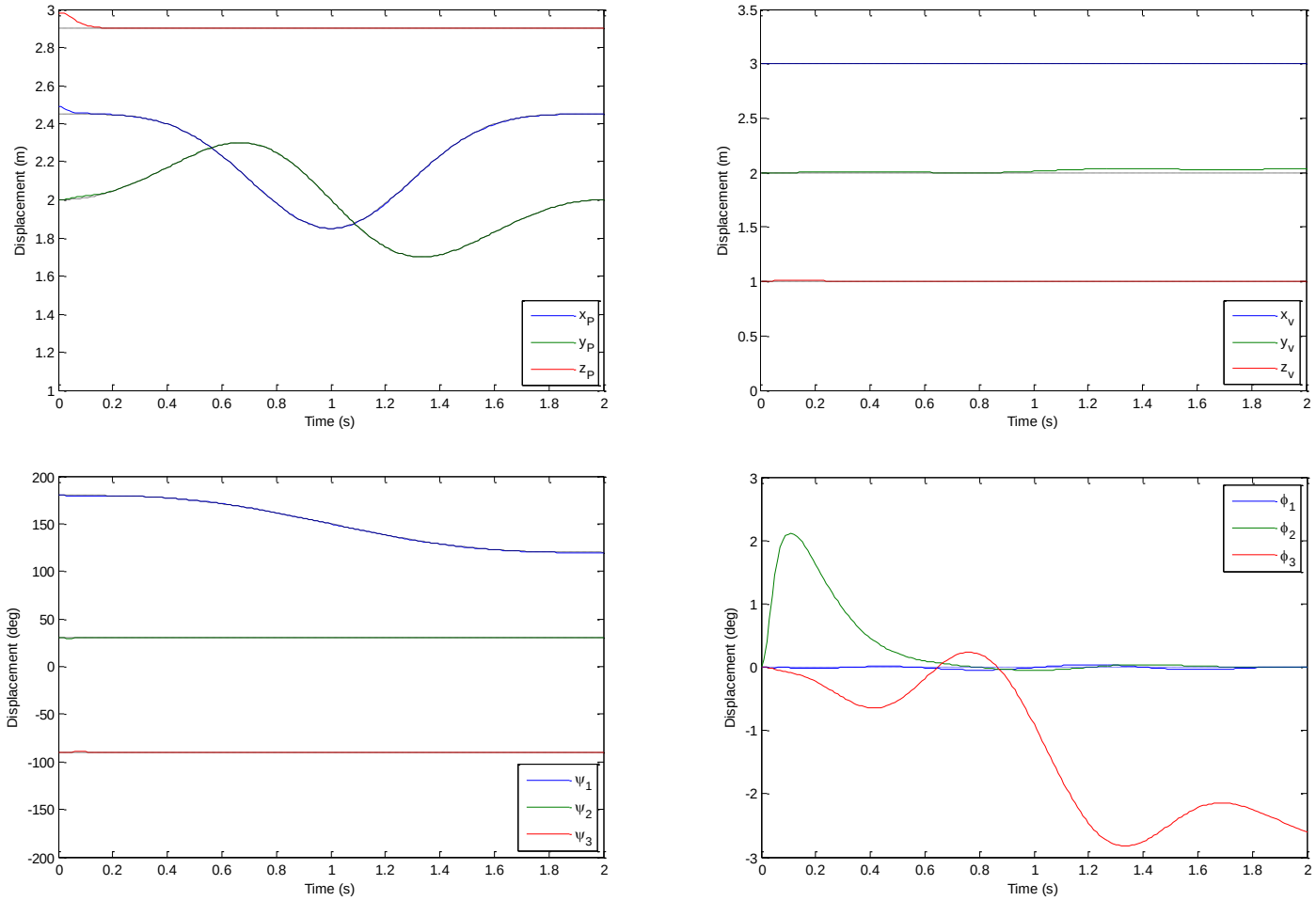

Figure 5.13 u-UVMS Closed Loop Responses (C1) (--- Desired, ― Response)

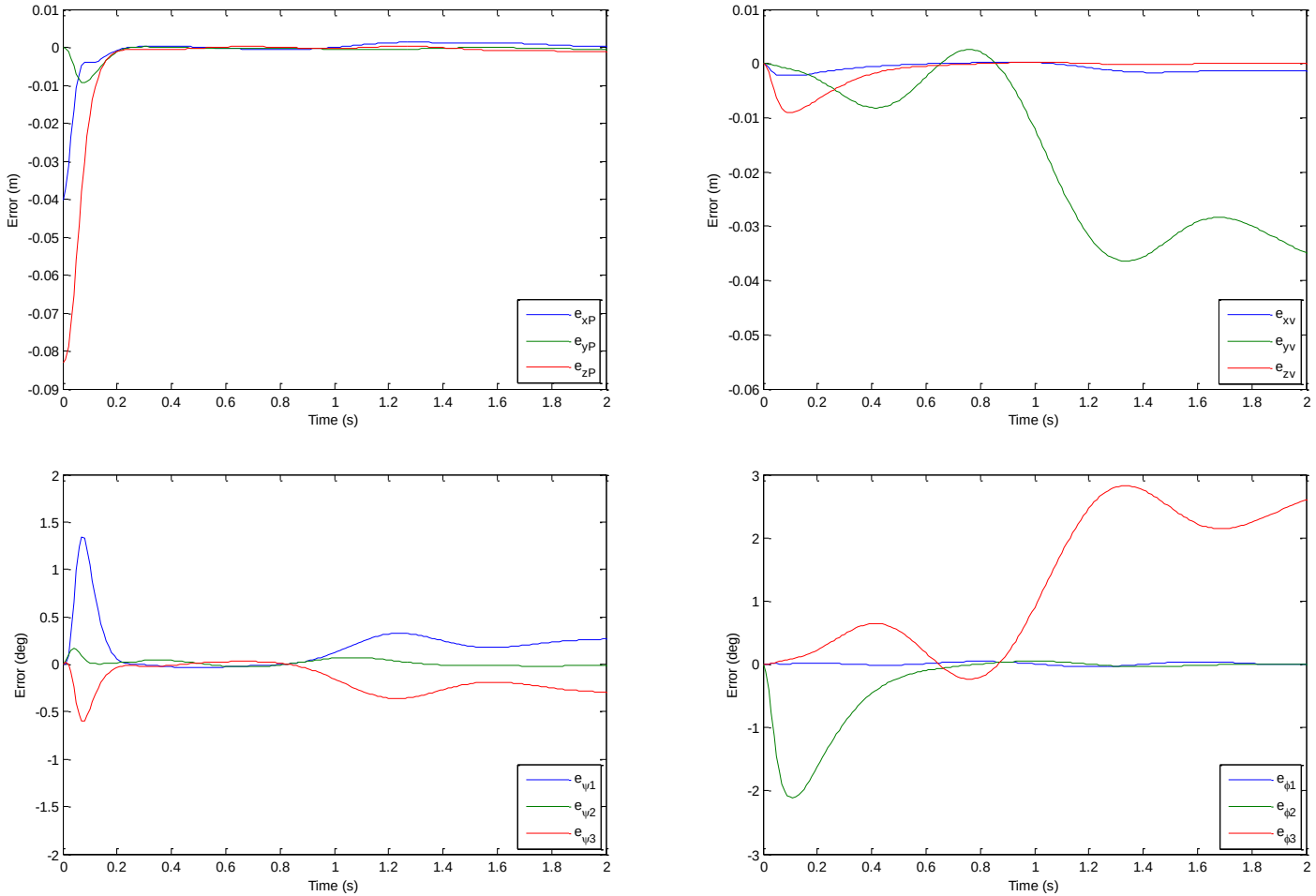

Figure 5.14 u-UVMS Position Errors (C1)

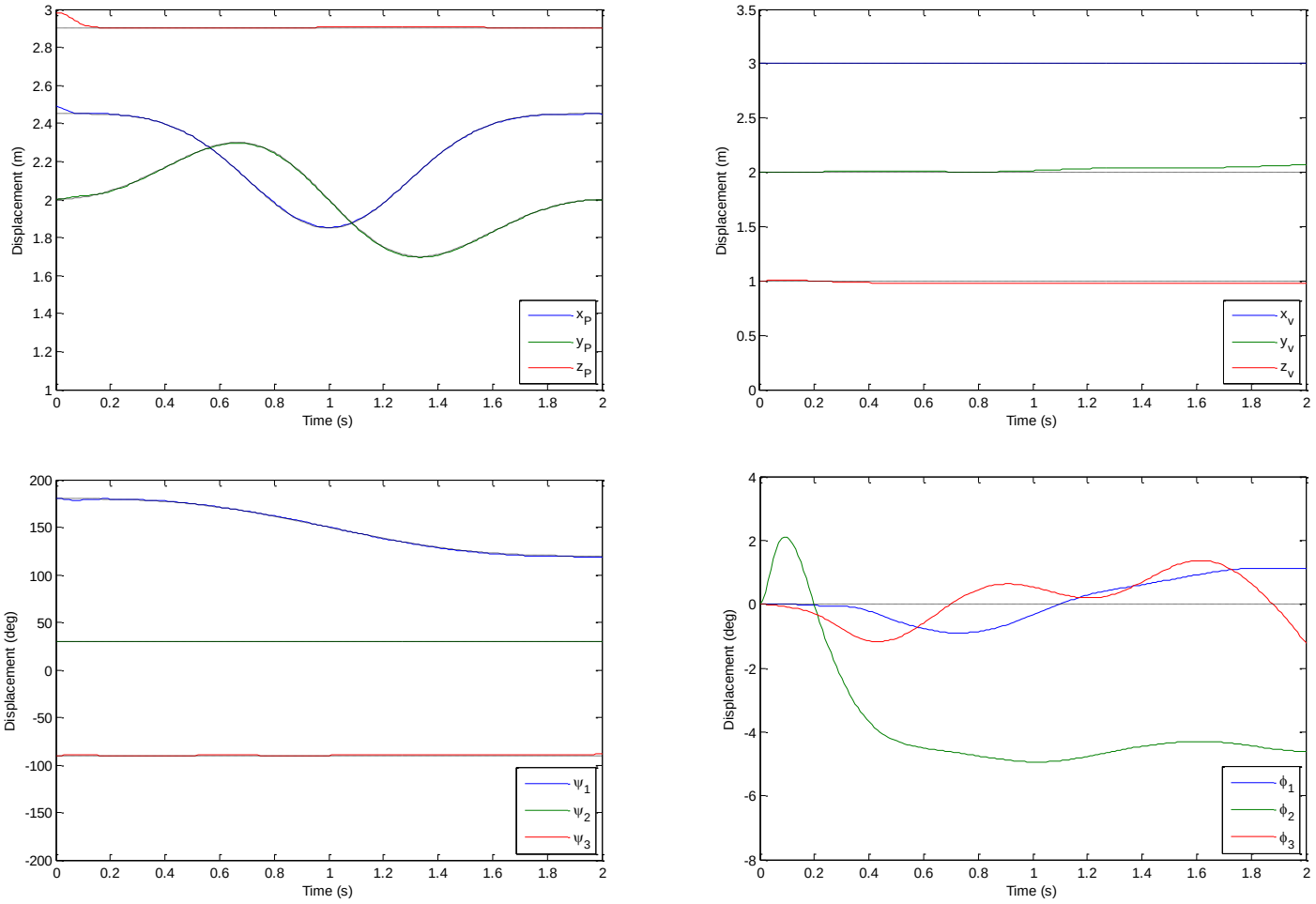

Figure 5.15 u-UVMS Closed Loop Responses (C2) (--- Desired, ─ Response)

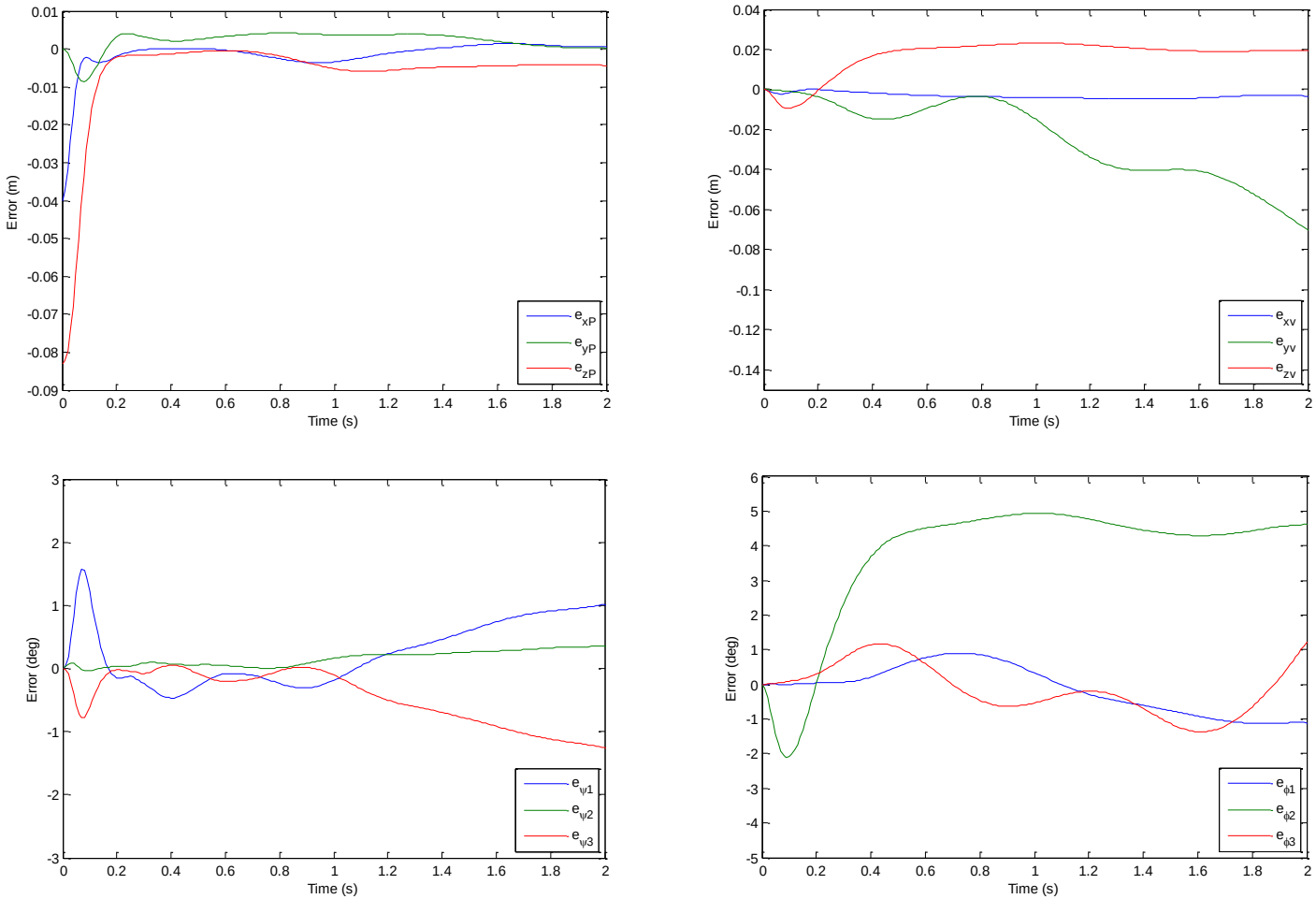

Figure 5.16 u-UVMS Position Errors (C2)

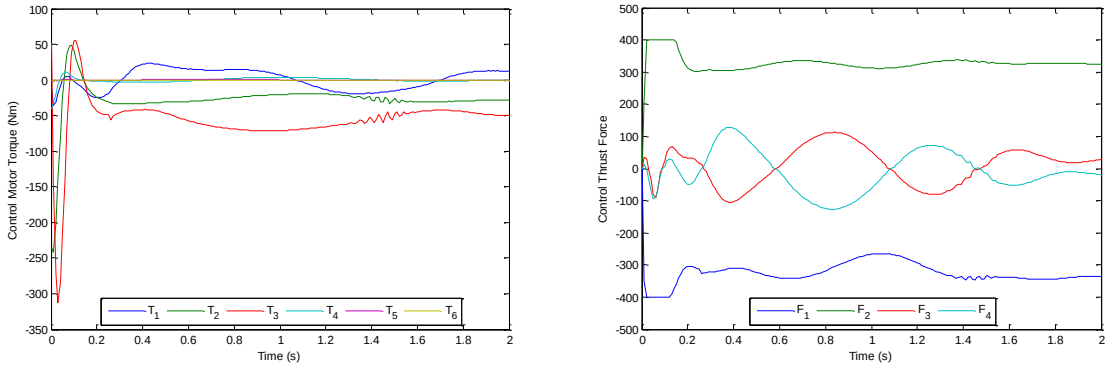

Figure 5.17 u-UVMS Control Forces and Torques (C2)

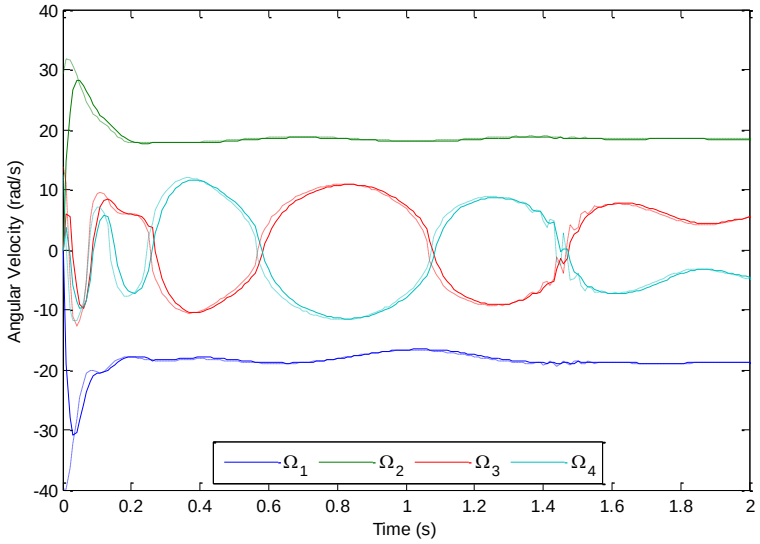

Figure 5.18 u-UVMS Propeller Speed Responses (C2) (--- Desired, — Response)

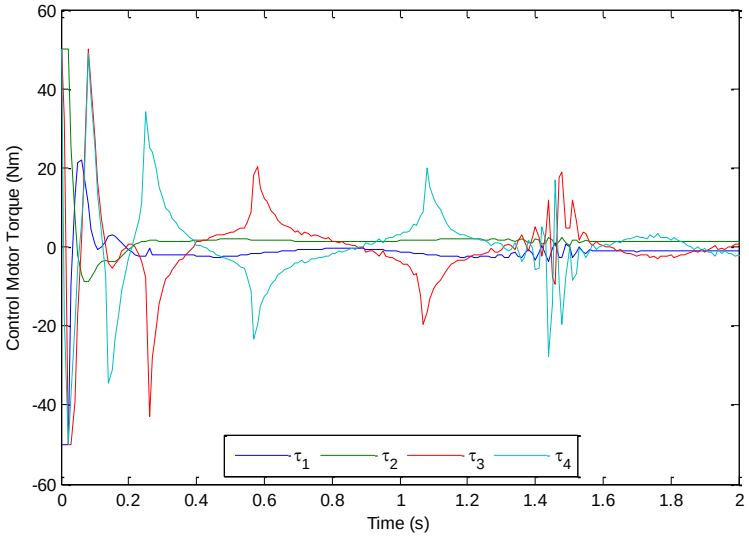

Figure 5.19 u-UVMS Thruster Motor Control Torques (C2)

5.2.3 Underactuated UVRMS Results

The underactuated UVRMS has an 8-DOF redundant manipulator and an underactuated AUV. It is also modeled as a neutrally buoyant system although the AUV and manipulator links are not so individually as specified in Table 5.5.

Table 5.5 UVRMS Mass and Geometry Properties

	Length (m)	**Radius (m)**	**Volume (m^3)**	**Mass (kg)**	**Buoyancy (N)**	**Weight (N)**
AUV	1.000	0.125	0.0654	60.21	654.90	590.70
Link-1	0.500	0.020	0.0006	1.70	6.29	16.64
Link-2	0.600	0.020	0.0008	2.04	7.54	19.97
Link-3	0.300	0.020	0.0004	1.02	3.77	9.99
Link-4	0.200	0.020	0.0003	0.68	2.51	6.66
Link-5	1.000	0.020	0.0013	3.39	12.57	33.28
Link-6	0.250	0.020	0.0003	0.85	3.14	8.32
Link-7	0.150	0.020	0.0002	0.51	1.89	4.99
Link-8	0.100	0.020	0.0001	0.34	1.26	3.33

The mass of the AUV is calculated after the calculation of the masses of the links and the total buoyant force acting on the system in a similar manner as $m_v = 60.2$ kg. Therefore, the ratio of the masses of two subsystems are kept the same as in Equation (5.1) in order to indicate the advantages and disadvantages of the systems.

The system is assumed to be at rest initially with its configuration given in Figure 5.20. The initial location and orientation of the AUV are specified as before while the initial joint angles of the manipulator are

$\theta_{1_0} = 0^\circ$
$\theta_{2_0} = 30^\circ$
$\theta_{3_0} = 0^\circ$

$$\theta_{4_0} = -30^\circ \tag{5.18}$$
$$\theta_{5_0} = 0^\circ$$
$$\theta_{6_0} = 60^\circ$$
$$\theta_{7_0} = 90^\circ$$
$$\theta_{8_0} = 0^\circ$$

The initial location and orientation of the end-effector corresponding to the initial AUV position and the initial joint angles are obtained as

$$x_{P_0} = 2.49\,\text{m},\ y_{P_0} = 2.00\,\text{m},\ z_{P_0} = 2.98\,\text{m} \tag{5.19}$$

$$\psi_{1_0} = 180^o,\ \psi_{2_0} = 30^o,\ \psi_{3_0} = 90^o \tag{5.20}$$

The initial desired coordinates of the tip point of the end-effector are taken as the same as ones given in Equation (5.8).

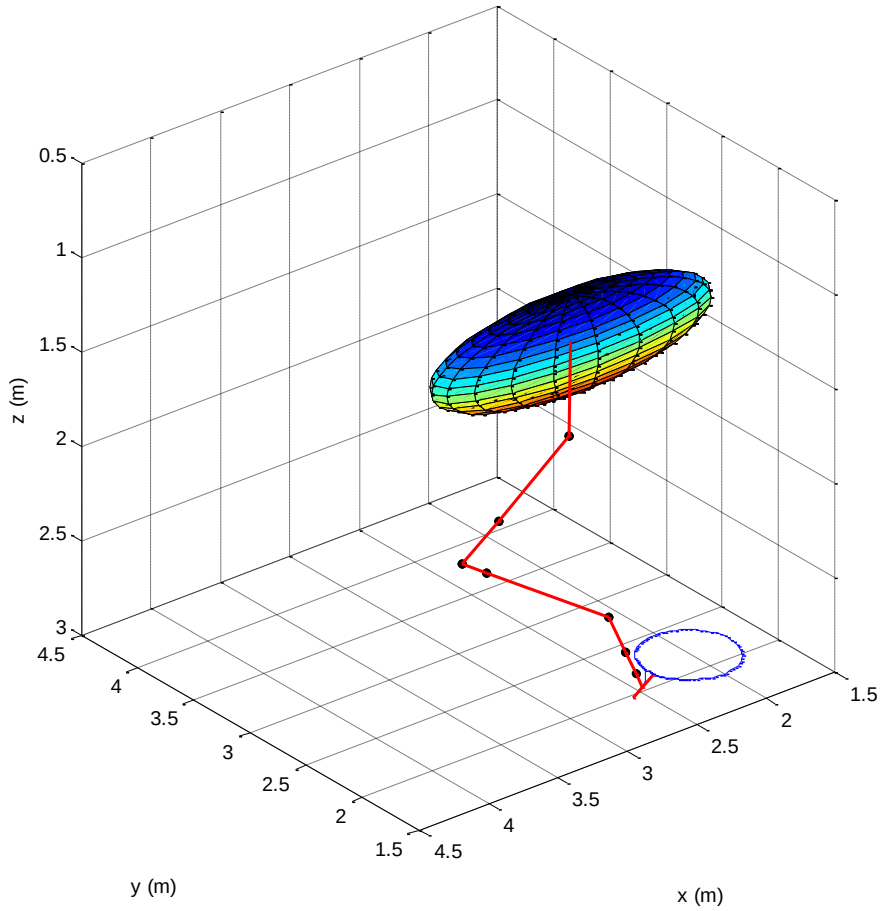

Figure 5.20 u-UVRMS Initial Configuration

The hydrodynamic effects on the links of the redundant manipulator having fineness ratio greater than 15 are taken into account. The design mainly concentrates not only on minimizing the energy this time but also reducing the interaction of the AUV and the manipulator subsystem for higher precision manipulation. For this purpose, the control parameter set for the AUV is kept the same and the upper value of $\omega_i(t)$ in the control parameter sets for the manipulator are selected as $\omega_i^u = 50$ rad/s to obtain satisfactory closed loop responses which are illustrated in Figure 5.21 and Figure 5.22. In the simulations, the period the deployment motion is taken as $T = 3\text{s}$.

The following statements can be listed as compared to the u-UVMS C1 results:

- Although the tracking errors of the AUV increase and the deviations in the sway and yaw directions are still observed, the amounts of them are nearly halved.
- The tracking errors of the end-effector of the manipulator subsystem decrease significantly since and the coupling effects are greatly reduced.
- The angular velocities and the torques provided by the motors of the thrusters decrease during motion.

As usual, u-UVRMS is also tested in the presence of parametric uncertainty and the disturbing ocean current. In such a condition, the closed loop responses and the errors illustrated in Figure 5.23 and Figure 5.24 reveal that

- The deviations increase up to 6 centimeters in sway and 4 degrees in yaw.
- The tracking errors of the end-effector of the manipulator subsystem increase as expected.
- The control forces/torques supplied to the system increase slightly while the angular velocities remain almost the same as depicted in Figures 5.25–5.27.

When the results are compared with those of UVMS C2, it can be expressed that tracking errors of the tip point coordinates of the end-effector are lower. As for the steady state values, they are a little bit higher because the feedback gains are not as

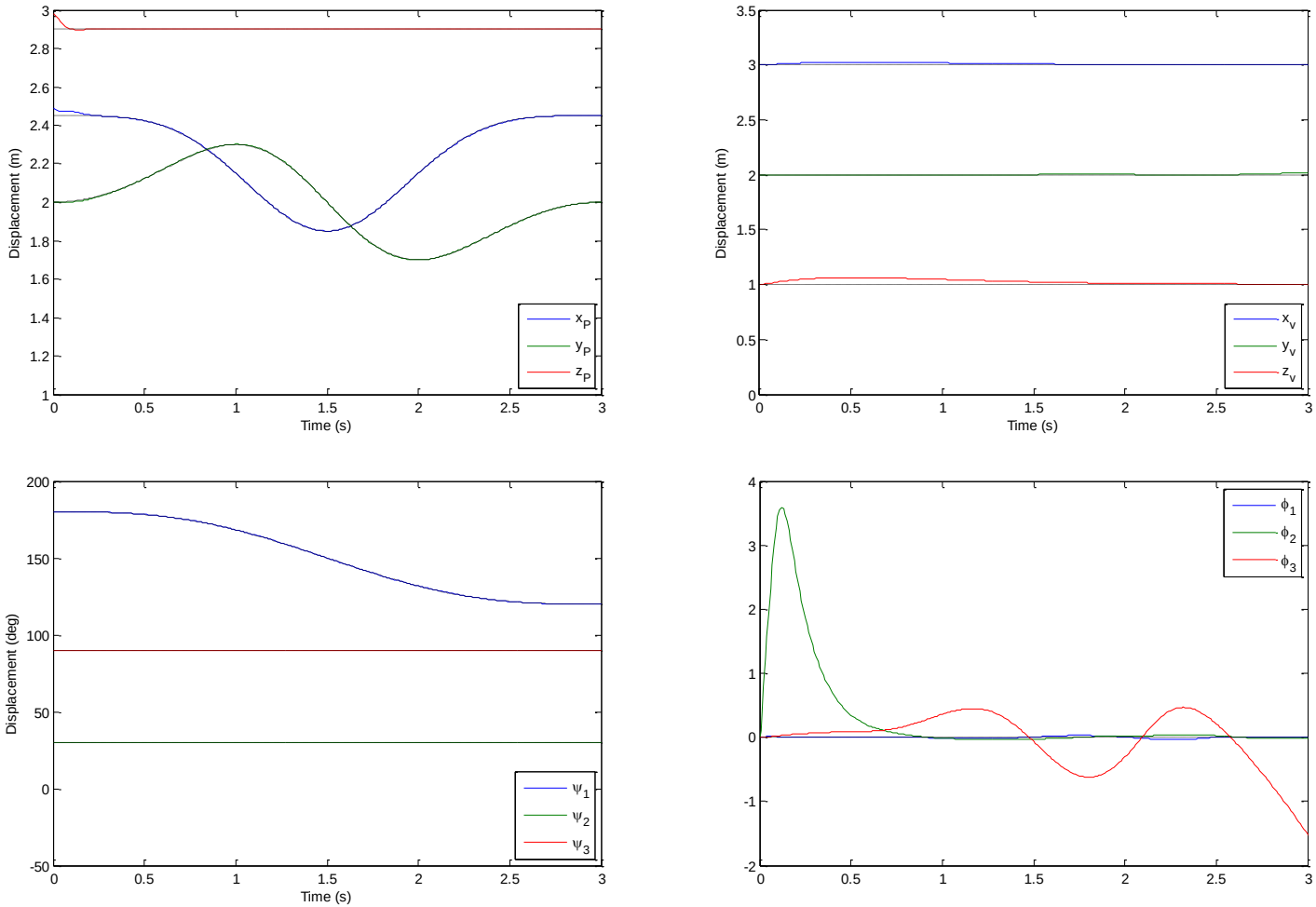

Figure 5.21 u-UVRMS Closed Loop Responses (C1) (--- Desired, ─ Response)

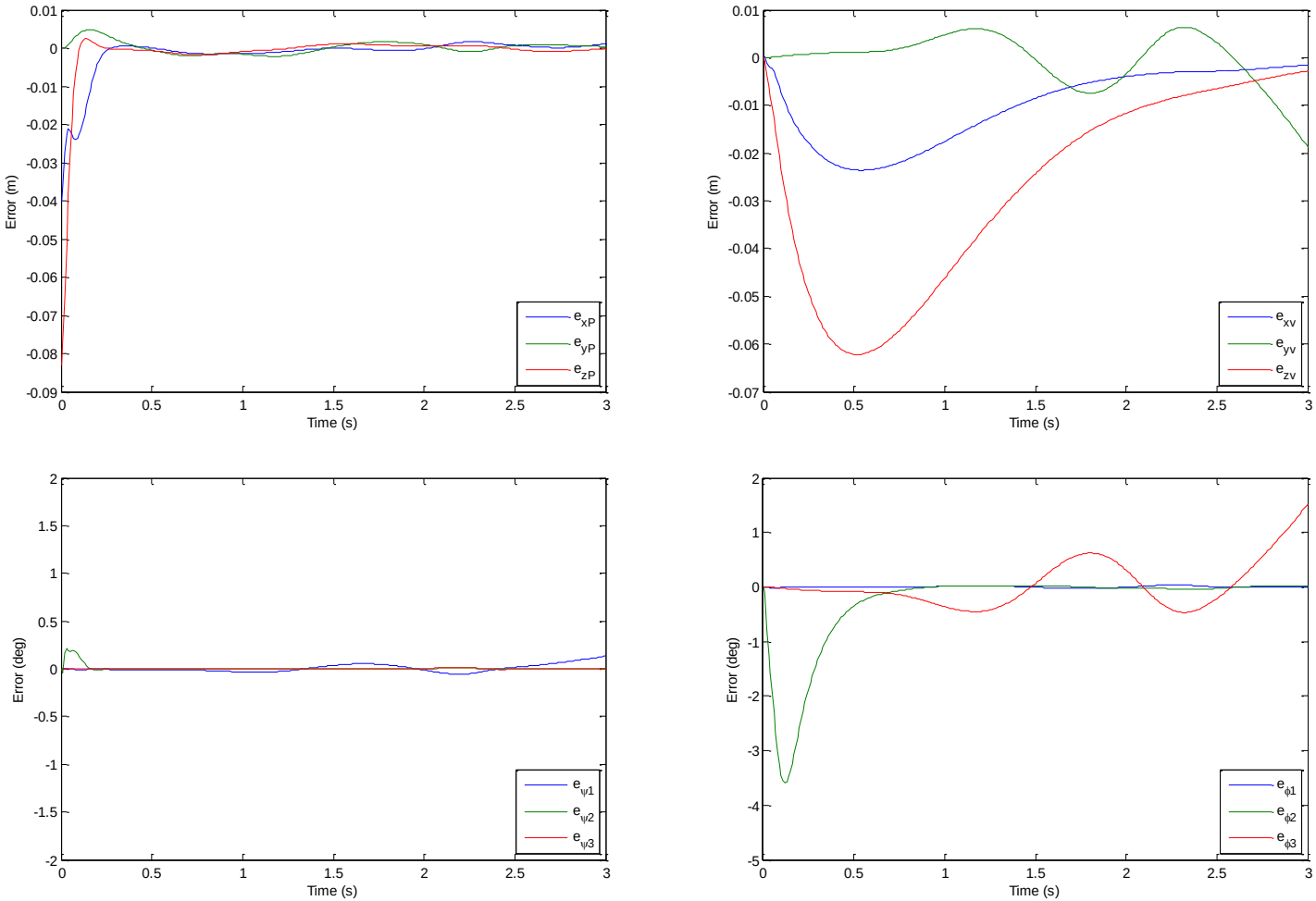

Figure 5.22 u-UVRMS Position Errors (C1)

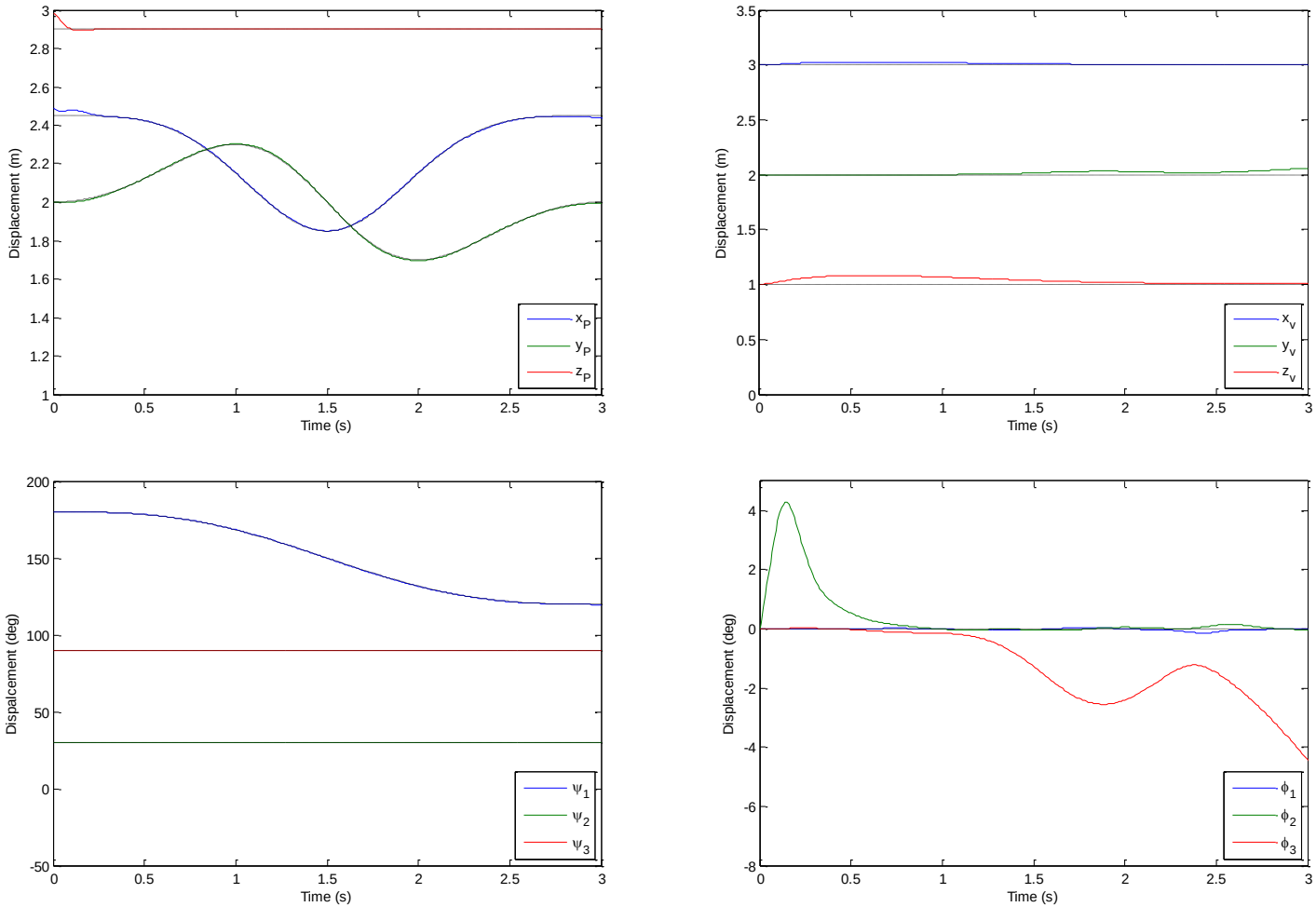

Figure 5.23 u-UVRMS Closed Loop Responses (C2) (--- Desired, ⎯ Response)

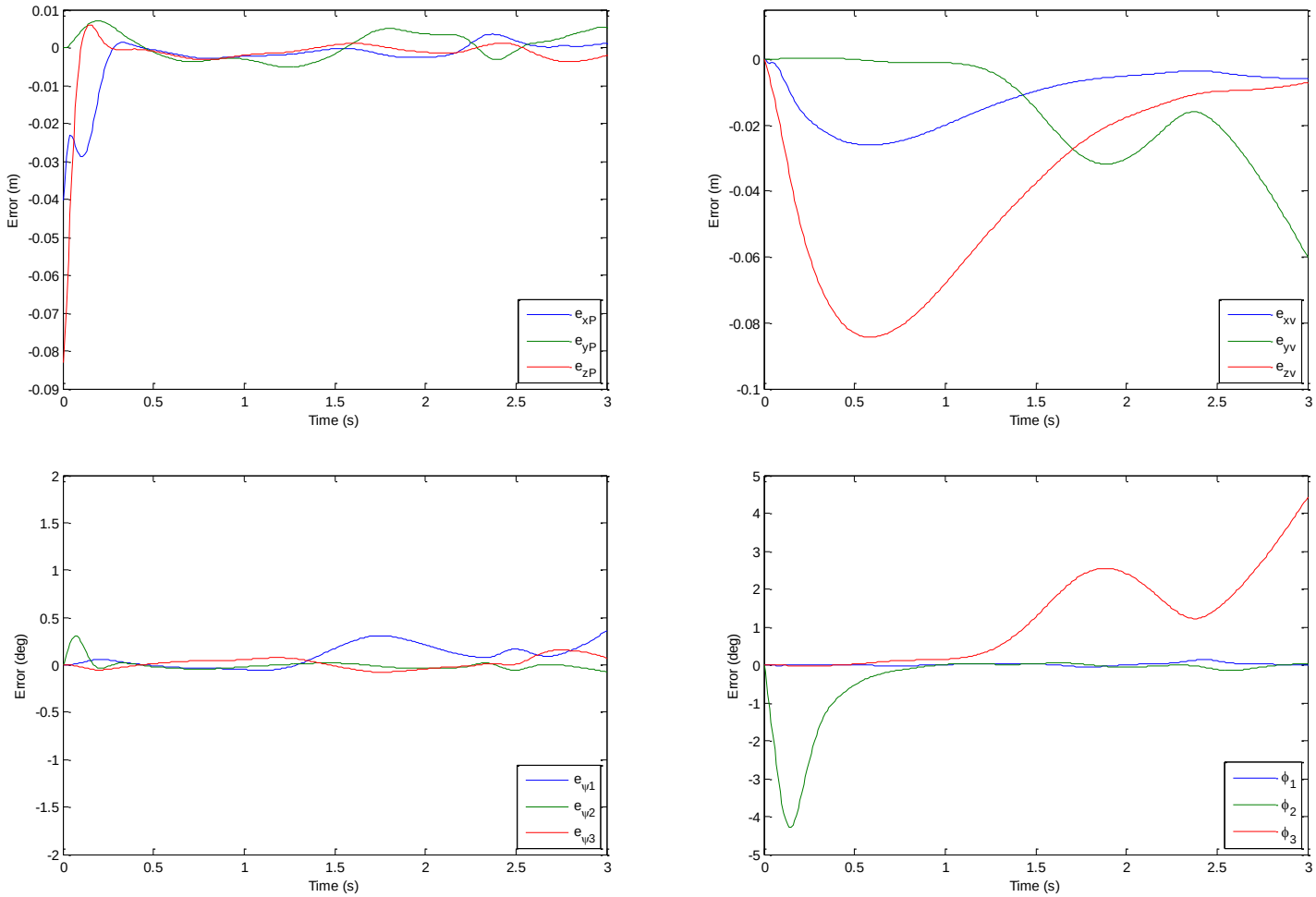

Figure 5.24 u-UVRMS Position Errors (C2)

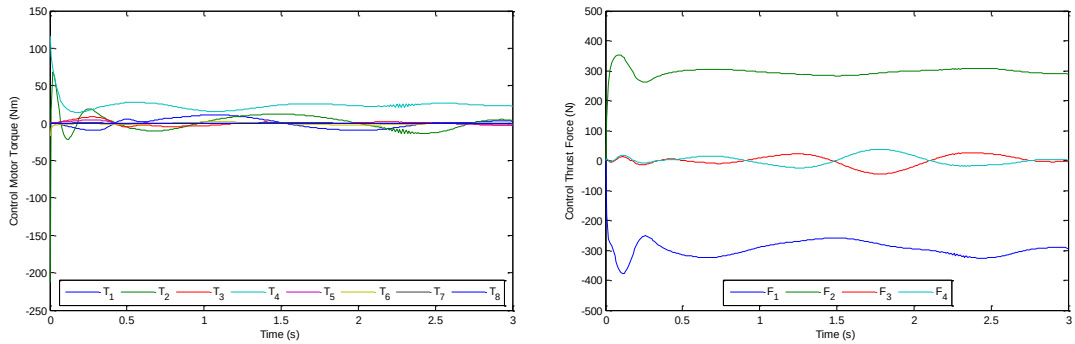

Figure 5.25 u-UVRMS Control Forces and Torques (C2)

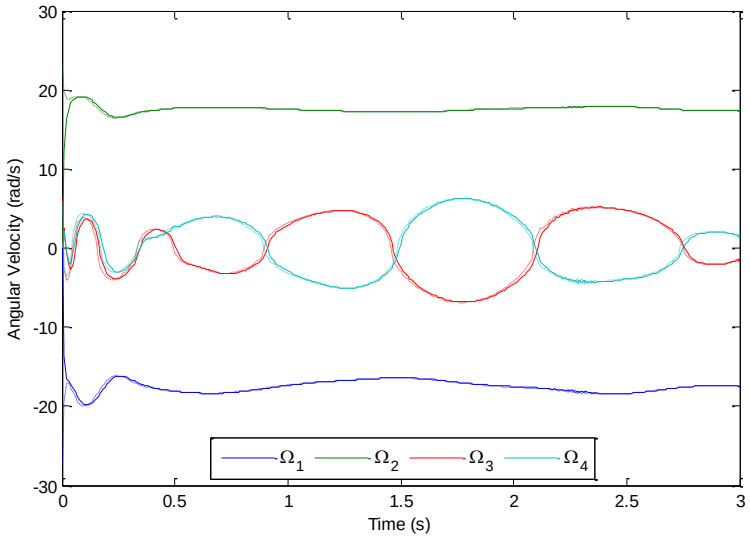

Figure 5.26 u-UVRMS Propeller Speed Responses (C2) (--- Desired, — Response)

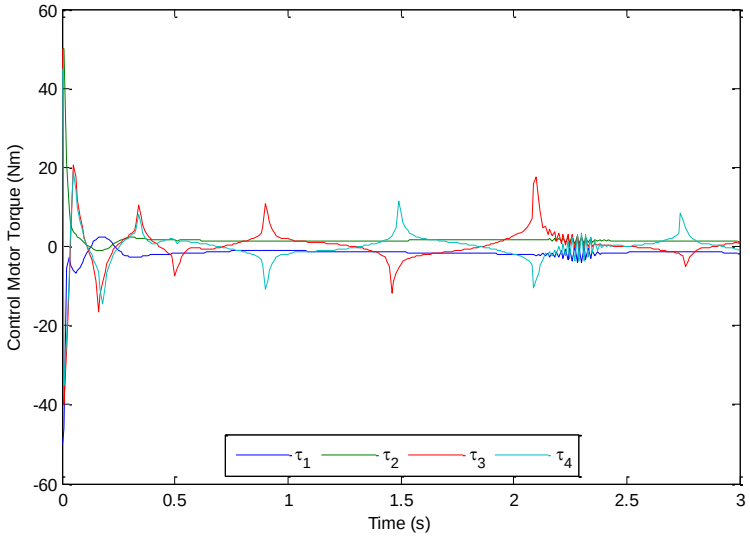

Figure 5.27 u-UVRMS Thruster Motor Control Torques (C2)

high as those of u-UVMS. However, these errors are acceptable for high precision manipulation. Not only that, the energy required to drive the system is notably minimized.

The effectiveness of the proposed control algorithms applied on the three systems can be rechecked for the other underwater mission called geological sampling by specifying separate tasks for both subsystems defined also in the Earth frame which are described by Equations (4.89) – (4.92).

In this mission, the period of the motion is taken to be the same as before with the following desired amounts of change in the tip point coordinates

$$\Delta x_P = 0,\ \Delta y_P = -0.3\ \text{m},\ \Delta z_P = -0.3\ \text{m} \tag{5.21}$$

and the desired amounts of change in the Euler angles

$$\Delta \psi_1 = -60^0,\ \Delta \psi_2 = 0^0,\ \Delta \psi_3 = 0^0 \tag{5.22}$$

Therefore, the mission is to follow a 30 cm straight line on yz plane with a 60^0 change in the azimuth angle of the end-effector while keeping the AUV fixed at its original position. The initial positions and the initial errors are kept the same as in the mine detection mission.

The position and velocity feedback gain diagonal matrices are chosen to have a smooth critically damped transition from the actual to the desired trajectory as in Equation (5.13). After several trials, the control parameter set $\{\omega_i = 10\ \text{rad/s} : i = 1,...,6\}$ for the AUV and the ones given in Equations (5.15) and (5.16) with $\omega_i^u = 50\ \text{rad/s}$ for the manipulator are observed to yield satisfactory closed loop responses for all the systems under consideration and the simulation results are tabulated in Table 5.6.

Table 5.6 Geological Sampling Mission Results

		Fully Actuated UVMS				u-UVMS				u-UVRMS			
		Maximum Position Error During Motion (m/deg)		Steady State Error (m/deg)		Maximum Position Error During Motion (m/deg)		Steady State Error (m/deg)		Maximum Position Error During Motion (m/deg)		Steady State Error (m/deg)	
		C3	C4	C3	C4	C3	C4	C3	C4	C3	C4	C3	C4
End Effector	x_P	1.073e-03	3.846e-03	2.416e-04	1.011e-03	4.287e-04	5.105e-03	7.661e-05	5.105e-03	1.203e-04	2.826e-03	1.203e-04	4.742e-04
	y_P	8.757e-03	7.305e-03	3.151e-04	2.189e-03	9.776e-03	9.718e-03	1.332e-05	6.393e-04	6.951e-04	1.399e-02	4.768e-04	1.967e-04
	z_P	1.864e-03	5.802e-03	6.231e-04	5.802e-03	2.764e-04	2.739e-03	3.723e-05	2.739e-03	1.565e-04	2.888e-03	1.565e-04	5.896e-04
	ψ_1	1.295e-00	1.665e-00	9.862e-03	7.882e-01	1.359e-00	1.572e-00	1.778e-01	1.572e-00	1.374e-01	2.967e-01	8.611e-03	2.059e-01
	ψ_2	1.685e-01	4.120e-01	1.360e-02	1.281e-02	1.668e-01	4.919e-01	4.078e-03	6.138e-02	2.059e-01	4.341e-01	7.775e-05	2.633e-03
	ψ_3	5.653e-01	9.798e-01	8.152e-03	9.575e-01	6.046e-01	1.649e-00	2.002e-02	1.649e-00	3.354e-04	4.868e-02	6.034e-05	2.825e-02
AUV	x_v	2.228e-03	6.081e-03	2.236e-04	3.480e-03	2.136e-03	1.189e-02	1.258e-05	1.189e-02	3.958e-03	8.279e-03	1.018e-05	7.655e-03
	y_v	2.493e-04	4.248e-03	2.348e-04	4.248e-03	1.199e-02	4.601e-02	2.818e-03	4.601e-02	4.260e-03	2.705e-02	3.228e-03	2.532e-02
	z_v	9.041e-03	2.296e-02	1.225e-04	2.163e-02	9.112e-03	1.189e-02	1.243e-06	1.189e-02	9.770e-03	1.158e-02	1.372e-05	2.980e-03
	ϕ_1	8.050e-02	1.245e-00	7.783e-02	1.245e-00	6.539e-03	1.767e-00	2.606e-04	1.767e-00	6.949e-04	6.501e-01	3.192e-05	1.225e-02
	ϕ_2	2.113 e-00	5.053e-00	1.850e-02	4.749e-00	2.112e-00	4.819e-00	2.932e-04	3.196e-00	1.227e-00	1.378e-00	1.477e-03	1.981e-02
	ϕ_3	2.037e-02	3.797e-02	2.801e-03	3.797e-02	9.612e-01	4.110e-00	2.227e-01	4.110e-00	3.377e-01	2.075e-00	2. 509e-01	1.925e-00

CHAPTER VI

DISCUSSIONS AND CONCLUSIONS

This thesis aims mainly at dynamic modeling of systems consisting of a 6-DOF AUV equipped with a 6-DOF manipulator subsystem (UVMS) and with an 8-DOF redundant manipulator subsystem (UVRMS) and proposing inverse dynamics control algorithms for them to execute tasks defined in Earth-fixed frame.

For this purpose, the basic kinematic equations of the systems are derived in Chapter-II. First, kinematic relations of the AUV subsystem are derived in body-fixed frame. Then, coordinate transformations are introduced to express these equations in inertial frame at velocity and acceleration levels. Next, recursive kinematic relations of multibody systems with a moving base are derived. Finally, these equations are used to derive the kinematic equations for systems under consideration.

In Chapter-III, the derivation of the dynamic models of the systems is covered. First, the dynamic equations of motion of the AUV and the manipulator subsystems are derived one by one. Then, using the kinematic and dynamic constraints, these equations are collected so as to get governing differential equations of motion of the entire systems. Basic hydrodynamic forces and the shadowing effects of the bodies on each other are explained in detail as well as the disturbing effect of the ocean currents. The thruster model is introduced and its incorporation to the dynamic equations is clarified to get more realistic dynamic models for rigid multibody systems working in underwater environment.

The inverse dynamics control methods developed for tracking the desired trajectories of the UVMS as well as the thrusters are presented in Chapter-IV. The task equations are formulated and the expressions relating the task variables to the joint variables are explained. The equations are further manipulated to get a relation between the system inputs (i.e. the thrust forces acting on the AUV and the actuator torques acting on the manipulator) and the system outputs (i.e. the location and orientation variables of the AUV and the end-effector of the manipulator). Trajectories for both of the AUV and the end-effector of the manipulator subsystem are defined for typical underwater missions like mine detection and geological sampling. The asymptotic stability and disturbance rejection ability are verified even in the presence of parametric uncertainty that exists in both constant model parameters of the propeller efficiency and the hydrodynamic coefficients such as the lift, drag, side force, and added mass coefficients. The position error dynamics of the systems under consideration are formulated.

In Chapter-V, the effectiveness of the control methods is tested in MATLAB/Simulink and the results are presented for all systems. Simulink models are developed in order to generate the system equations of motion and to apply the control algorithm at each sampling time.

It is shown that the control laws yielded satisfactory tracking properties for all of the systems in spite of the parametric uncertainty, disturbance and the thruster effects which create phase lag in the actual thrust forces. The results demonstrated that fully actuated UVMS can perform the tasks successfully with high precision and it can counteract the unwanted features of the surrounding media. The underactuated UVMS, on the other hand, can greatly handle the underwater manipulation yielding some deviations in uncontrolled directions and increase in steady state and tracking errors. These errors are assessed to be acceptable since less energy is required to perform these tasks. In order to increase the precision of the manipulation, the redundancy of the manipulator subsystem is increased while keeping the AUV underactuated. This is achieved by adding joints that are going to compensate the uncontrolled motions of the underwater vehicle. This way, it is believed to perform

12-DOF task defined in the Earth fixed frame with 12 actuating elements and to reduce interaction between the two subsystems. To the best of our knowledge, the idea of controlling the system having underactuated AUV and redundant manipulator is considered to be novel. The results revealed that the tracking errors of the end-effector of the manipulator subsystem are undeniably decreased and the end-effector motion is less affected from the uncontrolled AUV motion.

It is critical to verify that the systems are asymptotically stable and the proposed control scheme is effective and robust even in the presence of parameter uncertainties and disturbance. The tracking errors are in acceptable levels and can further be decreased if higher gains are used at the cost of a higher sampling rate. Evidently, the gains cannot be selected as high as desired because the real time computational requirements place an upper limit on them. Conversely, the sampling frequencies should not be chosen less than 10 times of the largest natural frequency of the closed loop system since instability and divergence of the control torques and responses may more likely be observed.

As stated, the dynamic models of the systems in concern are complicated. It is intended in this study to take into account any effect due to the surrounding medium as well as the effects that take place due to the motion of the bodies. The shadowing effect is one of these effects which have not been considered in the literature to the best of our knowledge. Therefore, this effect is included with its simplified but basic form in order to obtain a realistic but not unnecessarily complicated model. The original idea here is the inclusion of this effect with a reasonable modeling.

The motor dynamics of the joint actuators is not considered and it is assumed that the required control torques of the joints are applied without any delay. This assumption is justified if brushless DC motors are used which are commonly used in robotic applications. The frequency response of the current loop in brushless DC motors is wide enough to minimize any effect on outer control loops [70].

It is examined that the necessary measurements for the calculation of the control torques and forces that appear in the control law are the positions and velocities of the actuated joints of the manipulator and the translational acceleration and the angular velocity components of the AUV. The angular velocity components of the AUV are measured by the onboard rate gyros. The components of acceleration vector of the AUV, on the other hand, are measured by using the onboard accelerometers placed on the point where the origin of the body fixed frame of underwater vehicle and the base of the manipulator is coincident. In the study, it is also assumed that the noise and drift generated by the inertial sensors do not have considerable effect on the control performance. This assumption is based on the fact that gyros and accelerometers are low-noise sensors and on another assumption that some auxiliary equipment like magnetometers [71,72] are used to cope with gyro drift and a suitable terrain aided underwater navigation technique [73,74] is used to cope with accelerometer drift.

Consequently, the developed inverse dynamics control laws are assessed to be effective and applicable for systems working in underwater environment and performing different kinds of missions. Although the speeds of the missions are overwhelmingly limited by the physical and computational capability of the mission computers and accurate sensory feedback, this drawback will be defeated as the number of research and development studies on this area increases depending on the increase in the awareness on the strategic importance of these systems that can be utilized both in civil applications and in the military operations. In this research, a prolate spheroid underwater vehicle and cylindrical manipulator links have been considered. As another future research direction, it might be interesting to study the UVMSs having AUV with irregular shapes and noncircular manipulator links. Since the accurate dynamic modeling is achieved, several different control approaches may also be applied to the systems, i.e. UVMS and UVRMS including sliding mode, fuzzy logic, neural network and so on. More important than all, it will be very attention-grabbing to verify the dynamic models and the effectiveness of the proposed control algorithms experimentally for practical applications.

REFERENCES

[1] Antonelli, G., Underwater Robots: Motion and Force Control of Vehicle-Manipulator Systems, 2nd Ed., Springer-Verlag, 2006.

[2] Yuh, J., "Control of Underwater Robotic Vehicles", Proc. of IEEE International Conference on Intelligent Robots and Systems, 1993.

[3] Air France Flight 447, http://en.wikipedia.org/wiki/Air_France_ Flight_447# cite_note-3, last visited on May, 2012.

[4] Kosowatz, J., "Robots Plumb the Depths", http://www.asme.org/kb/news---articles/articles/robotics/robots-plumb-the-depths, last visited on May, 2012.

[5] Kosowatz, J., "New Images Illuminates the Titanic", http://www.asme.org /kb/news---articles/articles/robotics/new-images-illuminate-the-titanic, last visited on May, 2012.

[6] Associated Press, http://hosted.ap.org/dynamic/external/search.hosted.ap.org/ wireCoreTool/Search?type=Photo&output_format=PARA&query=This+composite+image%2C+released+by+RMS+Titanic+&SITE=AP&SECTION=HOME, last visited on May, 2012.

[7] RMS Titanic Inc., http://www.rmstitanic.net/expedition, last visited on May, 2012.

[8] Deepwater Horizon Oil Spill, http://en.wikipedia.org/wiki/Deepwater_Horizon _oil_spill, last visited on May, 2012.

[9] Monterey Bay Aquarium Research Institute, http://www.mbari.org/news /news_releases/2010/auv-gulf/auv-gulf-release.html, last visited on May, 2012.

[10] National Aeronautics and Space Administration, http://www.nasa.gov /topics/earth/features/oilspill /20100525_spill.html, last visited on May, 2012.

[11] Goheen, K.R., Jefferys, E.R., "The Application of Alternative Modelling Techniques to ROV Dynamics", Proc. of IEEE Conference on Robotics and Automation, 1990.

[12] Fossen, T.I., Fjellstad, O.E., "Nonlinear Modeling of Marine Vehicles in 6 Degrees of Freedom", Journal of Mathematical Modeling of Systems, Vol. 1, No. 1, pp. 17-27, 1995.

[13] Yuh, J., Choi, S.K., "Design of an Omni-Directional Underwater Robotic Vehicle and Its Coordinated Motion Control", Proc. of the American Control Conference, CA, 1993.

[14] Jun, B.H., Park, J.Y., Lee, F.Y., Lee, P.M., Lee, C.M., Kim, K, "Development of the AUV 'ISiMI' and a Free Running Test in an Ocean Engineering Basin", Ocean Engineering, Vol. 36, pp. 2-14, 2009.

[15] Marani, G., Choi, S.K., Yuh, J., "Underwater Autonomous Manipulation for Intervention Missions AUVs", Ocean Engineering, Vol. 36, pp. 15-23, 2009.

[16] Yuh, J., "Design and Control of Autonomous Underwater Robots: A Survey", Autonomous Robots, Vol. 8, pp. 7–24, 2000.

[17] Yoerger, D.R., Slotine, J.J.E., "Robust Trajectory Control of Underwater Vehicles", IEEE Journal of Oceanic Engineering, Vol. 10, No. 4, pp. 462–470, 1985.

[18] Healey, A.J., Lienard, D., "Multivariable Sliding Mode Control for Autonomous Diving and Steering of Unmanned Underwater Vehicles", IEEE Journal of Oceanic Engineering, Vol. 18, No. 3, pp. 327–339, 1993.

[19] Goheen, K.R., Jefferys, E.R., "Multivariable Self-Tuning Autopilots for Autonomous and Remotely Operated Vehicles", IEEE Journal of Oceanic Engineering, Vol. 15, No. 3, pp. 144–151, 1990.

[20] Nakamura, Y., Savant, S., "Nonlinear Tracking Control of Autonomous Underwater Vehicles", Proc. of IEEE Conference on Robotics and Automation, 1992.

[21] Yuh, J., West, M.E., Lee, P.M., "An Autonomous Underwater Vehicle Control with a Non-regressor Based Algorithm", Proc. of IEEE Conference on Robotics and Automation, pp. 2363–2368, 2001.

[22] Yuh, J., Nie, J., Lee, C.S.G., "Experimental Study on Adaptive Control of Underwater Robots", Proc. of IEEE Conference on Robotics and Automation, pp. 393–398, 1999.

[23] Tabaii, S.S., El-Hawary, F., El-Hawary, M., "Hybrid Adaptive Control of Autonomous Underwater Vehicle", Proc. of the Symposium on Autonomous Underwater Vehicle Technology, pp. 275–282, 1994.

[24] Hoang, N.Q., Kreuzer, E., "Adaptive PD-Controller for Positioning of a Remotely Operated Vehicle Close to an Underwater Structure: Theory and Experiments", Control Engineering Practice, Vol. 15, pp. 411–419, 2007.

[25] Wang, J.S., Lee, C.S.G., Yuh, J., "An On-Line Self-Organizing Neuro-Fuzzy Control for Autonomous Underwater Vehicles", Proc. of IEEE Conference on Robotics and Automation, pp. 2416–2421, 1999.

[26] Craven, P.J., Sutton, R., Burns, R.S., Dai, Y.M., "Multivariable Intelligent Control Strategies for an Autonomous Underwater Vehicle", International Journal of Systems Science, Vol. 30 No.9, pp. 965-980, 2009.

[27] Ishii, K., Fujii, T., Ura, T., "Neural Network System for On-line Controller Adaptation and Its Application to Underwater Robot", Proc. of IEEE Conference on Robotics and Automation, pp. 756-761, 1998.

[28] Tarn, T.J., Shoults, G.A., Yang, S. P., "A Dynamic Model of an Underwater Vehicle with a Robotic Manipulator Using Kane's Method", Autonomous Robots, Vol. 3, pp. 269–283, 1996.

[29] McMillan, S., Orin, D.E., McGhee, R.B., "Efficient Dynamic Simulation of an Underwater Vehicle with a Robotic Manipulator", IEEE Transactions on Systems, Man, and Cybernetics, Vol. 25, No. 8, pp. 1194-1206, 1995.

[30] Mahesh, H., Yuh, J., Lakshmi, R., "A Coordinated Control of an Underwater Vehicle and Robot Manipulator", Journal of Robotic Systems, Vol. 8, pp. 339–370, 1991.

[31] Diaz, E.O., De Wit, C.C., Perrier, M., "A Comparative Study of Neglected Dynamics on a UVMS under Nonlinear Robust Control", Proc. of Oceans Conference, pp. 936–940, 1998.

[32] De Wit, C.C., Diaz, E.O., Perrier, M., “Nonlinear Control of an Underwater Vehicle/Manipulator with Composite Dynamics”, IEEE Transactions on Control Systems Technology, Vol. 8, No. 6, pp. 948–960, 2000.

[33] Ishitsuka, M., Sagara, S., Ishii, K., “Dynamics Analysis and Resolved Acceleration Control of an Autonomous Underwater Vehicle Equipped with a Manipulator”, International Symposium on Underwater Technology, pp. 277-281, 2004.

[34] McLain, T. W., Rock, S. M., Lee, M. J., “Experiments in the Coordinated Control of an Underwater Arm/Vehicle System”, Autonomous Robots, Vol. 3, pp. 213–232, 1996.

[35] Antonelli, G., Chiaverini, S., “Adaptive Tracking Control of Underwater Vehicle-Manipulator Systems Based on the Virtual Decomposition Approach”, IEEE Transactions on Robotics and Automation, Vol. 20, No. 3, pp. 594–602, 2004.

[36] Chung, G.B., Eom, K.S., Yi, B.J., Suh, I.H., Oh, S.R., Cho, Y.J., “Disturbance Observer Based Robust Control for Underwater Robotic Systems with Passive Joints”, Proc. of IEEE International Conference on Robotics and Automation, pp. 1775–1780, 2000.

[37] Sarkar, N., Podder, T. K., “Coordinated Motion Planning and Control of Autonomous Underwater Vehicle-Manipulator Systems Subject to Drag Optimization”, IEEE Journal of Oceanic Engineering, Vol. 26, pp. 228–239, 2001.

[38] Podder, T. K., “Motion Planning of Autonomous Underwater Vehicle-Manipulator Systems”, Ph.D. Thesis, The University of Hawaii, USA, 2000.

[39] Antonelli, G., Chiaverini, S., “A Fuzzy Approach to Redundancy Resolution for Underwater Vehicle-Manipulator Systems”, Control Engineering Practice, Vol. 11, pp. 445–452, 2003.

[40] Antonelli, G., Chiaverini, S., “Fuzzy Redundancy Resolution and Motion Coordination for Underwater Vehicle-Manipulator Systems”, IEEE Transactions on Fuzzy Systems, Vol. 11, No. 1, pp. 109–120, 2003.

[41] Dos Santos, C.H., Bittencourt, G., Guenther, R., De Pieri, E., "A Fuzzy Hybrid Singularity Avoidance for Underwater Vehicle-Manipulator Systems", Information Control Problems in Manufacturing - MCOM, pp. 209-214, 2006.

[42] Soylu, S., Buckham, B.J., Podhorodeski, R.P., "Redundancy Resolution for Underwater Mobile Manipulators", Ocean Engineering, Vol. 37, pp. 325–343, 2010.

[43] Suboh, S.M., Rahman, I.A., Arshad, M.R., Mahyuddin, M.N., "Modeling and Control of 2-DOF Underwater Planar Manipulator", Indian Journal of Marine Sciences, Vol. 38, pp. 365–371, 2009.

[44] Han, J., Park, J., Chung, W.K., "Robust Coordinated Motion Control of an Underwater Vehicle-Manipulator System with Minimizing Restoring Moments", Ocean Engineering, Vol. 38, pp. 1197–1206, 2011.

[45] Cui, Y., Yuh, J., "A Unified Adaptive Force Control of Underwater Vehicle-Manipulator Systems (UVMS)", Proc. of IEEE/RSJ International Conference on Intelligent Robots and Systems, pp. 553 – 558, 2003.

[46] Lapierre, L., Fraisse, P., Dauchez, P., "Position/Force Control of an Underwater Mobile Manipulator", Journal of Robotic Systems, Vol. 20, pp. 707–722, 2003.

[47] Antonelli, G., Chiaverini, S., Sarkar, N., "External Force Control for Underwater Vehicle-Manipulator Systems", IEEE Transactions on Robotics and Automation, Vol. 17, No. 6, pp. 931–938, 2001.

[48] Yatoh, T., Sagara, S., "Resolved Acceleration Control of Underwater Vehicle-Manipulator Systems using Momentum Equation", Proc. of Oceans Conference, pp. 1–6, 2007.

[49] Fossen, T. I., "Guidance and Control of Ocean Vehicles", John Wiley & Sons, NY, 1994.

[50] Özgören, M. K., "Lecture Notes on Principles of Robotics", Middle East Technical University, 2005.

[51] Imlay, F. H., "The Complete Expressions for Added Mass of a Rigid Body Moving in an Ideal Fluid", Technical Report DTMB 1528, David Taylor Model Basin, Washington D.C., 1961.

[52] Bø, H., "Hydrodynamic Estimation and Identification", M.Sc. Thesis, Norwegian University of Science and Technology, Department of Engineering Cybernetics, Norway, 2004.

[53] Munk, M. M. Fluid Mechanics, Vol. VI, Aerodynamic Theory of Airships, Dover Publ. Inc, 1934.

[54] Bishop, R.E.D., Hassan A.Y., "The Lift and Drag Forces on a Circular Cylinder in a Flowing Fluid", Proc. of the Royal Society of London. Series A, Mathematical and Physical Sciences, Vol. 277, No. 1368, pp. 32-50, 1964.

[55] Sahin, I., Okita N., "Flow around Circular and Noncircular Cylinders by a Low-Order Panel Method", Ocean Engineering, Vol. 25, No. 7, pp. 529–539, 1998.

[56] Newman, J. N., "Marine Hydrodynamics", Cambridge, MA, MIT Press, 1977.

[57] Sarpkaya, T., "Hydrodynamic Damping, Flow Induced Oscillations and Biharmonic Response", Journal of Offshore Mechanics and Arctic Enginereering, Vol. 117, No. 4, pp. 232-238, 1995.

[58] Ferro, R.S.T., Hou, E.H., "A Selected Review of Hydrodynamic Force Coefficient Data on Stranded Wires Used in Fishing Gear", Department of Agriculture and Fisheries for Scotland. Marine Laboratory., 1984.

[59] Whitcomb, L. L., Yoerger, D. R., "Preliminary Experiments in Model-Based Thruster Control for Underwater Vehicle Positioning", IEEE Journal of Oceanic Engineering, Vol. 24, pp. 495-506, 1999.

[60] Yoerger, D.R., Cooke, J.G., Slotine, J.J.E., "The Influence of Thruster Dynamics on Underwater Vehicle Behavior and Their Incorporation into Control System Design", IEEE Journal of Oceanic Engineering, Vol. 15, pp. 167-178. 1990.

[61] Healey, A.J., Rock, S.M., Cody, S., Miles, D., Brown, J.P., "Toward an Improved Understanding of Thruster Dynamics for Underwater Vehicles", IEEE Journal of Oceanic Engineering, Vol. 20, No. 4, pp. 354-361, 1995.

[62] Kim, J., Chung, W.K., "Accurate and Practical Thruster Modeling for Underwater Vehicles", Ocean Engineering, Vol. 33, pp. 566–586, 2006.

[63] Bessa, W.M., Dutra, M.S., Kreuzer, E., "Thruster Dynamics Compensation for the Positioning of Underwater Robotic Vehicles Through a Fuzzy Sliding

Mode Based Approach", ABCM Symposium Series in Mechatronics, Vol. 2, pp.605-612, 2006.

[64] Roskam, J., "Airplane Flight Dynamics and Automatic Flight Controls", Design, Analysis and Research Corporation, U.S.A, 2007.

[65] Siouris, G.M., "Missile Guidance and Control Systems", Springer-Verlag, U.S.A, 2004.

[66] Korkmaz, O., Ider, S.K., Özgören M.K., "Trajectory Tracking Control of an Underwater Vehicle Manipulator System", SAVTEK-2012, Ankara, Turkey (in Turkish).

[67] Korkmaz, O., Ider, S.K., Özgören M.K., "Modeling and Dynamic Analysis of an Underwater Vehicle Manipulator System", TOK-2011, İzmir, Turkey (in Turkish).

[68] Ider, S.K., Amirouche, F.M.L., "Coordinate Reduction in the Dynamics of Constrained Multibody Systems-A New Approach", Journal of Applied Mechanics, Vol. 55, pp. 899-904, 1988.

[69] Shabana, A. A., "Computational Dynamics", Wiley, NY, 2001.

[70] Kollmorgen Inland Motor, "Handbook for Brushless Motors and Drive Systems", VA, 1996.

[71] Armstrong, B., Pentzer, J., Odell, D., Bean, T., Canning, J., Pugsley, D., Frenzel, J., Anderson, M., Edwards, D., "Field Measurement of Surface Ship Magnetic Signature Using Multiple AUVs", Proc. of Oceans Conference, art. no. 5422197, pp. 1–9, 2009.

[72] Claus, B., Bachmayer, R., "Development of a Magnetometry System for an Underwater Glider", 17th International Symposium on Unmanned Untethered Submersible Technology, 2011.

[73] Anonsen, K.B., Hagen, O.K., "Terrain Aided Underwater Navigation Using Pockmarks", Proc. of Oceans Conference, art. no. 5422265, pp. 1–6, 2009.

[74] Williams, S., Dissanayake, G., Durrant-Whyte, H., "Towards Terrain-Aided Navigation for Underwater Robotics", Advanced Robotics, Vol. 15, pp. 533–549, 2001.

APPENDIX A

SYSTEM JACOBIAN MATRICES

A.1. UVMS Jacobian Matrices

The Jacobian matrix $\hat{J}_\theta \in \Re^{6x6}$ has the form

$$\hat{J}_\theta = \begin{bmatrix} \overline{J}_{\theta_{11}} & \overline{J}_{\theta_{12}} & \dots & \overline{J}_{\theta_{16}} \\ \overline{J}_{\theta_{21}} & \overline{J}_{\theta_{22}} & \dots & \overline{J}_{\theta_{26}} \end{bmatrix} \tag{A.1}$$

where

$$\overline{J}_{\theta_{11}} = a_1\tilde{u}_3\overline{u}_3 + a_2\tilde{u}_3\hat{C}^{(0,2)}\overline{u}_1 + a_3\tilde{u}_3\hat{C}^{(0,3)}\overline{u}_1 + a_4\tilde{u}_3\hat{C}^{(0,4)}\overline{u}_1 + a_5\tilde{u}_3\hat{C}^{(0,5)}\overline{u}_3 + a_6\tilde{u}_3\hat{C}^{(0,6)}\overline{u}_3 \tag{A.2}$$

$$\begin{aligned}\overline{J}_{\theta_{12}} = {} & a_2\hat{C}^{(0,1)}\tilde{u}_3\hat{C}^{(0,2)}\overline{u}_1 + a_3\hat{C}^{(0,1)}\tilde{u}_3\hat{C}^{(0,3)}\overline{u}_1 \dots \\ & + a_4\hat{C}^{(0,1)}\tilde{u}_3\hat{C}^{(0,4)}\overline{u}_1 + a_5\hat{C}^{(0,1)}\tilde{u}_3\hat{C}^{(0,5)}\overline{u}_3 + a_6\hat{C}^{(0,1)}\tilde{u}_3\hat{C}^{(0,6)}\overline{u}_3\end{aligned} \tag{A.3}$$

$$\overline{J}_{\theta_{13}} = a_3\hat{C}^{(0,2)}\tilde{u}_3\hat{C}^{(0,3)}\overline{u}_1 + a_4\hat{C}^{(0,2)}\tilde{u}_3\hat{C}^{(0,4)}\overline{u}_1 + a_5\hat{C}^{(0,2)}\tilde{u}_3\hat{C}^{(0,5)}\overline{u}_3 + a_6\hat{C}^{(0,2)}\tilde{u}_3\hat{C}^{(0,6)}\overline{u}_3 \tag{A.4}$$

$$\overline{J}_{\theta_{14}} = a_4\hat{C}^{(0,3)}\tilde{u}_3\hat{C}^{(0,4)}\overline{u}_1 + a_5\hat{C}^{(0,3)}\tilde{u}_3\hat{C}^{(0,5)}\overline{u}_3 + a_6\hat{C}^{(0,3)}\tilde{u}_3\hat{C}^{(0,6)}\overline{u}_3 \tag{A.5}$$

$$\overline{J}_{\theta_{15}} = a_5\hat{C}^{(0,4)}\tilde{u}_3\hat{C}^{(0,5)}\overline{u}_3 + a_6\hat{C}^{(0,4)}\tilde{u}_3\hat{C}^{(0,6)}\overline{u}_3 \tag{A.6}$$

$$\overline{J}_{\theta_{16}} = a_6\hat{C}^{(0,5)}\tilde{u}_3\hat{C}^{(0,6)}\overline{u}_3 \tag{A.7}$$

$$\overline{J}_{\theta_{21}} = \overline{u}_3 \tag{A.8}$$

$$\overline{J}_{\theta_{22}} = \hat{C}^{(0,1)}\overline{u}_3 \tag{A.9}$$

$$\overline{J}_{\theta_{23}} = \hat{C}^{(0,2)}\overline{u}_3 \tag{A.10}$$

$$\overline{J}_{\theta_{24}} = \hat{C}^{(0,3)}\overline{u}_3 \tag{A.11}$$

$$\overline{J}_{\theta_{25}} = \hat{C}^{(0,4)}\overline{u}_3 \tag{A.12}$$

$$\overline{J}_{\theta_{26}} = \hat{C}^{(0,5)}\overline{u}_3 \tag{A.13}$$

The Jacobian matrix $\hat{J}_\eta \in \Re^{6x6}$ has the form

$$\hat{J}_\eta = \begin{bmatrix} \overline{J}_{\eta_{11}} & \overline{J}_{\eta_{12}} & \ldots & \overline{J}_{\eta_{16}} \\ \overline{J}_{\eta_{21}} & \overline{J}_{\eta_{22}} & \ldots & \overline{J}_{\eta_{26}} \end{bmatrix} \tag{A.14}$$

where

$$\overline{J}_{\eta_{11}} = \overline{J}_{\eta_{24}} = \overline{u}_1 \tag{A.15}$$

$$\overline{J}_{\eta_{12}} = \overline{J}_{\eta_{25}} = \overline{u}_2 \tag{A.16}$$

$$\overline{J}_{\eta_{13}} = \overline{J}_{\eta_{26}} = \overline{u}_3 \tag{A.17}$$

$$\begin{aligned} \overline{J}_{\eta_{14}} = a_1\tilde{u}_1\overline{u}_3 + a_2\tilde{u}_1\hat{C}^{(0,2)}\overline{u}_1 + a_3\tilde{u}_1\hat{C}^{(0,3)}\overline{u}_1 + a_4\tilde{u}_1\hat{C}^{(0,4)}\overline{u}_1 + a_5\tilde{u}_1\hat{C}^{(0,5)}\overline{u}_3 \ldots \\ + a_6\tilde{u}_1\hat{C}^{(0,6)}\overline{u}_3 + \tilde{u}_1\left(\overline{p}_{O_v} + \overline{p}_{O_1} + \overline{p}_{O_2} + \overline{p}_{O_3} + \overline{p}_{O_4} + \overline{p}_{O_5}\right) \end{aligned} \tag{A.18}$$

$$\begin{aligned} \overline{J}_{\eta_{15}} = a_1\tilde{u}_2\overline{u}_3 + a_2\tilde{u}_2\hat{C}^{(0,2)}\overline{u}_1 + a_3\tilde{u}_2\hat{C}^{(0,3)}\overline{u}_1 + a_4\tilde{u}_2\hat{C}^{(0,4)}\overline{u}_1 + a_5\tilde{u}_2\hat{C}^{(0,5)}\overline{u}_3 \ldots \\ + a_6\tilde{u}_2\hat{C}^{(0,6)}\overline{u}_3 + \tilde{u}_2\left(\overline{p}_{O_v} + \overline{p}_{O_1} + \overline{p}_{O_2} + \overline{p}_{O_3} + \overline{p}_{O_4} + \overline{p}_{O_5}\right) \end{aligned} \tag{A.19}$$

$$\begin{aligned} \overline{J}_{\eta_{16}} = a_1\tilde{u}_3\overline{u}_3 + a_2\tilde{u}_3\hat{C}^{(0,2)}\overline{u}_1 + a_3\tilde{u}_3\hat{C}^{(0,3)}\overline{u}_1 + a_4\tilde{u}_3\hat{C}^{(0,4)}\overline{u}_1 + a_5\tilde{u}_3\hat{C}^{(0,5)}\overline{u}_3 \ldots \\ + a_6\tilde{u}_3\hat{C}^{(0,6)}\overline{u}_3 + \tilde{u}_3\left(\overline{p}_{O_v} + \overline{p}_{O_1} + \overline{p}_{O_2} + \overline{p}_{O_3} + \overline{p}_{O_4} + \overline{p}_{O_5}\right) \end{aligned} \tag{A.20}$$

$$\overline{J}_{\eta_{21}} = \overline{J}_{\eta_{22}} = \overline{J}_{\eta_{23}} = \overline{0} \tag{A.21}$$

A.2. UVRMS Jacobian Matrices

The Jacobian matrix $\hat{J}_\theta \in \Re^{6x8}$ has the form

$$\hat{J}_\theta = \begin{bmatrix} \overline{J}_{\theta_{11}} & \overline{J}_{\theta_{12}} & \dots & \overline{J}_{\theta_{18}} \\ \overline{J}_{\theta_{21}} & \overline{J}_{\theta_{22}} & \dots & \overline{J}_{\theta_{28}} \end{bmatrix} \tag{A.22}$$

where

$$\overline{J}_{\theta_{11}} = a_1\tilde{u}_3\overline{u}_3 + a_2\tilde{u}_3\hat{C}^{(0,2)}\overline{u}_1 + a_3\tilde{u}_3\hat{C}^{(0,3)}\overline{u}_1 + a_{45}\tilde{u}_3\hat{C}^{(0,4)}\overline{u}_3 + a_6\tilde{u}_3\hat{C}^{(0,6)}\overline{u}_1 \dots + a_7\tilde{u}_3\hat{C}^{(0,7)}\overline{u}_3 + a_8\tilde{u}_3\hat{C}^{(0,8)}\overline{u}_3 \tag{A.23}$$

$$\overline{J}_{\theta_{12}} = a_2\hat{C}^{(0,1)}\tilde{u}_3\hat{C}^{(0,2)}\overline{u}_1 + a_3\hat{C}^{(0,1)}\tilde{u}_3\hat{C}^{(0,3)}\overline{u}_1 + a_{45}\hat{C}^{(0,1)}\tilde{u}_3\hat{C}^{(0,4)}\overline{u}_3 \dots + a_6\hat{C}^{(0,1)}\tilde{u}_3\hat{C}^{(0,6)}\overline{u}_1 + a_7\hat{C}^{(0,1)}\tilde{u}_3\hat{C}^{(0,7)}\overline{u}_3 + a_8\hat{C}^{(0,1)}\tilde{u}_3\hat{C}^{(0,8)}\overline{u}_3 \tag{A.24}$$

$$\overline{J}_{\theta_{13}} = a_3\hat{C}^{(0,2)}\tilde{u}_3\hat{C}^{(0,3)}\overline{u}_1 + a_{45}\hat{C}^{(0,2)}\tilde{u}_3\hat{C}^{(0,4)}\overline{u}_3 + a_6\hat{C}^{(0,2)}\tilde{u}_3\hat{C}^{(0,6)}\overline{u}_1 \dots + a_7\hat{C}^{(0,2)}\tilde{u}_3\hat{C}^{(0,7)}\overline{u}_3 + a_8\hat{C}^{(0,2)}\tilde{u}_3\hat{C}^{(0,8)}\overline{u}_3 \tag{A.25}$$

$$\overline{J}_{\theta_{14}} = a_{45}\hat{C}^{(0,3)}\tilde{u}_3\hat{C}^{(0,4)}\overline{u}_3 + a_6\hat{C}^{(0,3)}\tilde{u}_3\hat{C}^{(0,6)}\overline{u}_1 + a_7\hat{C}^{(0,3)}\tilde{u}_3\hat{C}^{(0,7)}\overline{u}_3 + a_8\hat{C}^{(0,3)}\tilde{u}_3\hat{C}^{(0,8)}\overline{u}_3 \tag{A.26}$$

$$\overline{J}_{\theta_{15}} = a_{45}\hat{C}^{(0,4)}\tilde{u}_3\hat{C}^{(0,4)}\overline{u}_3 + a_6\hat{C}^{(0,4)}\tilde{u}_3\hat{C}^{(0,6)}\overline{u}_1 + a_7\hat{C}^{(0,4)}\tilde{u}_3\hat{C}^{(0,7)}\overline{u}_3 + a_8\hat{C}^{(0,4)}\tilde{u}_3\hat{C}^{(0,8)}\overline{u}_3 \tag{A.27}$$

$$\overline{J}_{\theta_{16}} = a_6\hat{C}^{(0,5)}\tilde{u}_3\hat{C}^{(0,6)}\overline{u}_1 + a_7\hat{C}^{(0,5)}\tilde{u}_3\hat{C}^{(0,7)}\overline{u}_3 + a_8\hat{C}^{(0,5)}\tilde{u}_3\hat{C}^{(0,8)}\overline{u}_3 \tag{A.28}$$

$$\overline{J}_{\theta_{17}} = a_7\hat{C}^{(0,6)}\tilde{u}_3\hat{C}^{(0,7)}\overline{u}_3 + a_8\hat{C}^{(0,6)}\tilde{u}_3\hat{C}^{(0,8)}\overline{u}_3 \tag{A.29}$$

$$\overline{J}_{\theta_{18}} = a_8\hat{C}^{(0,7)}\tilde{u}_3\hat{C}^{(0,8)}\overline{u}_3 \tag{A.30}$$

$$\overline{J}_{\theta_{21}} = \overline{u}_3 \tag{A.31}$$

$$\overline{J}_{\theta_{22}} = \hat{C}^{(0,1)}\overline{u}_3 \tag{A.32}$$

$$\overline{J}_{\theta_{23}} = \hat{C}^{(0,2)}\overline{u}_3 \tag{A.33}$$

$$\bar{J}_{\theta_{24}} = \hat{C}^{(0,3)}\bar{u}_3 \tag{A.34}$$

$$\bar{J}_{\theta_{25}} = \hat{C}^{(0,4)}\bar{u}_3 \tag{A.35}$$

$$\bar{J}_{\theta_{26}} = \hat{C}^{(0,5)}\bar{u}_3 \tag{A.36}$$

$$\bar{J}_{\theta_{27}} = \hat{C}^{(0,6)}\bar{u}_3 \tag{A.37}$$

$$\bar{J}_{\theta_{28}} = \hat{C}^{(0,7)}\bar{u}_3 \tag{A.38}$$

The Jacobian matrix $\hat{J}_\eta \in \Re^{6x6}$ has the form

$$\hat{J}_\eta = \begin{bmatrix} \bar{J}_{\eta_{11}} & \bar{J}_{\eta_{12}} & \dots & \bar{J}_{\eta_{16}} \\ \bar{J}_{\eta_{21}} & \bar{J}_{\eta_{22}} & \dots & \bar{J}_{\eta_{26}} \end{bmatrix} \tag{A.39}$$

where

$$\bar{J}_{\eta_{11}} = \bar{J}_{\eta_{24}} = \bar{u}_1 \tag{A.40}$$

$$\bar{J}_{\eta_{12}} = \bar{J}_{\eta_{25}} = \bar{u}_2 \tag{A.41}$$

$$\bar{J}_{\eta_{13}} = \bar{J}_{\eta_{26}} = \bar{u}_3 \tag{A.42}$$

$$\begin{aligned} \bar{J}_{\eta_{14}} = {} & a_1\tilde{u}_1\bar{u}_3 + a_2\tilde{u}_1\hat{C}^{(0,2)}\bar{u}_1 + a_3\tilde{u}_1\hat{C}^{(0,3)}\bar{u}_1 + a_{45}\tilde{u}_1\hat{C}^{(0,4)}\bar{u}_3 + a_6\tilde{u}_1\hat{C}^{(0,6)}\bar{u}_1 \dots \\ & + a_7\tilde{u}_1\hat{C}^{(0,7)}\bar{u}_3 + a_8\tilde{u}_1\hat{C}^{(0,8)}\bar{u}_3 + \tilde{u}_1\left(\bar{p}_{O_v} + \bar{p}_{O_1} + \bar{p}_{O_2} + \bar{p}_{O_4} + \bar{p}_{O_5} + \bar{p}_{O_6} + \bar{p}_{O_7}\right) \end{aligned} \tag{A.43}$$

$$\begin{aligned} \bar{J}_{\eta_{15}} = {} & a_1\tilde{u}_2\bar{u}_3 + a_2\tilde{u}_2\hat{C}^{(0,2)}\bar{u}_1 + a_3\tilde{u}_2\hat{C}^{(0,3)}\bar{u}_1 + a_{45}\tilde{u}_2\hat{C}^{(0,4)}\bar{u}_3 + a_6\tilde{u}_2\hat{C}^{(0,6)}\bar{u}_1 \dots \\ & + a_7\tilde{u}_2\hat{C}^{(0,7)}\bar{u}_3 + a_8\tilde{u}_2\hat{C}^{(0,8)}\bar{u}_3 + \tilde{u}_2\left(\bar{p}_{O_v} + \bar{p}_{O_1} + \bar{p}_{O_2} + \bar{p}_{O_4} + \bar{p}_{O_5} + \bar{p}_{O_6} + \bar{p}_{O_7}\right) \end{aligned} \tag{A.44}$$

$$\begin{aligned} \bar{J}_{\eta_{16}} = {} & a_1\tilde{u}_3\bar{u}_3 + a_2\tilde{u}_3\hat{C}^{(0,2)}\bar{u}_1 + a_3\tilde{u}_3\hat{C}^{(0,3)}\bar{u}_1 + a_{45}\tilde{u}_3\hat{C}^{(0,4)}\bar{u}_3 + a_6\tilde{u}_3\hat{C}^{(0,6)}\bar{u}_1 \dots \\ & + a_7\tilde{u}_3\hat{C}^{(0,7)}\bar{u}_3 + a_8\tilde{u}_3\hat{C}^{(0,8)}\bar{u}_3 + \tilde{u}_3\left(\bar{p}_{O_v} + \bar{p}_{O_1} + \bar{p}_{O_2} + \bar{p}_{O_4} + \bar{p}_{O_5} + \bar{p}_{O_6} + \bar{p}_{O_7}\right) \end{aligned} \tag{A.45}$$

$$\bar{J}_{\eta_{21}} = \bar{J}_{\eta_{22}} = \bar{J}_{\eta_{23}} = \bar{0} \tag{A.46}$$

APPENDIX B

HYDRODYNAMIC DATA

B.1. Added Mass/Inertia Coefficients

Table B.1.1 UVMS Added Mass/Inertia Coefficients

	$X_{a_{i_1}}$	$Y_{a_{i_2}}$	$Z_{a_{i_3}}$	$K_{\alpha_{i_1}}$	$M_{\alpha_{i_2}}$	$N_{\alpha_{i_3}}$
AUV	-2.9520	-54.8374	-54.8374	0	-9.1585	-9.1585
Link-1	-0.1696	-1.6965	-1.6965	0	-0.0353	-0.0353
Link-2	-0.3054	-3.0536	-3.0536	0	-0.2061	-0.2061
Link-3	-0.4072	-4.0715	-4.0715	0	-0.4886	-0.4886
Link-4	-0.0848	-0.8482	-0.8482	0	-0.0044	-0.0044
Link-5	-0.0509	-0.5089	-0.5089	0	-0.0010	-0.0010
Link-6	-0.0339	-0.3393	-0.3393	0	-0.0003	-0.0003

Table B.1.2 UVRMS Added Mass/Inertia Coefficients

	$X_{a_{i_1}}$	$Y_{a_{i_2}}$	$Z_{a_{i_3}}$	$K_{\alpha_{i_1}}$	$M_{\alpha_{i_2}}$	$N_{\alpha_{i_3}}$
AUV	-2.9520	-54.8374	-54.8374	0	-9.1585	-9.1585
Link-1	-0.1696	-1.6965	-1.6965	0	-0.0353	-0.0353
Link-2	-0.2036	-2.0358	-2.0358	0	-0.0611	-0.0611
Link-3	-0.1018	-1.0179	-1.0179	0	-0.0076	-0.0076
Link-4	-0.0679	-0.6786	-0.6786	0	-0.0023	-0.0023
Link-5	-0.3393	-3.3929	-3.3929	0	-0.2827	-0.2827
Link-6	-0.0848	-0.8482	-0.8482	0	-0.0044	-0.0044
Link-7	-0.0509	-0.5089	-0.5089	0	-0.0010	-0.0010
Link-8	-0.0339	-0.3393	-0.3393	0	-0.0003	-0.0003

B.2. Damping Coefficients

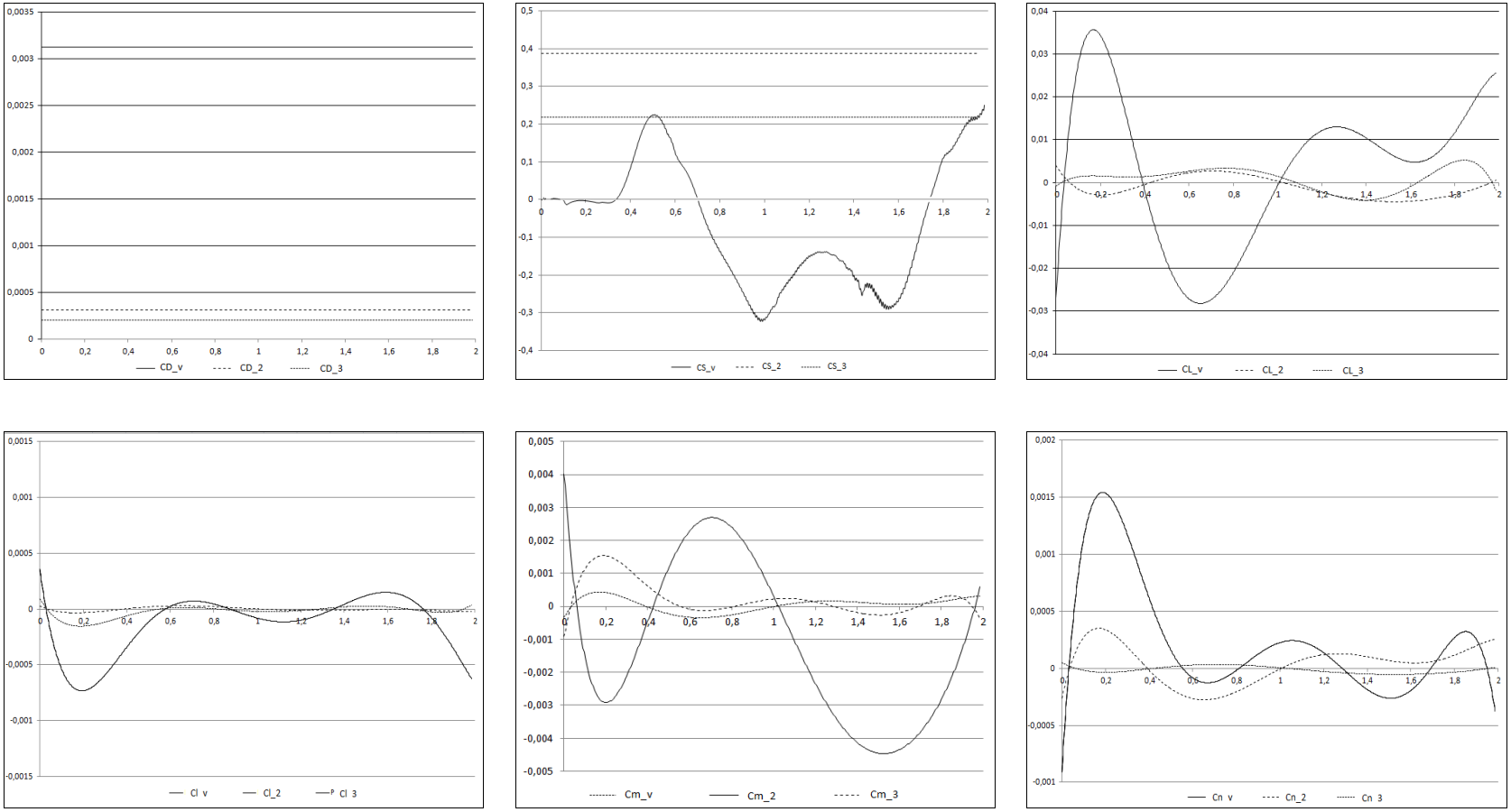

Figure B.1. Force/Moment Coefficients

CURRICULUM VITAE

PERSONAL INFORMATION

Surname, Name	:	KORKMAZ, Ozan
Date & Place of Birth	:	17 March 1982 – Ankara/Turkey
Nationality	:	Turkish
Work Address	:	TÜBİTAK SAGE The Scientific & Technological Research Council of Turkey Defense Industries R&D Institute P.K. 16, 06261, Mamak, Ankara /Turkey Tel: +90 312 590 90 00 Fax: +90 312 590 91 48 E-mail: ozan.korkmaz@tubitak.gov.tr

EDUCATION

Degree	Institution	Years, Grade
Ph.D.	Middle East Technical University Department of Mechanical Engineering	2007-2012, 3.56/4.00
M.Sc.	Middle East Technical University Department of Mechanical Engineering	2004-2006, 3.29/4.00
B.Sc.	Gazi University Department of Mechanical Engineering	2000-2004, 3.16/4.00
High School	50. Yıl Foreign Language Weighted Lycee	1996-2000, 5.00/5.00

WORK EXPERIENCE

The Scientific and Technological Research Council of Turkey-TÜBİTAK

2012-ongoing	Senior Researcher Defense Industries Research and Development Institute-SAGE
2010-2012	Researcher Defense Industries Research and Development Institute-SAGE
2006-2010	Scientific Programs Assistant Expert Engineering Research Grant Committee-MAG

Middle East Technical University-METU

2004-2006	Research Assistant Department of Mechanical Engineering

Summer Internships

2003	Coca-Cola İçecek Production Department
2002	ASELSAN Directorate of Product Quality

FOREIGN LANGUAGES

English (advanced)
German (beginner)

PUBLICATIONS

INTERNATIONAL JOURNAL ARTICLES:

- Korkmaz, O., Ider, S.K., Özgören, M.K, Inverse Dynamics Control of an Autonomous Underwater Vehicle Manipulator System, *submitted to journal*

- Ider, S.K., Korkmaz, O., Trajectory Tracking Control of Parallel Robots in the Presence of Joint Drive Flexibility, Journal of Sound and Vibration, Vol. 319 pp. 77-90, 2009.

INTERNATIONAL CONFERENCE PAPER:

- Korkmaz, O., Ider, S.K., Control of Parallel Manipulators Having Joint Drive Flexibility, 14th IFAC IEEE International Conference on Methods and Models in Automation and Robotics, Miedzyzdroje, Poland, 2009.

NATIONAL CONFERENCE PAPERS:

- Korkmaz, O., Ider, S.K., Özgören, M.K., Trajectory Tracking Control of an Underwater Vehicle Manipulator System, SAVTEK-2012, Ankara, Turkey (in Turkish).

- Korkmaz, O., Ider, S.K., Özgören, M.K., Modeling and Dynamic Analysis of an Underwater Vehicle Manipulator System, TOK-2011, İzmir, Turkey (in Turkish).

- Korkmaz, O., Ider, S.K., Force and Position Control of Flexible Joint Parallel Manipulators, 14th National Machine Theory Symposium, Güzelyurt, Turkish Republic of Northern Cyprus, 2009 (in Turkish).